CURRENT FLOW PATTERNS GENERATED BY COCHLEAR IMPLANTS

Punita Christopher

A dissertation submitted to the faculty of the University of North Carolina at Chapel Hill in partial fulfillment of the requirements for the degree of Doctor of Philosophy in the Department of Biomedical Engineering, School of Medicine.

Chapel Hill
2007

Approved by:

Dr. Charles Finley

Dr. John Grose

Dr. Henry Hsiao

Dr. David Lalush

Dr. Mark Tommerdahl

ABSTRACT

Punita Christopher: Current Flow Patterns Generated by Cochlear Implants
(Under the direction of Dr. Charles Finley)

Cochlear implants are neural prosthetic devices that restore partial hearing in many, but not all, hearing impaired individuals. In a cochlear implant device, sound is processed by an external speech processor, encoded as a data stream, and transmitted via a radio-frequency link across the skin to a subcutaneously-implanted receiver/stimulator located near the external ear. The signals are decoded, converted to current pulses and delivered into the cochlea by means of a surgically-implanted, multiple-contact, electrode array to stimulate surviving auditory nerve fibers in a tonotopic manner. Stimuli are typically delivered in a monopolar-coupled manner relative to a remote return electrode. Specific knowledge of how currents flow within and out of the implanted cochlea are important for understanding how present devices recruit surviving auditory fibers, as well as improving the design and clinical application of future devices. Few studies have addressed this problem to date, so our specific knowledge is limited. Consequently, the goal of this dissertation was to better understand the routes taken by the stimulus current as it leaves the cochlea in individual cochlear implant subjects. This study assumes that a better understanding of the injected current flow patterns would lead to improved control over stimulus current, which may result in the reduction of extracochlear stimulation and better-targeted stimulation of the auditory nerve. Because current flow cannot be directly measured in cochlear implant users, this

study uses surface artifact potentials to test predictions about how current may flow within and outside the cochlea. These surface potentials represent the *far field* of the stimulation delivered by the device, and are recorded non-invasively on the scalp, neck, and face of cochlear implant subjects during the active stimulation by the device. Results from the study indicate that differences exist in the primary current flow pathways for stimulation of apical and basal electrode contacts. This observation is counter to long held assumptions about current flow within the cochlea. Analytical head models and inverse dipole source localization methods have been developed to interpret these results further. Knowledge gained from this study may eventually lead to higher levels of performance for all cochlear implant users.

ACKNOWLEDGEMENTS

I wish to acknowledge several people that helped me start, survive, and complete this dissertation….

I would like to express my deepest gratitude to my advisor, Charlie Finley, for the many years of patience, guidance, and support. Charlie was extremely helpful, and always genuinely excited about what we were doing. I would not have finished without his encouragement and gentle prodding, especially when I was struggling with my writing. I am thankful to him for the resources and opportunities that he provided me with during my time in his laboratory. It has been a privilege and pleasure to work with someone who is as dedicated to his work as he is, and I will forever be grateful for this opportunity.

I wish to thank my committee members John Grose, Henry Hsiao, David Lalush, and Mark Tommerdahl for providing me with valuable insights. I am grateful to them for all their efforts in evaluating my progress through the course of my research and for helping me achieve my goals.

I very much appreciate the assistance provided by Marcia Clark, Emily Buss, and Holly Teagle in recruiting subjects for my study. This work would not have been possible without the subjects that participated in this study, and I would like to thank them for their time and cooperation.

I would like to express my appreciation to the cochlear implant manufacturing companies - Advanced Bionics Corporation and Cochlear Corporation for their technical assistance and

research software. I would also like to acknowledge the financial support from the NIH-NIDCD through which this work was made possible.

My thanks go out to the faculty, staff, and students of the BME department, as well as to my laboratory colleagues who have helped me in various capacities over the years.

I am deeply indebted to my friends here in Chapel Hill. They were my support system and I would not have survived graduate school in a foreign land without their help. I am especially thankful to my thesis support group for patiently listening to me and giving me valuable advice.

Finally, I am extremely grateful to my parents and my sister for always being there for me. I wish to thank them for their encouragement and understanding. Most of all, I want to thank them for their unconditional love and support; I know I could not have done it without them.

TABLE OF CONTENTS

LIST OF TABLES

LIST OF FIGURES

LIST OF ABBREVIATIONS

ABC	Advanced Bionics Corporation
AGC	automatic gain control
BTE	behind-the-ear
CIS	Continuous Interleaved Sampling
CPI	clinical programming interface
CSF	cerebrospinal fluid
DAQ	data acquisition card
dB	decibel
EAM	external auditory meatus
ECG	electrocardiogram
EEG	electroencephalography
EFI	Electrical Field Imaging
EFIM	Electrical Field Imaging and Modeling
ENT	Ear, Nose, and Throat
ERP	event related potential
FDA	Food and Drug Administration
GD	global dissimilarity
GFP	global field power
Hz	hertz
IAM	internal auditory meatus
IRB	Institutional Review Board
kHz	kilohertz

MEG	magnetoencephalography
PCMCIA	Personal Computer Memory Card International Association
p-p	peak to peak
RF	radio frequency
SE	standard error
μs	microsecond
μA	microampere

LIST OF SYMBOLS

A_L	left (external) auditory meatus
A_R	right (external) auditory meatus
Ca^{2+}	calcium ion
C_z	center midline
I_0	dipole strength
K^+	potassium ion
o_c	origin of the cochlea coordinate system
o_d	origin of the digitizer coordinate system
o_h	origin of the head coordinate system
q	dipole moment
q_r	radial dipole intensity
q_t	tangential dipole intensity
q_x	dipole moment in the X direction
q_y	dipole moment in the Y direction
q_z	dipole moment in the Z direction
r	radius
r_L	longitudinal resistor
r_q	dipole location
r_T	transversal resistor
v^H	potential in a homogeneous model
v^M	potential in a multiple shell model

v_r^H	radial component of the potential in a homogenous model
v_t^H	tangential component of the potential in a homogeneous model
X_c	X axis of the cochlea coordinate system
X_d	X axis of the digitizer coordinate system
X_h	X axis of the head coordinate system
Y_c	Y axis of the cochlea coordinate system
Y_d	Y axis of the digitizer coordinate system
Y_h	Y axis of the head coordinate system
Z_c	intracochlear electrode impedance
Z_c	Z axis of the cochlea coordinate system
Z_d	Z axis of the digitizer coordinate system
Z_h	Z axis of the head coordinate system
α	angle between dipole location and dipole moment
γ	angle between recording location and dipole position
θ	polar angle between Z axis and radius vector
λ	Berg magnitude factor
μ	Berg eccentricity factor
σ	conductivity
φ_d	potential field

1. INTRODUCTION

Hearing loss affects more than 278 million people worldwide (World Health Organization, 2005). Approximately 10% of Americans have some form of hearing loss, typically classified as either conductive or sensorineural. Conductive hearing loss occurs when sound is not mechanically transmitted efficiently from the outer ear through the middle ear resulting in a decrease in acoustic sensitivity and audibility of normal sounds. This type of hearing loss can often be corrected by medical treatment, surgical intervention and/or supplementary amplification provided by a hearing aid. Sensorineural hearing loss, on the other hand, is permanent in nature, and occurs as a result of damage to and/or irreversible loss of the sensory hair cells of the inner ear. While the primary function of hearing aid devices is to amplify sound, their effectiveness is reduced in the case of advanced sensorineural loss. Damaged hair cells produce distorted responses to acoustic energy, whereas lost hair cells result in complete gaps in the spectral and temporal information presented to the central nervous system. Considering the most extreme cases, severely hearing impaired patients are able to detect sounds with the aid of strong amplification but are unable to discern much useful speech information, whereas profoundly hearing impaired patients have sensory threshold shifts of >100 dB and essentially live in a world of silence. According to current medical practice, pediatric and adult patients with severe or profound hearing loss are candidates for cochlear implantation.

Cochlear implants are evolving neural prosthetic devices that work differently from hearing aid devices. In a cochlear implant device, sound is processed by an external speech

processor, encoded as a data stream, and transmitted via a radio-frequency link across the skin to an implanted stimulator. The encoded signals are converted by the implanted stimulator into the form of current pulses which are applied to the surviving portions of the auditory nerve in the cochlea by means of a surgically-implanted electrode array. These current pulses depolarize the targeted auditory nerve fibers, produce centrally conducted action potentials which are processed by central auditory relay nuclei and result in percepts perceived as sound by the central auditory nervous system. Cochlear implants were first available commercially in the 1970's as single channel devices providing limited benefit. In the 1980's multiple channel devices providing tonotopic representation of acoustic information became available and have been very successful in helping severely and profoundly deaf individuals recognize sounds and understand speech. According to the Food and Drug Administration's (FDA) 2005 data (National Institute on Deafness and other Communication Disorders, 2006), there are in excess of 100,000 cochlear implant users worldwide.

1.1 Research Question

The surgically-implanted electrode array consists of multiple electrode contacts that provide electrical stimulation in the form of current pulses to the neighboring auditory nerve fibers within the cochlea. In principle, the electrical current is targeted to stimulate only neural fibers in the immediate vicinity of each electrode contact. At the cellular level, this current spreads through the tissue volume creating extracellular voltage gradients along the neural fibers that result in the flow of transmembrane current across neighboring neurons and the generation of propagating action potentials. The details of where injected current flows

in the tissue volume to produce the extracellular potential profiles is an essential, but poorly understood, aspect of cochlear implant operation.

Several studies, a comprehensive description of which is provided in Section 2.3, have contributed to the current knowledge regarding the electrical properties of the cochlea, as well as the current flow within the cochlea in response to electrical stimulation. The classical view is that the low-impedance pathway for monopolar current (i.e. the current generated due to monopolar stimulation between an intracochlear electrode contact and a remote reference electrode) to leave the cochlea is through the central modiolar core, via the internal auditory meatus, and into brain tissue. However, recent studies have suggested the existence of other current pathways as well. At the macroscopic level, stimulus current often spreads across larger areas in and around the cochlea, even targeting regions that are not meant to be electrically stimulated. These regions include other untargeted regions of the cochlea itself and/or extracochlear locations such as the facial nerve, the vestibular apparatus and nerve, somatic innervation in the middle ear, and regions of the scalp in the vicinity of the implanted device or brain tissue beneath the device.

In spite of the existing knowledge, the pathways of current flow within and around the electrically-stimulated human cochlea are still not completely understood. This limited knowledge and theoretical understanding of cochlear implants directly impacts the design and application of implant systems. The effects of electrical stimulation often vary among cochlear implant subjects, and may be a possible basis for the significant across-subject variation of speech reception performances observed among implant users. Other factors that may lead to wide variability in the performance levels of patients include the following: age of onset and duration of deafness, age at implantation, duration of cochlear implant use,

biological status of the cochlea with regard to the degree and spatial pattern of auditory nerve survival, the ability of the central auditory nervous system to process information, surgical placement of the electrode and insertion depth within the cochlea, electrical dynamic range, signal processing strategies of the sound processor system, and/or malfunction of the cochlear implant device itself.

Consequently, the overall goal of this study is to better understand the routes taken by the stimulus current as it leaves the cochlea in individual cochlear implant subjects. While cochlear implants are extremely successful in some subjects, it remains a significant challenge for the field to extend such benefits to the remaining population of implantees. This study assumes that a better understanding of the flow patterns of injected current in individual subjects would lead to improved control over stimulus current, which may result in the reduction of extracochlear stimulation and better-targeted stimulation of the auditory nerve. Knowledge gained from this study may eventually lead to an improvement in electrode design and configuration, and higher levels of performance for all cochlear implant users.

Because current flow cannot be directly measured in cochlear implant users, this study uses surface artifact potentials to test predictions about how current may flow within and outside the cochlea. These surface potentials represent the *far field* of the stimulation delivered by the device, and are recorded non-invasively on the scalp, neck, and face of cochlear implant subjects during the active stimulation by the device. To relate the surface potentials measured on the scalp to the intracochlear current flow, several impedance measures of the electrode/skin/tissue interfaces are made. The following section states the specific aims of the study.

1.2 Specific Aims

(1) To test the hypothesis that surface potentials measured on the scalp are influenced linearly by the flow of current within and outside the cochlea and throughout the volume of the head during device stimulation (Hypothesis 1).

This specific aim tests the hypothesis that surface potentials measured non-invasively on the scalp can be used to infer patterns of current flow within the cochlea. An input stimulus consisting of a biphasic pulse train of constant amplitude is delivered to the cochlea. The resulting potential distribution that appears on the scalp is measured. The amplitude of the pulse train is then varied and the subsequent potential distribution is recorded. The scalp distributions obtained in each case are scaled to unit magnitude. The system exhibits homogeneity if the respective scaled distributions are similar in structure. The additive property of the system is verified by injecting a stimulus whose magnitude equals the sum of amplitudes from two individual stimuli. The resulting potential distribution is compared to the distribution obtained by summing the two distributions from individual stimuli. A system that satisfies the property of homogeneity and additivity follows the superposition theorem and can be considered to be linear in nature.

(2) To test the hypothesis that the bulk head tissue can be considered to be purely resistive in nature for the range of frequencies of stimulation delivered by modern cochlear implant systems (Hypothesis 2).

Electrode-fluid interface impedances are non-linear in nature, and are highly dependent on the frequency and magnitude of currents passing across them (Geddes, 1997). The use of a constant current source to generate stimulus pulses removes the non-linear

effects of the interface components. In order to model the system appropriately it is important to determine the impedance characteristics for the bulk tissue of the head. To test Hypothesis 2, a series of stimuli varying in magnitude and frequency over the range of 10 Hz – 70 kHz are injected through surface electrodes on the scalp. The resulting voltage on the surface of the head is measured using surface electrodes. The frequency response of these voltage measures is examined, and if it is found to be level and frequency independent, the bulk head tissue component is modeled as a resistive network.

(3) To test the hypothesis that depending on the choice of electrode configurations, there are different routes for stimulation current to flow within or exit the cochlea (Hypothesis 3).

The goal of this section is to test the hypothesis that there are different routes for stimulation current to flow within or exit the cochlea, depending on the choice of stimulation electrode configurations. To test this hypothesis, *global dissimilarities* (Skrandies, 1990) are computed for scalp surface potential distribution patterns across all electrodes. If adjacent electrodes have similar distribution patterns, and apical electrodes have patterns of distribution that are different from those for basal electrodes, the hypothesis is accepted. How the similarity of surface potential distributions changes as a function of stimulus electrode position within the cochlea may provide insight into the general patterns of where current flows out of the cochlea. In addition, *hierarchical clustering* methods (Duda, Hart, & Stork, 2000) are also used to study the differences between potential distributions. The differences reflected in electrodes that are farther away from each other compared to electrodes that are closer to each other vary depending on the location of the electrode contact, the depth of insertion of the array, and the anatomy of the individual subject.

(4) To test the hypothesis that multiple alternate paths exist for current to exit the cochlea, in addition to the classical view that current injected into the cochlea flows into the modiolar core and exits via the internal auditory meatus into the cranium (Hypothesis 4).

To test Hypothesis 4, *inverse dipole analysis* techniques are used to compute the dipole sources from measured surface potential data. If the predicted dipoles vary in terms of location and orientation depending on the electrode being stimulated, this suggests that there exist other routes by which current leaves the cochlea. If the resulting dipoles calculated for all individual electrodes have the same location and orientation coinciding with a location outside the cochlea and near the internal auditory meatus, this is consistent with the classical view of current flow patterns. Computational techniques used to solve the inverse electrical field problem and generate a simple dipole model that best fits as a generator source for the measured surface potential data are described in Chapter 3. These techniques are commonly used in electroencephalography (EEG) and magnetoencephalography (MEG) source analysis. Intracochlear electrical field measures, whose slopes represent voltage drops across the intracochlear electrodes, may also provide valuable information regarding the paths of current flow.

1.3 General Overview and Organization

This dissertation has the following organization. *Chapter 2. Background*, which follows this introduction, provides a brief summary of the auditory system and the cochlear implant device. A literature review of studies related to electrical properties of the cochlea and current flow patterns within the cochlea is provided. Surface artifact potentials, which are used in this study to test predictions regarding how current may flow within and outside the cochlea, are described in detail.

In this study, inverse source localization techniques are used to test various hypotheses regarding current flow in the cochlea. *Chapter 3. Methodology - Dipole Source Localization*, explains the computational techniques developed to solve the inverse electrical field problem. A description of the implementation of the spherical head model and the inverse model in computing dipole sources from surface potential measured in cochlear implant subjects is provided.

Chapter 4. Methodology – Data Collection explains the experimental measures obtained and the protocol followed in this study. Surface potential measures are recorded non-invasively on the scalp and face. Recordings at each measurement location are made using a custom-built recording electrode probe in conjunction with a 3D-digitizer and a biopotential amplifier. The digitizer enables highly accurate and rapid recording of the measurement location. The probe is designed to allow rapid recording of potentials on the scalp without traditional scalp preparation to reduce skin impedance. The intracochlear potentials are obtained non-invasively in one subject using an on-board data telemetry system. Measures of the electrical characteristics of the bulk tissue are also recorded in non-implanted subjects.

Chapter 5. Results presents the findings of this study. The analyzed data suggest that there are differences in the current flow patterns for apical and basal electrode contacts. In the case of apical electrode contacts, the return pathway for monopolar current appears to be through the modiolus and internal meatus into the cranium. For basal electrode contacts, however, the majority of the current that exits the cochlea seems to flow out laterally.

Chapter 6. Discussion and Conclusions focuses on the significance of results obtained from this study. Problems encountered are discussed along with the general

limitations of the approach. Future work is discussed as well. Finally, the *Appendix* contains subject informed consent forms used in this Institutional Review Board (IRB)-approved study.

2. BACKGROUND

The purpose of this chapter is to provide the appropriate background information and a relevant literature review to understand the rationale for this study. First, a summary of the anatomy and function of the auditory system is presented. A brief overview of cochlear implant technology then follows. Existing studies describing the electrical properties of the cochlea and implant-generated current flow patterns in and around the cochlea are discussed. Prior work that deduces patterns of current flow in cochlear implant subjects from surface potential measures and intracochlear electrical field measures, which represent the *far field* and the *near field* respectively of the electrical stimulation provided to the cochlea, is discussed in detail.

2.1 The Peripheral Auditory System

A diagram of the human ear is given in Figure 2.1. The ear is divided into the outer, middle, and inner ear sections. The outer ear consists of the pinna/auricle and the external auditory meatus/ear canal. The pinna helps to collect sound energy from the external environment and direct it into the external auditory meatus toward the middle ear. The tympanic membrane, which is also known as the eardrum, is a thin membrane that separates the outer and middle ear. This structure converts the acoustic pressure wave in the external meatus into mechanical displacement of the middle ear ossicles. The middle ear ossicles, which are the smallest bones in the human body, include the malleus, incus and stapes. They serve in conjunction with the tympanic membrane to form a mechanical transformer which

matches the low acoustic impedance of the external canal to the high impedance of the fluid-filled cochlea to maximize acoustic energy transfer into the cochlea. The Eustachian tube in the middle ear connects to the pharynx in the oral cavity and provides a mechanism for equalizing ambient air pressure across the tympanic membrane to minimize static loading.

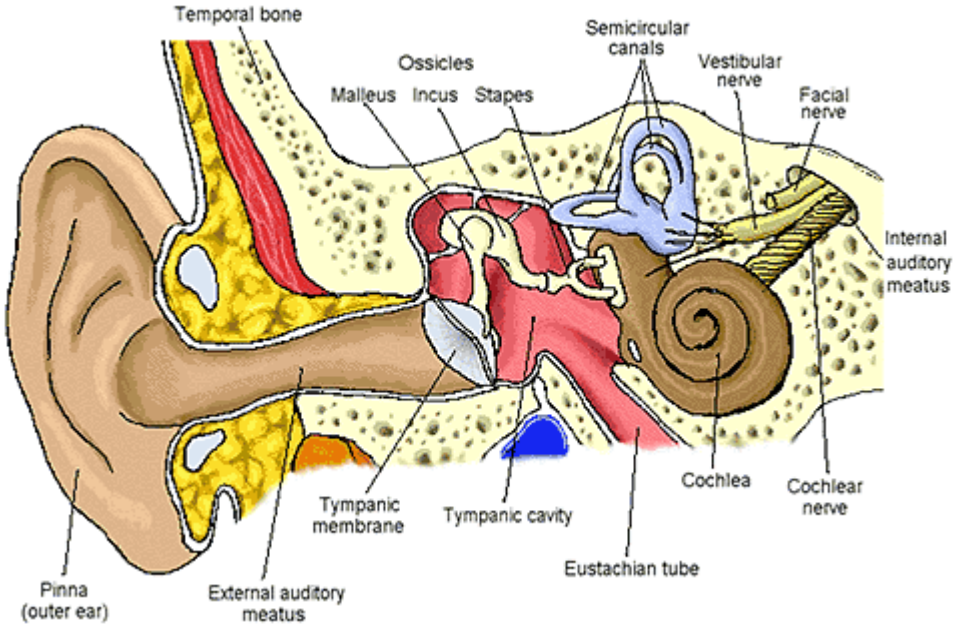

Figure 2.1: Diagram of the human ear (from the "Hearing Professionals Limited" website http://www.hearingprofessionals.co.nz/)

2.1.1 The Inner Ear

The inner ear section is made up of the vestibular apparatus and the cochlea. The vestibular apparatus, which controls the balance mechanism in the body, contains three semicircular canals and the vestibule. The cochlea is a spiral-shaped, coiled structure

enclosed within the temporal bone. The human cochlea is about 35 mm long. It is wide at the base and tapers towards the apex in a spiral. The modiolus forms the bony central core of the cochlear spiral. The auditory/cochlear nerve fibers pass through the modiolar core, and along with the facial and vestibular nerves extend into the internal auditory meatus, towards the cranium. The vestibular nerve and the auditory/cochlear nerve constitute the VIII cranial nerve.

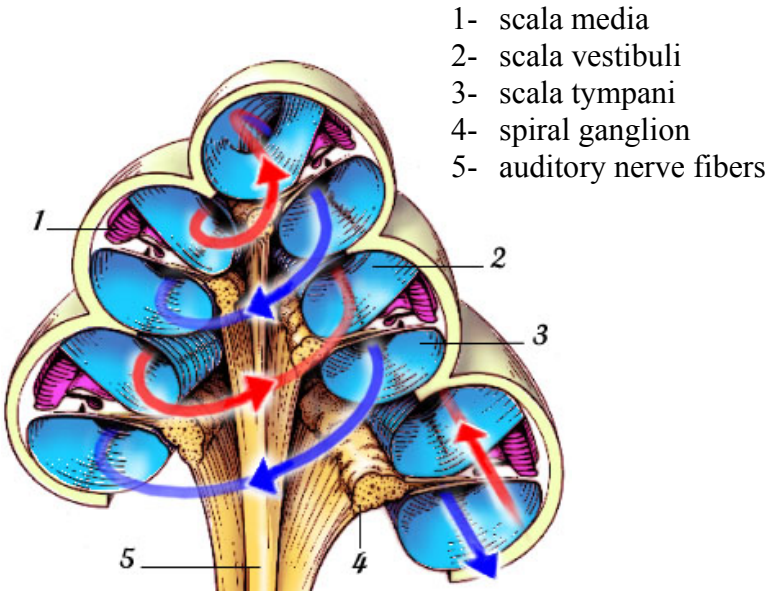

Figure 2.2: Cross-sectional view of the cochlea (Figure by S. Blatrix, from the "Promenade around the Cochlea" website <www.cochlea.org> by R Pujol et al., Montpellier, France)

A cartoon image of the cross sectional view through the cochlea is provided in Figure 2.2. The cochlea is divided into three spiraled chambers: scala vestibuli at the top, scala tympani at the bottom, and scala media in between. At the base, the scala vestibuli and the scala tympani terminate at the oval window (red arrow pathway) and round window (blue arrow pathway), respectively. The scala media is separated from the scala tympani by means

of the basilar membrane. The organ of Corti, which is the organ of hearing, lies on the basilar membrane. Within the organ of Corti are four rows of hair cells. The innermost row comprises the inner hair cells, which are the sensory receptor cells in the auditory system. The outer hair cells in the outer three rows are innervated by efferent fibers projecting from the central nervous system and actively work to regulate the mechanical properties of the basilar membrane. The apical cilia of the inner hair cells extend into the scala media and are deflected in response to basilar membrane motion. The base of these hair cells connects to nerve fibers of the cochlear nerve, which pass through the modiolus. In Figure 2.2, the spiral ganglion cells and cochlear nerve fibers within the modiolar core are also shown.

2.1.2 Sensory Transduction

Sensory transduction in the normal functioning ear occurs in the following manner. Sound waves enter through the outer ear in the form of vibrations. The frequency and magnitude of these vibrations are directly related to the pitch and intensity of the sound, respectively. The waves travel inwards and produce vibrations in the tympanic membrane. The vibrations are carried to the middle ear bones and cause movement of the oval window, which is connected to the foot of the stapes bone. This results in the propagation of pressure waves in the perilymphatic fluid of the scala vestibuli. These pressure variations are transmitted through the basilar membrane. The basilar membrane vibrates with maximum amplitude at different positions along its length depending on the frequency of the stimulation. Low-frequency sounds cause maximum displacement of the basilar membrane toward the apex, while high-frequency sounds create maximum displacement toward the base of the basilar membrane of the cochlea. Consequently, each location along the basilar membrane is maximally sensitive to a particular frequency, and this mechanism is known as

place theory. The vibrations in the basilar membrane cause the cilia of the inner hair cells to bend, as a result of which the ion channels open and potassium (K^+) ions enter the cell. This leads to cell depolarization, bringing about an influx of calcium (Ca^{2+}) ions into the cell. Subsequently, the calcium influx causes neurotransmitter release from the hair cell to stimulate auditory nerve fibers at the base of the hair cell. The nerve impulse propagates to the brain via the auditory nerve and this is perceived as sound.

A healthy auditory system can be compared to a transducer, which transforms acoustic energy to neural impulses. If the hair cells are damaged, energy transformation does not take place appropriately, and sound never reaches the brain. Hair cell damage causes atrophy of neighboring auditory neurons as well. Deafness occurs when a large number of auditory neurons and hair cells within the cochlea are damaged. In a deafened cochlea, cochlear implants bypass the damaged hair cells, and directly provide electrical stimulation to the surviving auditory neurons in the cochlea.

2.2 Cochlear Implant Basics

Cochlear implant devices consist of the following components: (1) microphone, (2) signal processor, (3) transmitter, (4) receiver/stimulator, and (5) multi-contact electrode array. A diagram of the functional components of a cochlear implant is shown in Figure 2.3. The transmitter is in the form of a magnetic headpiece worn above the ear. The microphone is housed in the headpiece, or worn as a behind-the-ear (BTE) device. Signal processors are either worn as BTE devices or carried in a pouch or pocket. The stimulator is surgically implanted under the skin in the region above the ear. Part of the bone is drilled out during surgery and the stimulator is held securely to the bone. The multi-contact electrode array is surgically placed in the basilar membrane of the cochlea.

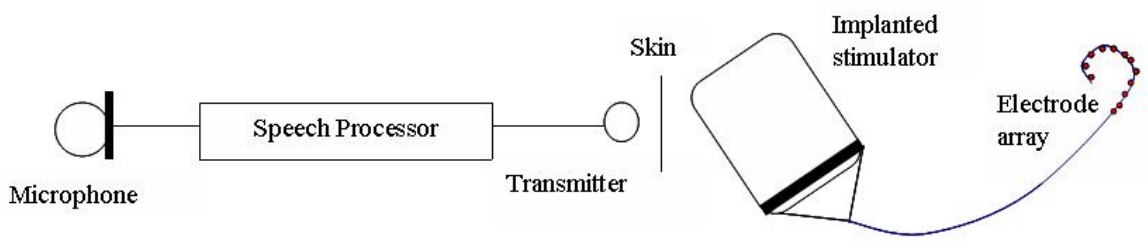

Figure 2.3: Functional components of a cochlear implant

The incoming, broad dynamic range, acoustic input is picked up by the microphone and is compressed by an automatic gain-controlled (AGC) amplifier into the electrical dynamic range of the signal processor's analog-to-digital converter. The compressed signal is sampled by an analog–to-digital converter, processed using a speech-processing algorithm, and transmitted across the skin to the implanted stimulator via a radio-frequency (RF) link. The stimulator in turn delivers the coded signals to the cochlea via the implanted electrode array in a patterned manner determined by the speech processing strategy. In the analog form of stimulation, the information presented to the electrodes is in the form of continuous analog signals that are applied directly to the electrode contacts. More common in use is the *continuous interleaved sampling* (CIS) strategy, which was proposed by Eddington and developed by researchers at the Research Triangle Institute (Wilson et al., 1991). In the CIS approach, discrete, biphasic pulses are presented to each electrode in a non-overlapping manner, such that at a particular point in time only one electrode is stimulated. This form of sequential, pulsatile stimulation decreases the interactions between the electrical fields for each electrode, compared to that which would occur with simultaneous stimulation across the electrodes.

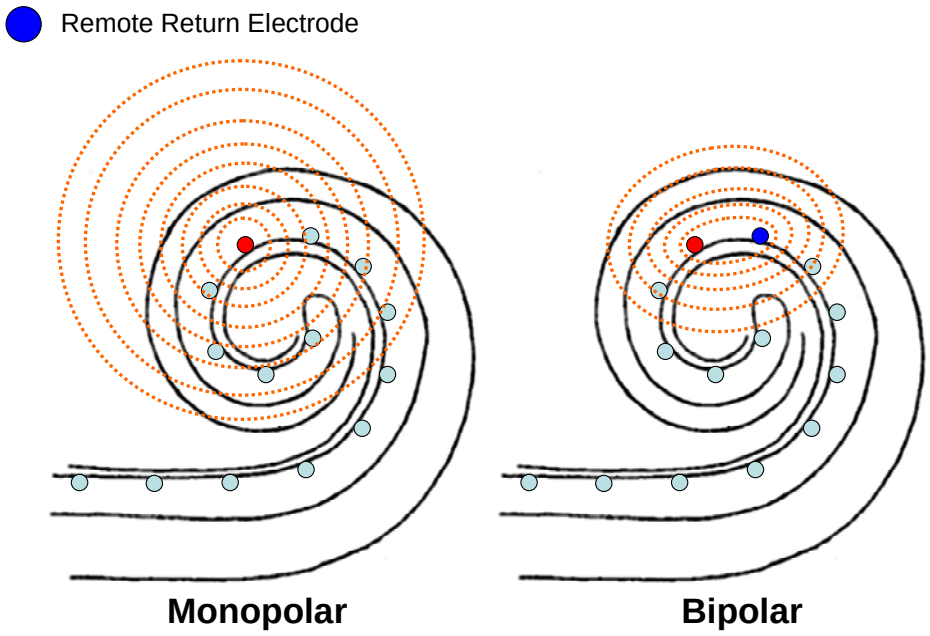

Figure 2.4: Monopolar and bipolar mode of stimulation

The multi-contact electrode array placed beneath the basilar membrane exploits the *place theory* mechanism of the cochlea by stimulating the surviving auditory neurons on a sector-by-sector basis to convey tonotopic information. Electrode contacts near the base are stimulated to encode high frequency acoustic information while contacts near the apex are stimulated to encode low frequency information. The stimulation delivered can either be in *monopolar* or *bipolar* mode. In the monopolar configuration, the active electrode is placed away from the ground reference. Here, stimulation is provided through one of the intracochlear electrode contacts and a remote reference plate electrode located on the surface of the subcutaneously implanted receiver/stimulator or via a ball electrode placed beneath the temporalis muscle. In the bipolar mode of stimulation, the active and ground electrodes are

close to each other, and current stimuli are provided through two intracochlear electrode contacts. Figure 2.4 shows the two modes of stimulation.

The commercially available and FDA-approved cochlear implant devices in the United States include the Nucleus device (Cochlear Corporation, Sydney, Australia), the Clarion device (Advanced Bionics Corporation, Valencia, CA, USA), and the MedEl device (MedEl Corporation, Innsbruck, Austria). All three of these cochlear implant systems function similarly according to the general principles described above.

2.3 Current Flow in the Cochlea

Current flow within and outside of the cochlea has been studied by several researchers over the years. Here, these studies are divided into three categories based on the following measures that were used: intracochlear potential measures in animal cochleae, scalp potential measures, and non-invasive intracochlear electrical field measures in human cochlear implant subjects.

2.3.1 Intracochlear Potentials - Animal Studies

Some of the earliest studies in this field (von Békésy, 1951; von Békésy, 1960) were conducted in guinea pigs to determine the resistivities of various anatomical regions within the cochlea. In his experiments, von Békésy used two separate pairs of electrodes inserted at various locations within and around the cochlea to inject current and record the change in potential, respectively. Results from the experiments proved that the cochlear bone was a good insulator. Furthermore, the study also found a low impedance pathway through the central core of the cochlea, namely the modiolus, continuing through the internal auditory meatus containing the facial, auditory, and vestibular nerves, and towards the brain. This

early description of conductive pathways in the cochlea has had a pervasive effect on the theoretical principles and assumptions used in the design of cochlear implants for the past three decades.

Other animal studies (Clopton & Spelman, 1982; Spelman et al., 1980; Spelman, Clopton, Pfingst, & Miller, 1980; Spelman, Clopton, & Pfingst, 1982) were conducted in guinea pigs and monkeys to find experimentally the current pathways during stimulation by intracochlear electrodes, and verify the results obtained using behavioral threshold measures and brain stem evoked potential responses. Electrodes were placed either in the scala of the cochlea or at an external site. The later studies (Clopton & Spelman, 1982; Spelman et al., 1982) used a four-electrode method to separate out the electrode and tissue impedances, and placed the external electrodes in the internal auditory meatus in the guinea pig. These studies suggested that the regions being activated by the stimuli were outside the scala tympani, and hence current would have to exit the cochlea through the modiolus. This work, while appearing to confirm the earlier findings of von Békésy (1951 and 1960), was also strongly biased in experimental design by the earlier concepts posed by von Békésy due to the placement of the return electrode in the internal auditory meatus, instead of a more distant remote site. Also, an underlying assumption of these studies was that the inner ear represented a linear, resistive model. This assumption was tested and verified up to a frequency range of 12.5 kHz. Modern implant systems however present primarily short duration biphasic pulses which have significant frequency content above this range. Consequently, the general assumption in cochlear implant design that the biological tissue of the inner ear is essentially electrically resistive remains untested and may not be true.

Some other studies (Micco and Richter, 2006) have been conducted to determine the differences between a deafened cochlea and a normal cochlea. Two models were used in this study - the in vivo model where resistivity measures were obtained from anesthetized gerbils, and the in vitro model, also referred to as a hemicochlea model, in which measurements were made using cochlear tissue from a sacrificed gerbil. The study reported that the resistivity of the modiolus decreased as a result of neural degeneration in a deafened cochlea. It was also found that both models produced similar results in terms of the change in resistivity. This study also assumed that the cochlear tissue is completely resistive.

All of the studies described so far inferred insight into current flow in the cochlea by examining the distribution of potentials measured within or near the cochlea itself, essentially the *near field* of the broadly spreading electrical potential distribution created by electrical stimulation. Most of these studies have been limited to animal models and may not be good predictors of conditions in human subjects where anatomical features differ and electrical properties may be different and/or altered by disease or surgical intervention. An alternative approach, which is more relevant to clinical application, is to examine the *far field* of the electrical potentials generated by stimulation, namely potentials appearing on the surface of the scalp.

2.3.2 Surface Potentials

Scalp artifact potentials represent a scaled version of the electrical stimulation delivered by the device, and have primarily been used in various studies (Battmer, Gnadeberg, Lehnhardt, & Lenarz, 1994; Carter, 2001; Christopher, 2003; Cullington & Clarke, 1997; Garnham, Cope, & Mason, 2000; Heller, Sinopoli, Fowler-Brehm, & Shallop, 1991; Kileny, Meiteles, Zwolan, & Telian, 1995; Mens, Oostendorp, & van den Broek,

1994b; Mens & Mulder, 2002; Shallop, 1993) as a means to objectively test the integrity and the functional operation of cochlear implant devices. Most of these studies examined one or two biphasic output pulses during a specified recording time interval. One study (Christopher, 2003; Finley, Christopher, Eddington, & Herrmann, 2003) expanded this approach to record and analyze long series of records that spanned several hundred artifact pulses, in an effort to increase the chances of identifying certain rare stimulation events which may otherwise be undetected when only few pulses are examined. This study used speech stimuli, and the devices were tested in their normal "speech processor" mode. The generic nature of the approach used in this study allowed for the testing of devices from the three major manufacturers of clinically-applied devices. These objective tests using stimulus artifact events recorded from the scalp are of great value, especially in testing the pediatric population, where a child's behavioral response is either absent, unreliable, and/or extremely limited.

Surface artifact potential measures have also been used to measure the flow of current within and around the cochlea in response to electrical stimulation of the multiple electrode contacts. Significant contributions to this field were made in a study (Mens, Oostendorp, & van den Broek, 1994a), in which surface potentials were measured in 16 users of the Cochlear (Nucleus) Mini System 22 (Cochlear Corporation). Two out of the sixteen subjects tested had a history of otosclerosis, which is a pathological condition that causes the compacted cochlear bone to become spongiform in nature. The stimulation by the implanted device was provided sequentially through a series of bipolar combinations of all active electrodes. Differential recording electrodes were placed on the ipsilateral mastoid (positive), contralateral mastoid (reference/negative), and the arm (ground). Peak-to-peak

amplitudes of measured scalp potentials were computed for the averaged data, and plotted as a function of the electrode contact numbers (*E-E maps*) of the electrodes actively used for each bipolar condition (Mens, Oostendorp, & van den Broek, 1994b). It was found that two different potential distribution patterns emerged for subjects with and without otosclerosis. In subjects without otosclerosis, the potentials decreased as a function of the position of the active electrode from the round window, and increased as a function of the distance between the stimulating bipolar electrode pair. In the two subjects that had a history of otosclerosis, the potentials were the greatest in amplitude when the distance between the stimulating electrodes was about half of a complete cochlear turn. These different patterns suggested that in subjects without otosclerosis, the injected current spread primarily along the highly conductive scalar fluids and not through the highly resistive bony walls, spiraling from apex to base, and finally exited the cochlea through basally located openings into the temporal bone to eventually produce the measured artifact on the scalp.. This result was in agreement with the earlier work conducted in cochlear implant subjects (Kasper, Pelizzone, & Montandon, 1991), which found a low-resistance pathway at the basal openings of the cochlea, suggesting a significant current pathway through the basal turn with monopolar coupled stimuli. In patients with a history of otosclerosis, however, Mens et al. found that the major current pathway appeared to be directly through the cochlear bone as a result of increased conductivity due to the spongiform bone pathology in such patients.

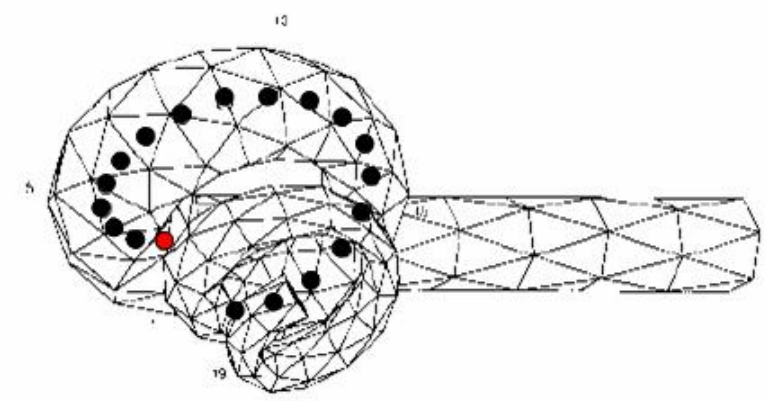

Figure 2.5: Cochlea and EAM model (from Mens et al., 1999; Figure 3 and www.informaworld.com)

In a subsequent study (Mens, Huiskamp, Oostendorp, & van den Broek, 1999), simple volume conduction head models were used to interpret the surface potential data obtained from the previous study (Mens, Oostendorp, & van den Broek, 1994a). In these models, the skin, skull, and brain regions were represented by nested spheres. The cochlea was represented by a spiral tube that spanned 2.5 turns, as shown in Figure 2.5. The cochlea was further attached to a tube, which represented the external auditory meatus (EAM). Monopoles were placed from the base to the apex in the cochlea, and these 19 monopolar source locations are shown in Figure 2.5. The positive monopole (indicated by the red dot) was represented by the source located at the most basal position. The other 18 positions served as possible locations for the negative source, depending on the bipolar electrode pair that was being stimulated.

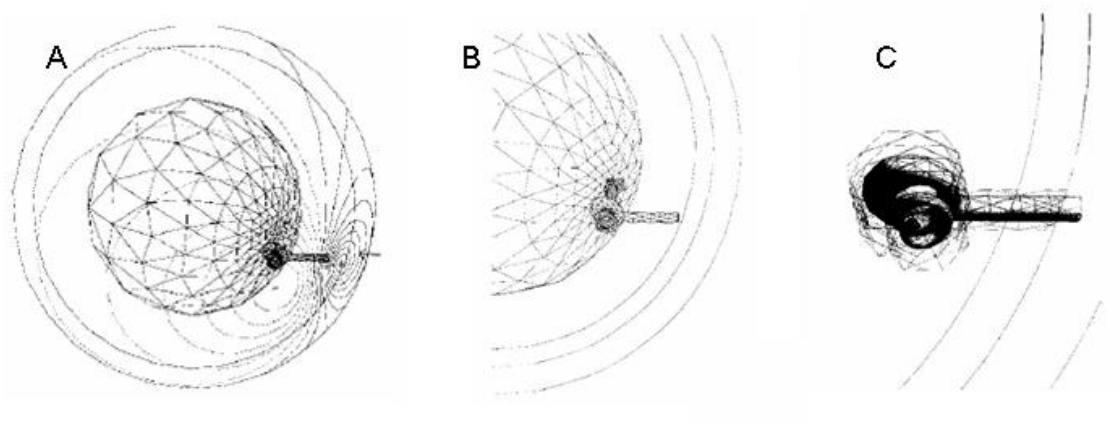

Figure 2.6: Mens' volume conduction models – A: thick skull, B: IAM, and C: petrous bone (from Mens et al., 1999; Figures 4, 5A, and 6 and www.informaworld.com)

The basic model consisted of the skull, skin, and brain compartments. Different anatomical structures were added to the basic model to determine the effect of these structures in the flow of stimulus current around the cochlea. The following three models, which are represented in Figure 2.6, were constructed: (A) *thick skull model*, in which the cochlea and EAM were placed within a large skull compartment, (B) *modiolus/internal auditory meatus (IAM) model*, which was identical to the thick skull model except for a canal placed very close to the cochlea that extended into the brain region, and (C) *petrous bone model*, in which the cochlea was surrounded by a bony chamber, that represented the petrous bone (the petrous bone is the part of the temporal bone that surrounds the middle and inner ear) and extended into the brain region. In the petrous bone model, the EAM extended into the skin compartment. The resistivity of the petrous bone was equal to that of the skull region. For resistivity ratios of 1:1 and 1:10 (other compartments vs. skull), all the models produced potential patterns that were similar to the data obtained from the subjects with otosclerosis.

However, the petrous bone model best represented the surface potential data from subjects without otosclerosis when the resistivity ratio was increased. The resistivity ratio between the compartments of this model and the bone/skull was 1:100. Mens et al. (1999) concluded that the failure of the other models to accurately represent the potentials from subjects without otosclerosis suggests that the primary return current pathway from the cochlea is a non-specific path through the cochlear wall across the petrous bone and back into the cranial cavity.

2.3.3 Intracochlear Electrical Field Measures

Modern cochlear implant systems such as the Clarion® CII and 90K devices (Advanced Bionics Corporation, ABC) have in-built capabilities to make objective intracochlear electrical field measures. "Electrical Field Imaging" or EFI is a widely used commercial term for these intracochlear electrical field measures applying only to the ABC cochlear implant systems. It has little to do with traditional imaging techniques per se, and is more closely related to impedance tomography. The stimulation protocol consists of injecting a known monopolar current across a single intracochlear electrode contact relative to a remote return electrode. In this mode, current flows between a single electrode contact and the remote reference electrode. The voltage is recorded systematically from each of the sixteen electrodes along the array using on-board backward telemetry capabilities of the implant system. Such measures are repeated until all the 16 electrodes have been stimulated individually and a complete EFI voltage map has been obtained. The voltages are usually divided by the injected current to represent normalized measures described in terms of ohm units (volt/amp). Hence the resulting EFI map represents impedance values, sometimes referred to as *transimpedances*.

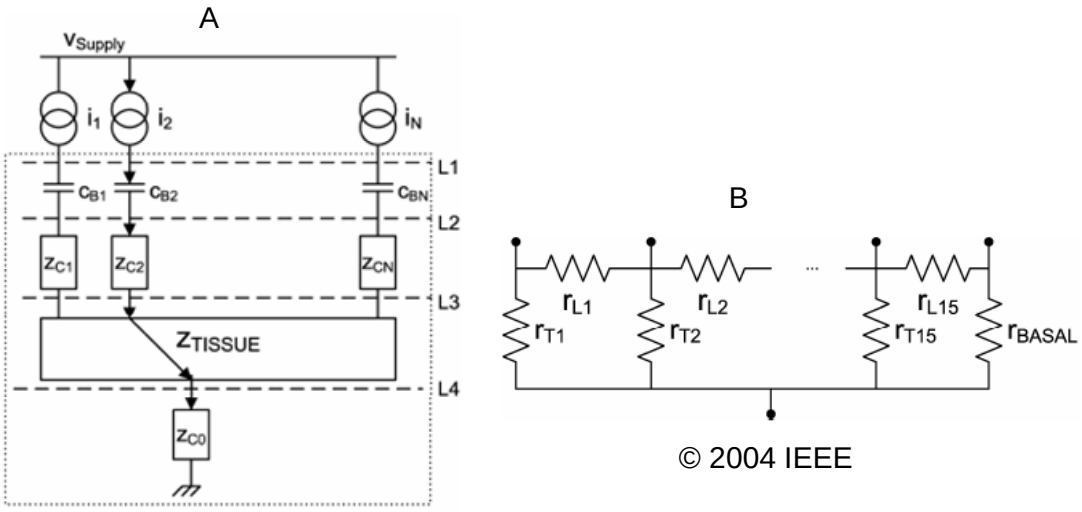

A: General impedance model containing current sources, blocking capacitors, interface impedances Z_c, tissue impedance network Z_{tissue}, and reference electrode, B: Tissue impedance network model

Figure 2.7: EFI Impedance Model (from Vanpoucke et al, 2004; Figures 3 and 8)

Researchers in Antwerp, Belgium (Advanced Bionics, 2003; Vanpoucke, Zarowski, & Peeters, 2004) developed a lumped-element, electrical network model to interpret EFI measures in individual subjects with Clarion CII devices. This network model is shown in Figure 2.7. Stimulation current flows between the electrode contact and the remote reference electrode. C_B represents the blocking or coupling capacitors of the implant device's current sources.. The impedance of the intracochlear electrode contacts is represented as Z_c. The bulk tissue is represented by a purely resistive ladder network, which consists of a longitudinal resistor r_L, which represents the current flow within the scala, and a transversal resistor r_T, which represents the current flow from the scala to the bone. Again, the

underlying assumption of this model is that the tissue is resistive in nature. This was confirmed in experiments for a frequency up to 12 kHz (Vanpoucke, Zarowski, Casselman, Frijns, & Peeters, 2004); however this frequency is low given the faster stimulation rates up to 50 kHz in modern cochlear implant systems. In a related clinical study (Vanpoucke et al., 2004), the EFI data from Clarion® CII subjects suggested that a significant current pathway can exist along the facial nerve in some subjects for stimulation on some electrodes. This stands in contrast to the long-held assumption that current flows via the modiolus and internal auditory meatus into the cranium as originally described by von Békésy.

2.3.4 Discussion

The studies discussed above suggest that there can be four possible pathways for injected stimulus current to flow out of the cochlea. The following, which is an extension of the summary provided by Mens et al. (1999), are the four possible pathways:

1) through the modiolar wall via the internal auditory meatus and into the brain tissue, which is the classical view based on intracochlear potential and impedance measures in animals (Clopton & Spelman, 1982; Spelman et al., 1982; von Békésy, 1951; von Békésy, 1960),
2) through basally-located openings of the cochlea during monopolar (Kasper et al., 1991) and bipolar (Mens, Oostendorp, & van den Broek, 1994a) stimulation in human subjects,
3) non-specifically through the cochlear bone to the brain tissue, especially in patients with otosclerosis (Mens, Oostendorp, & van den Broek, 1994a; Mens et al., 1999), and
4) along the facial nerve (Vanpoucke et al., 2004).

Several volume conduction models of the cochlea have been developed in the past (Briaire & Frijns, 2000; Finley, Wilson, & White, 1990; Frijns, de Snoo, & Schoonhoven, 1995; Girzon, 1987; Hanekom, 2001; Hanekom, 2005; Rattay, Leao, & Felix, 2001; Rattay, Lutter, & Felix, 2001; Whiten, 2007) and have increased the existing knowledge regarding current flow in the cochlea. However, all of these previous models are constructed on the basis of the assumption that current will flow out of the base of the cochlea and consequently are constructed in a manner to create or favor a primary current pathway out of the core of the cochlea and into the internal auditory meatus. This is most often achieved by anatomically placing the "remote" reference electrode at the base of the cochlea and/or within the internal meatus if the model includes this detail. Another technique used to favor basal cochlear outflow is to increase the ratio of bone to fluid resistivity in the model to increase current flow longitudinally down the cochlear spiral. The present study makes no such assumptions, and attempts to understand the current flow pathways due to various stimulation modes by using simple dipole models of empirically derived electrical fields.

This study is further motivated by certain shortcomings of the Nucleus surface potential study (Mens, Oostendorp, & van den Broek, 1994a), in which surface potentials were measured only at a single location on the scalp, namely at the ipsilateral mastoid, relative to the contralateral mastoid. Significant additional information may be gained by examining the pattern of potential distribution throughout the surface of the head. The present study maps these patterns by recording potentials at multiple locations on the surface of the head, scalp, and neck.

Another limitation that this study addresses is the assumption made in earlier studies that the inner ear represents a linear, resistive model. While this assumption was tested and

verified up to a frequency of 12.5 kHz, this study will extend this testing to 70 kHz given the higher frequency content of short duration current pulses used in contemporary cochlear implant devices.

3. METHODOLOGY - DIPOLE SOURCE LOCALIZATION

Dipole source localization, which is widely used in analyzing electroencephalography (EEG) and other event related potential (ERP) data, refers to the technique of estimating the location, strength, and orientation of the unknown bioelectric source that generates electrical potentials on the surface of the scalp. Several researchers (Lagerlund, 1999; Musha & Okamoto, 1999; Scherg, 1990) have provided a comprehensive review of EEG dipole source localizations techniques.

The electrical potentials are measured by attaching recording electrodes to the scalp. To solve for the unknown bioelectric source, a mathematical model of the head is constructed. A current source is placed in the head model and the resulting electrical potential distribution that would appear on the scalp is generated. This provides the solution to the *forward problem*. The estimation of the unknown bioelectric source that generates the measured potential distribution constitutes the *inverse problem.* The solution to the inverse problem is usually computed through a series of iterations during which the parameters of the bioelectrical source in the forward head model are varied until the difference between the modeled and measured potential data is minimized. This results in a bioelectric source that best fits as the generator source for the measured scalp electrical potentials. The bioelectric source is modeled as a dipole, which is described in Section 3.1.

In this study, inverse dipole source localization techniques are used in order to compute the dipole sources from surface potential data measured in cochlear implant

subjects, and test various hypotheses about current flow in the cochlea for the apical and basal electrode contacts within the cochlea.

3.1 The Dipole Source

A dipole, which is represented in Figure 3.1A, consists of a current source and sink. The source and sink are of opposite and equal strength I_0, and are separated by a distance d. The dipole vector represented in 3-D space is shown in Figure 3.1B. The dipole vector's direction is defined from the sink to the source. The maximum and minimum potential values of the dipole-generated field lie on either side of the dipole vector, depending on the orientation of the dipole. The dipole can be represented as (Malmivuo & Plonsey, 1995):

$$\vec{q} = I_o \vec{d} \tag{3.1}$$

where $\vec{q}$ = dipole moment

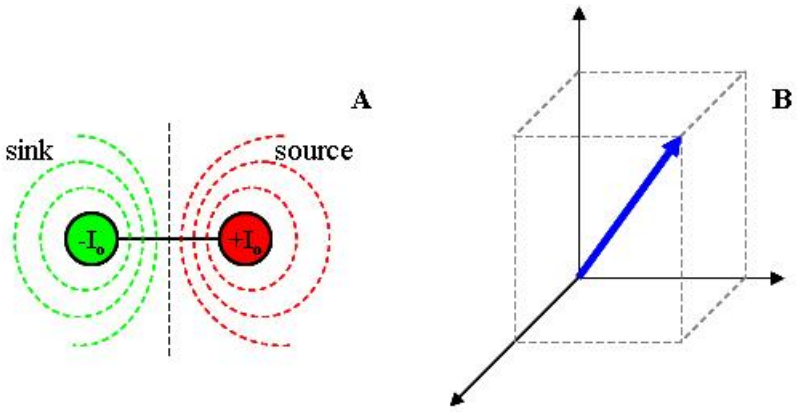

Figure 3.1: A - Dipole source and sink, B – Dipole vector in a 3-D space

Figure 3.2 represents a dipole source in an infinite, homogeneous space. The sink $-I_0$ lies at the origin and the source I_0 lies at a distance d. The field point r at which the potential is measured is located at *(x' y' z')*. Unit vectors $\vec{a}_r$ and $\vec{a}_z$ lie along the radius vector $\vec{r}$ and the Z axis respectively.

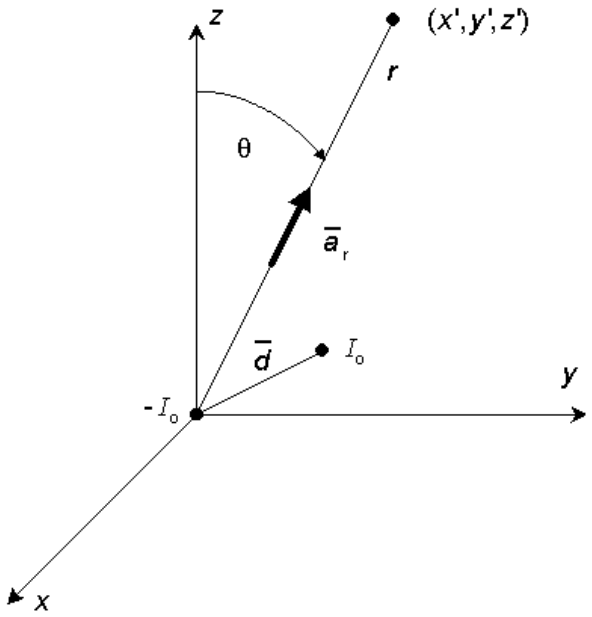

Figure 3.2: Dipole in an infinite space (from Malmivuo & Plonsey, 1995; Figure 8.1)

The potential field due to a dipole source in an infinite, homogeneous medium, whose moment q is defined in Equation (3.1), can be represented by the following equations (Malmivuo & Plonsey, 1995):

$$\phi_d = \frac{q}{4\pi\sigma}\frac{\vec{a}_r \cdot \vec{a}_z}{r^2} \tag{3.2}$$

$$\phi_d = \left(\frac{q}{4\pi\sigma}\right)\frac{\cos\theta}{r^2} \tag{3.3}$$

where ϕ_d = potential field

σ = conductivity of the medium

θ = polar angle that the Z axis makes with the radius vector

The model described by Equations (3.2) and (3.3) represents an infinite volume conductor. In comparison, spherical head models describe a bounded space. In this study, spherical models are used to solve the forward problem.

3.2 The Forward Problem

Using the head model to generate the electrical potentials on the surface of the head due to an internal bioelectric source constitutes the forward problem. Head models vary in terms of complexity of design. The simplest head model is represented by a single homogeneous sphere of uniform conductivity, which was first derived by researchers (Wilson & Bayley, 1950) to study the relationship between the electrical source and the generated electrical potentials in electrocardiogram (ECG) studies. Later, a more determinate form to calculate the potential in a homogeneous spherical volume was formulated (Brody, Terry, & Ideker, 1973). Because the homogeneous model is too simple and unrealistic, more accurate models such as the multilayer spherical head models are used widely.

In general, the multilayer heterogeneous spherical head model (Rush & Driscoll, 1969) consists of concentric shells, each shell representing regions of the head that have different conductivities such as the scalp, skull, cerebrospinal fluid (CSF), and brain. These

models are unrealistic in that they vastly oversimplify the anatomy of the head in making the basic assumption that the head is spherical in shape. However, the advantage of using spherical models when compared to more anatomically-realistic models is that the solution to the problem can be obtained analytically.

As noted in Chapter 2, more complex and realistically-shaped head models exist that are built using numerical techniques such as boundary element and finite-element analysis techniques. These numerical models are more accurate and can possibly better describe the surface potentials generated by dipole sources. However, in order to find the dipole that best fits as the generator source for the measured data, these forward computations need to be run several times. The initial approach in this study is to use simpler models such as the homogeneous and heterogeneous shell models to analyze the surface potential data. These models are described in more detail in subsequent sections. Future work may include the implementation of more complex models to explore hypotheses generated by the current work.

3.2.1 The Single Sphere Homogeneous Head Model

This homogeneous model is based on reformulated equations (Mosher, Leahy, & Lewis, 1999) of the Zhang homogeneous model (Zhang, 1995). The geometry for the homogenous model is provided in Figure. 3.3. Consider a spherical volume with center o of constant conductivity σ. The radius of the spherical volume r also represents the position on the surface of the head where the generated potential is measured. A dipole with moment q is located at r_q within the sphere. The angle between the dipole location r_q and the dipole moment q is α. The angle that the recording electrode makes with the dipole position is γ. The planes formed by q and r_q, and r_q and r are given by P1 and P2. The angle between P1

and P2 is β. The distance between r and r_q is d. The quantities r, q, and r_q are vectors that are represented in the Cartesian coordinate form.

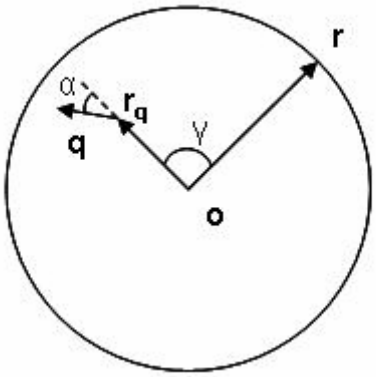

Figure 3.3: Homogeneous head model (after Mosher, Leahy, & Lewis, 1999; Figure 1)

The potential measured at r due to a dipole q at r_q for a homogeneous model is denoted $v^H(r; r_q, q)$ and is expressed as the sum of the potentials due to the radial component $v_r^H(r; r_q, q)$ and the tangential component $v_t^H(r; r_q, q)$. The superscript H denotes a homogeneous model, and the subscripts r and t represent the radial and tangential component, respectively. The equations representing the radial and tangential components are given by (Zhang, 1995):

$$v_r^H(r; r_q, q) = \left(\frac{q_r}{4\pi\sigma}\right)\left(\frac{2(r\cos\lambda - r_q)}{d^3} + \frac{1}{r_q d} - \frac{1}{r r_q}\right) \tag{3.4}$$

$$v_t^H(r;\, r_q,\, q) = \left(\frac{q_t}{4\pi\sigma}\right)\cos\beta\sin\gamma\left(\frac{2r}{d^3} + \frac{d+r}{rd(r - r_q\cos\gamma + d)}\right) \tag{3.5}$$

where $q_r = q\cos\alpha$ is the radial dipole intensity

$q_t = q\sin\alpha$ is the tangential dipole intensity

This model was further simplified (Mosher et al., 1999) by removing the transcendental functions and separating out the linear dipole moment q from the non-linear dipole location r_q. The equations then reduce to:

$$v_r^H(r;\, r_q,\, q) = c_1 r_q \cdot q \tag{3.6}$$

$$v_t^H(r;\, r_q,\, q) = (r_q^{\,2}(r\cdot q) - (r\cdot r_q)(r_q\cdot q))c_2 \tag{3.7}$$

where c_1 and c_2 are scalar coefficients, and $F(r,r_q)$ is a scalar function:

$$c_1 = \frac{1}{4\pi\sigma r_q}\left(2\frac{(d\cdot r_q)}{d^3} + \frac{1}{d} - \frac{1}{r}\right) \tag{3.8}$$

$$c_2 = \frac{1}{4\pi\sigma r_q^{\,2}}\left(\frac{2}{d^3} + \frac{d+r}{rF(r\cdot r_q)}\right) \tag{3.9}$$

$$F(r,r_q) = d\left(rd + r^2 - (r_q\cdot r)\right) \tag{3.10}$$

Finally, the closed-form solution to the homogeneous head model, which is a sum of the potentials due to the tangential and the radial components, is given by:

$$V^H(r;\, r_q,\, q) = v_r^h(r;\, r_q,\, q) + v_t^h(r;\, r_q,\, q) \tag{3.11}$$

$$\text{i.e. } v^H(r;\, r_q,\, q) = \left((c_1 - c_2(r\cdot r_q))r_q + c_2 r_q^{\,2} r\right)\cdot q \tag{3.12}$$

A thorough literature search for existing spherical models found few models such as this particular one that provided analytical solutions that are explained in detail. Another reason why this model was chosen is because the parameters of the dipole are unconstrained in nature compared to some other models in which dipoles are subject to fixed locations and/or orientations. In addition, this model provides a clear separation of the non-linear dipole location parameter r_q from the linear dipole moment parameter q, which simplifies the inverse calculation.

3.2.2 The Multiple Shell Heterogeneous Head Model

The multiple shell heterogeneous head model consists of nested concentric spheres that represent the scalp (skin), skull, cerebrospinal fluid (CSF), brain cavities, and etc. Rush and Driscoll (1969) provide a review of several such models that have been derived and tested.

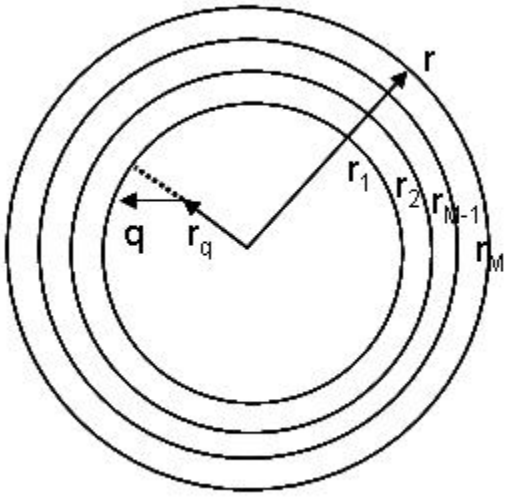

Figure 3.4: Multiple shell model (after Zhang, 1995; Figure 1)

As seen in Figure 3.4, the sphere has M layers or shells, each of whose conductivity is isotropic (i.e. the radial and tangential conductivities within each layer are equal). The conductivities for the shells starting from the innermost to the outermost shell are represented as $\sigma_1, \sigma_2, \ldots\ldots \sigma_M$, and the corresponding radii of the shells are $r_1, r_2, \ldots r_M$. The location at which the potential is measured is represented as r. The dipole q is geometrically similar to the dipole described in Section 3.2.1. The superscript M denotes a multilayer model. The potential generated at r due to a dipole q at r_q is denoted $v^M(r; r_q, q)$ and is expressed as (Zhang, 1995):

$$v^M(r;r_q,q) = \frac{q}{4\pi\sigma_M r^2}\sum_{n=1}^{\infty}\frac{2n+1}{n}\left(\frac{r_q}{r}\right)^{n-1}\cdot f_n\begin{pmatrix} n\cos\alpha P_n(\cos\gamma) \\ +\cos\beta\sin\alpha\cdot P_n^1(\cos\gamma)\end{pmatrix} \qquad (3.13)$$

where P_n^1 and P_n are the Legendre polynomials

n = number of Legendre terms

$$f_n = \frac{n}{nm_{22}+(1+n)m_{21}} \qquad (3.14)$$

Coefficients m_{22} and m_{21} are calculated from the following equation:

$$\begin{bmatrix} m_{11} & m_{12} \\ m_{21} & m_{22}\end{bmatrix} = \frac{1}{(2n+1)^{M-1}}\prod_{k=1}^{M-1}\begin{bmatrix} n+\dfrac{(n+1)\sigma_k}{\sigma_{k+1}} & (n+1)\left(\dfrac{\sigma_k}{\sigma_{k+1}}-1\right)\left(\dfrac{r}{r_k}\right)^{2n+1} \\ n\left(\dfrac{\sigma_k}{\sigma_{k+1}}-1\right)\left(\dfrac{r_k}{r}\right)^{2n+1} & (n+1)+\dfrac{n\sigma_k}{\sigma_{k+1}}\end{bmatrix} \qquad (3.15)$$

As shown above the solution in Equation (3.13) is in the form of an infinite series and contains several terms, thereby making the computation a slow process. Hence to improve the computational speed of the multilayer model, various approximations have been

developed (Ary, Klein, & Fender, 1981; Berg & Scherg, 1994; de Munck & Peters, 1993). Results from previous work (Ary et al., 1981) suggested that a simple homogeneous model could be used to calculate the potential in a 3-shell model after making adjustments for the eccentricity (i.e. the distance from the center of the sphere). Later studies (Zhang & Jewett, 1993) however showed that this approximation was inaccurate and produced errors.

In the present study, Zhang's *multilayer approximated head model* (Zhang, 1995) is used. This model is an extension of Zhang's homogeneous model, which was described earlier in Section 3.2.1. This model is based on Berg and Scherg's approximation (Berg & Scherg, 1994). Berg and Scherg (1994) determined that the potential distribution due to a single dipole in a multiple shell model could be described by scaling and summing the potentials due to three or more similar dipoles in a homogeneous model. Figure 3.5 provides a description of this approximation. The dipoles are chosen such that they are parallel to the original dipole. The corresponding angles of the parallel dipoles are at right angles to each other.

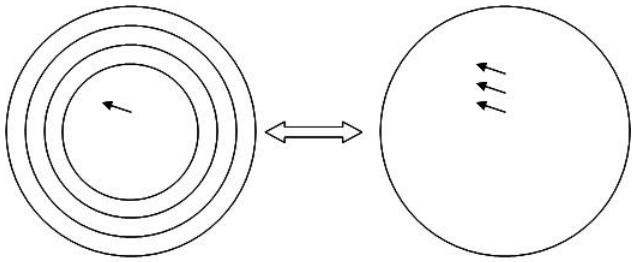

Figure 3.5: Berg and Scherg's approximation (after Berg and Scherg, 1994; Figure 1)

The potentials from the homogeneous model are multiplied by scaling factors and then summed. These scaling factors are referred to as the *Berg parameters*. These parameters could not be computed analytically; rather they were derived empirically. Berg and Scherg (1994) calculated the potential distribution due to a single dipole at 80% eccentricity using a 4-shell head model. The potential distributions for three suitably-located dipoles, which are parallel to the original dipole in the 4-shell model, were also computed using the homogeneous model. The data from the homogeneous model was then fitted to the data from the 4-shell model to determine the scaling factors. It was found that the scaling factors comprise three magnitude factors and three eccentricity factors. The eccentricity factors are linearly related to the original source's eccentricity, but the magnitude factors are independent of eccentricity. None of the Berg parameters are dependent on the orientation of the original dipole source.

The dipole moments for the new dipole sources are obtained by multiplying the original dipole source's moment q with the calculated Berg's magnitude factors. Likewise, locations for the new sources are computed by multiplying the original location r_q with the Berg eccentricity factors. The potential distributions for the new dipole sources are then computed using the homogeneous model in Equation (3.12). The homogeneous model is assumed to have the same radius and conductivity value as the outermost shell in the multiple shell model. Berg and Scherg's approximated multiple shell model can be represented as:

$$V^M(r; r_q, q) = \sum_{j=1}^{J} v^H(r; \mu_j r_q, \lambda_j q) \tag{3.16}$$

where J = number of new dipoles (usually 3)

μ = Berg eccentricity factor

λ= Berg magnitude factor

Zhang (1995) derived an analytical expression for these Berg factors. The weighting factor f_n, as given in Equation (3.14), is computed as a function only of the radii and conductivity values of the shells in the model. The Berg parameters are then determined by minimizing the following function Δ:

$$\Delta = \sum_{n=2}^{N_{\max}} \left[\left(\frac{r_1}{r_M} \right)^{n-1} \left(f_n - f_1 \mu_1^{n-1} - \sum_{j=2}^{J} \lambda_j (\mu_j^{n-1} - \mu_1^{n-1}) \right) \right]^2 \qquad (3.17)$$

where N_{max} = number of Legendre Series terms

This multiple shell model, like the homogeneous model discussed earlier, places no constraints on the orientation of the dipole, and separates the non-linear dipole location from the linear dipole moment. Furthermore, this method of approximation proved to be accurate and increased computing speed over 30 times compared to older multiple shell models.

3.3 The Inverse Solution

The goal of dipole source localization in this study is to find the equivalent dipole that generates a computed scalp potential distribution that best approximates a measured and/or known scalp potential distribution. Basically, there are only a limited number of recording locations at which scalp potentials are usually recorded. Also noise, artifacts, and processing errors often contaminate the signal of interest. Thus the inverse problem does not necessarily have a unique solution and more than one source may fit as the estimated generator source

for a particular potential distribution. Thus it is necessary to constrain the source model based on some a *priori* information about the dipole source.

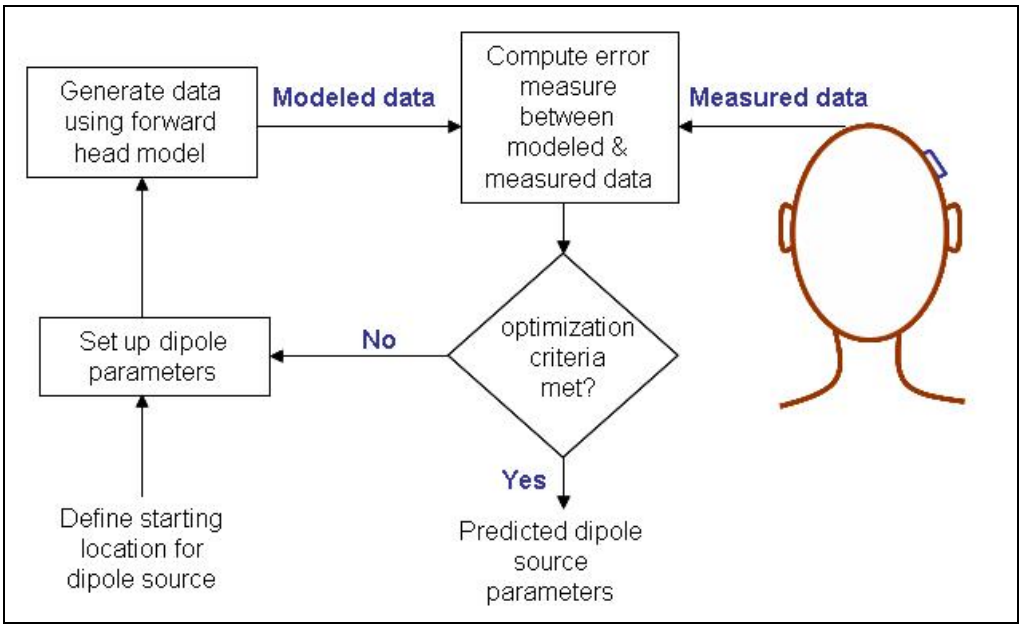

Figure 3.6: Flowchart for inverse problem

The general technique in solving this inverse problem is to find the best fit between the measured and modeled data. The flowchart for this process is described in Figure 3.6. The modeled data is generated by the use of appropriate head models which are discussed in Section 3.2. A starting condition is first defined for the dipole source, and the estimated dipole is placed in the forward model. The following are the six parameters that define the dipole source: the spatial coordinates *x, y*, and *z* that represent the 3-dimensional location of the dipole in the Cartesian coordinate system, and the dipole moment vectors q_x, q_y, and q_z that define the orientation along the three axes X, Y, and Z, respectively. The best fit

between the modeled and measured data is found by varying the parameters of the estimated dipole source until the difference between the modeled and measured data sets (the error measure) is minimum. The model-generated and measured data sets correspond to the same locations on the surface of the head. The error measure is usually computed as the sum of the squares of differences between the modeled and measured potential values at the respective recording locations on the scalp and face (Scherg, 1990).

The inverse problem is usually solved using a non-linear least square fitting process (Lagerlund, 1999). This fitting process, however, is sensitive to a number of factors such as noise, artifacts, starting location for the estimated dipole source, etc. (Lagerlund, 1999), which may result in estimating the dipole based on a local minimum value rather than a global minimum error measure. Because of these limitations, the inverse model used in this study is based on a faster and improved method. Salu's approach (Salu & Mehrotra, 1984; Salu et al., 1990) uses a combination of linear and non-linear fitting methods. Basically the dipole moments q_x, q_y, and q_z are determined using a linear approach, and the spatial coordinates *x, y*, and *z* are found using a non-linear fitting process. *Optimal dipoles* are first found for the measured data. An optimal dipole is one whose orientation causes it to describe the generated data better than any other dipole placed at that very location. The orientation parameters of the optimal dipole at a particular location $i = (x_i\ y_i\ z_i)$ are represented as P_x, P_y, and P_z. The voltage generated at *j* by the optimal dipole located at *i* is expressed as V_j and is a function of transfer coefficients T_{xij}, T_{yij}, and T_{zij}. Transfer coefficients T_{xij}, T_{yij}, and T_{zij} basically represent the potential distribution generated at *j* by three unit dipoles located at *i* and oriented along the positive X, Y, and Z directions respectively. The equation describing this relation is:

$$V_j = P_x \cdot T_{xij} + P_y \cdot T_{yij} + P_z \cdot T_{zij} \tag{3.18}$$

The transfer coefficients for the multiple shell head model are found from Equation (3.16). The dipole parameters P_x, P_y, and P_z are then calculated by minimizing the error measure S which is the sum of the squares of differences between the potential distribution generated by the optimal dipole and the measured potential values Fj at the recording location j.

$$S = \sum_{j=1}^{J} \left(P_x \cdot T_{xij} + P_y \cdot T_{yij} + P_z \cdot T_{zij} - F_j \right)^2 \tag{3.19}$$

where J = total number of recording locations

Equation (3.19) represents a linear least squares problem. After all the optimal dipoles are found for the specified locations i, the *equivalent dipole* is found as the optimal dipole with the least error. The error function is checked to confirm that the smallest error is actually a global minimum value rather than a local minimum value. The equivalent dipole may be found in several different ways. Often, optimal dipoles are first found in a small search region. Then, the search region is redefined based on the error function, and new optimal dipoles are found. This process is repeated until the best optimal dipole is found. However, if there is some prior knowledge about where the dipole may exist, the search region is defined as a dense grid in the vicinity of the dipole's location, and the best optimal dipole in that search region is found to be the equivalent dipole.

3.4 Model Implementation

In this section, the implementation of the forward and inverse models used in this study is described in detail. These models are implemented using software tools written in MatLab (The MathWorks Inc., Natick, MA, USA).

3.4.1 The Forward Model

This study uses the multiple shell heterogeneous head model that is described in Section 3.2.2. The head model consists of 4 shells that represent the skin, skull, CSF, and brain compartments. The radii of these shells are estimated based on the radius of the head in each subject. Ferree and colleagues (Ferree, Eriksen, & Tucker, 2000) provide a summary of the conductivity values of head tissue obtained experimentally (Baumann, Wozny, Kelly, & Meno, 1997; Burger & van Milaan, 1943; Geddes & Baker, 1967; Law, 1993). The mean conductivity values for each tissue type are presented in Table 3.1, and these values are used in this study.

Table 3.1: Head tissue conductivity values (after Ferree et al., 2000)

Tissue Type	Mean Conductivity $(\Omega m)^{-1}$
Brain	0.25
CSF	1.79
Skull	0.018
Scalp	0.44

The following are the inputs provided to the forward head model in order to compute the potential distribution in Equation (3.16): (1) the spatial coordinates of the recording electrode locations, (2) the radius of the head, (3) the location and moment of the dipole.

3.4.1.1 Inputs to the Model

The spatial coordinates of the recording sites are measured using a 3-D digitizer. The complete protocol followed in defining and measuring the locations on the scalp and face is discussed in Chapter 4. The recorded spatial coordinates are expressed in terms of the *digitizer coordinate* system, which is referenced to the base of the digitizer system. Data are collected during multiple short sessions, during which the subject maintains a constant head position. Reference markers are placed on three locations (the left and right auditory meatuses A_L and A_R respectively, and the center midline C_z) on the subject's head to establish a reference frame by which recording site coordinates are related across sessions and head positions. The coordinates in the digitizer coordinate system are transformed to the *head coordinate system* using an affine transformation routine, which involves both rotation and translation of the digitizer coordinate system. The positive X axis of the head coordinate system is directed towards the right external auditory meatus A_R while the positive Y axis extends from the origin (center of the head) towards the nasion, as shown in Figure 3.7. The positive Z axis is towards C_z at the top of the head.

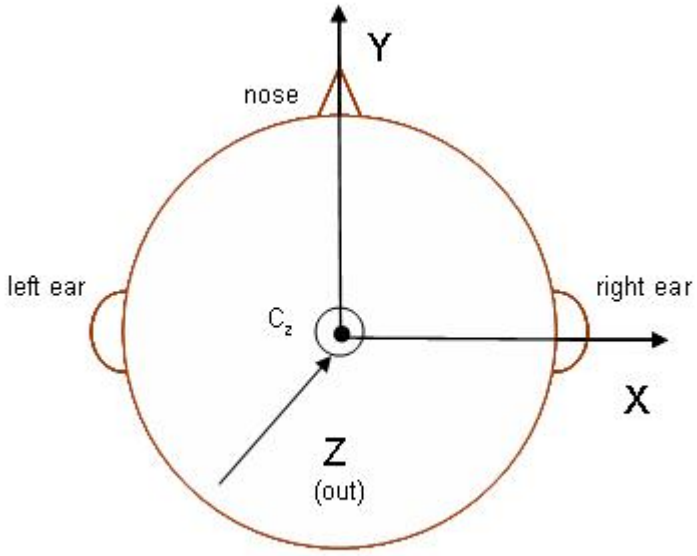

Figure 3.7: Head coordinate system

Reference points C_z, A_L, and A_R are denoted P_0, P_1, and P_2 respectively. The origin of the head coordinate system, $o_h = (x_0\ y_0\ z_0)$, is defined as the midpoint of the line segment connecting *P1* and *P2*. X_h, Y_h, and Z_h represent the X, Y, and Z axes of the head coordinate system. A perpendicular line from the origin pointing towards P_0 defines the direction of Z_h. The vector from o_h to P_2 defines the direction of X_h. The vector normal to the plane containing P_0, P_1, and P_2 represents Y_h. The vectors that represent the X_h, Y_h, and Z_h axes are normalized into unit vectors *i'*, *j'*, and *k'* respectively. The origin of the digitizer coordinate system is represented as $o_d = (0\ 0\ 0)$. X_d Y_d, and Z_d represent the X, Y, and Z axes of the digitizer coordinate system. The unit vectors for the X_d Y_d, and Z_d axes are $i = (1\ 0\ 0)$, $j = (0\ 1\ 0)$, and $k = (0\ 0\ 1)$ respectively.

The affine transformation (Youngworth, Bates, Romero, & Aronstein, 2005), which is used to convert the coordinates from the digitizer coordinate system $(X_d\ Y_d\ Z_d)$ to the head coordinate system $(X_h\ Y_h\ Z_h)$, is represented as:

$$X_h = l_{11}(X_d - x_0) + l_{12}(Y_d - y_0) + l_{13}(Z_d - z_0) \tag{3.20}$$

$$Y_h = l_{21}(X_d - x_0) + l_{22}(Y_d - y_0) + l_{23}(Z_d - z_0) \tag{3.21}$$

$$Z_h = l_{31}(X_d - x_0) + l_{32}(Y_d - y_0) + l_{33}(Z_d - z_0) \tag{3.22}$$

where position vectors $l_{11}, l_{12}, l_{13}, l_{21}, l_{22}, l_{23}, l_{31}, l_{32}, l_{33}$ are defined as:

$$l_{11} = i \cdot i' \tag{3.23}$$

$$l_{12} = j \cdot i' \tag{3.24}$$

$$l_{13} = k \cdot i' \tag{3.25}$$

$$l_{21} = i \cdot j' \tag{3.26}$$

$$l_{22} = j \cdot j' \tag{3.27}$$

$$l_{23} = k \cdot j' \tag{3.28}$$

$$l_{31} = i \cdot k' \tag{3.29}$$

$$l_{32} = j \cdot k' \tag{3.30}$$

$$l_{33} = k \cdot k' \tag{3.31}$$

The spatial coordinates of the recording locations which are expressed in terms of the head coordinate system are then projected to the surface of a sphere whose radius r is approximately equal to the radius of the subject's head. This further transformation from a

realistic head surface to a spherical head surface is necessary because a spherical model is used to interpret the surface potential data. First, the coordinates from the Cartesian form *(x y z)* are converted to a spherical coordinate system ($r\ \varphi\ \theta$):

$$\theta = \tan^{-1}\left(\frac{y}{x}\right) \tag{3.32}$$

$$\phi = \tan^{-1}\left(\frac{\sqrt{x^2 + y^2}}{z}\right) \tag{3.33}$$

Then, the spherical coordinates are transformed back to the Cartesian system, using the value of r which equals the approximate radius of the subject's head, using the following relations:

$$x = r\sin\phi\cos\theta \tag{3.34}$$

$$y = r\sin\phi\sin\theta \tag{3.35}$$

$$z = r\cos\phi \tag{3.36}$$

Because the head is not spherical in nature, the radius of the head r is an approximate value. It is computed as the mean of the distances between the extremities of the head surface, along the X_h, Y_h, and Z_h axes. The vectors representing the location and moment of the dipole source are provided to the model in Cartesian coordinate form. The model makes certain assumptions about the dipole source, which are discussed in the subsequent section.

3.4.1.2 Cochlea Model

This section describes how the location of the cochlea within the subject's head may be estimated. The spatial locations for the intracochlear electrode contacts vary from subject to subject, but can be approximated based on existing computed tomography (CT) imaging data. These spatial coordinates for the stimulating electrode contacts are obtained in the *cochlear coordinate system* and then transformed to the *head coordinate system*. The head coordinate system is described in Section 3.4.1.1. Figure 3.8 represents the geometry of the right cochlea related to the head, in which basically, the subject's head is rotated to obtain the "cochlear view" (Xu, Cohen, & Clark, 2000). X_c, Y_c, and Z_c represent the axes in the cochlea coordinate system, while X_h, Y_h, and Z_h represent those in the head coordinate system. The origin of the cochlear coordinate system o_c lies on the base of the mid-modiolar axis. The origin o_c lies on the same transverse plane as the head coordinate system and is located approximately mid-way between the head coordinate system's origin o_h and the positive end of X_h, and can be represented as $(x_0\ y_0\ z_0)$, when referenced to the head coordinate system. The mid-modiolar axis is tilted 10° downward from the transverse plane. The angle between X_c and X_h is $C = (90° - A)$, and A is found to have a mean value of 52.5° (Xu et al., 2000).

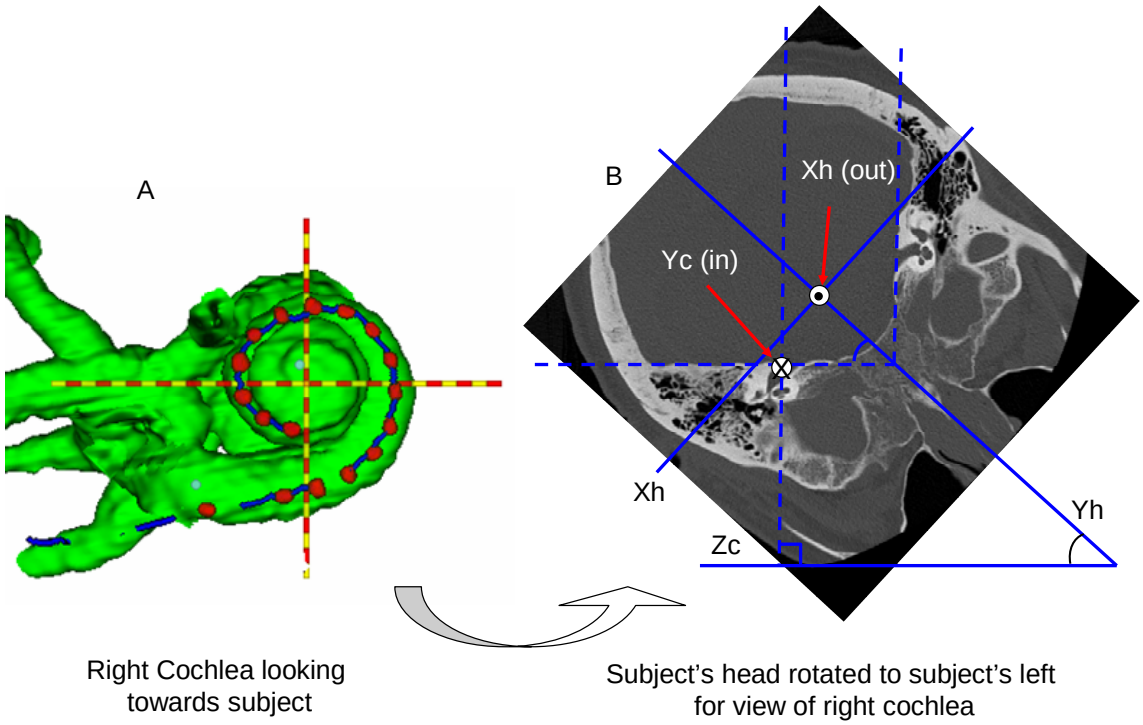

Figure 3.8: Geometry of right cochlea (Panel B after Xu et al., 2000; Figure 1B)

The following transformation equations (Youngworth, Bates, Romero, & Aronstein, 2005), which use Euler's angular rotations, are used to convert the spatial coordinates for the electrode contacts from the cochlear coordinate system $(x_c\ y_c\ z_c)$ to the head coordinate system $(x_h\ y_h\ z_h)$:

$$x_h = x_0 + x_c \cos\gamma - \left(y_c \cos\delta + z_c \sin\delta\right)\sin\gamma \tag{3.37}$$

$$y_h = y_0 + x_c \sin\gamma + \left(y_c \cos\delta + z_c \sin\delta\right)\cos\gamma \tag{3.38}$$

$$z_h = z_0 + z_c \cos\delta - y_c \sin\delta \tag{3.39}$$

where $\gamma = C$, i.e. the angle between X_h and X_h

δ = angle between Z_h and Z_c

3.4.1.3 Model Assumptions

The dipole source provides the stimulus to the cochlea. Basically, two modes of stimulation exist. In the bipolar mode of stimulation, the two intracochlear electrodes that are being stimulated within the cochlea represent the source and the sink of the dipole source that are closely-spaced. In the monopolar mode of stimulation, the intracochlear stimulating electrode and the remote reference electrode form the dipole, in which the source and the sink are relatively widely-spaced.

Spherical models are primarily built for the analyses of EEG and ERP data, wherein the source of the generated potentials lies completely in the innermost shell (brain compartment). Hence, the dipole source in the multiple shell model is assumed to lie in the innermost shell. For the bipolar mode of stimulation, this assumption holds true because both the source and the sink lie in the same compartment (i.e. the innermost "brain" shell). However, in the monopolar mode, the dipole source is unique; the remote reference electrode usually lies in the third shell, which is the bone compartment, and the stimulating electrode lies in the innermost (first) shell.

When the dipole lies in a layer k other than the innermost layer, the r_1 term in Equation (3.17) is replaced by r_k, the radius of the shell in which the dipole lies, such that $r_{k-1} < r_d < r_k$ (Zhang, 1995), where r_d represents the length of the dipole. The minimization function Δ is thus modified as follows:

$$\Delta = \sum_{n=2}^{N_{\max}} \left[\left(\frac{rk}{r_M} \right)^{n-1} \left(f_n - f_1 \mu_1^{n-1} - \sum_{j=2}^{J} \lambda_j (\mu_j^{n-1} - \mu_1^{n-1}) \right) \right]^2 \tag{3.40}$$

Using the principle of superposition, the large dipole *d* that spans across three different layers in the case of monopolar stimulation is split into smaller dipoles d_{brain}, d_{CSF}, and d_{bone}, which represent the constituent dipoles in the brain, CSF, and bone compartments respectively. The potential distribution due to each of these small dipoles is computed, using the multiple shell model. The values of *k* substituted in Equation (3.37) for d_{brain}, d_{CSF}, and d_{bone}, are 1, 2, and 3 respectively. The potentials are summed, and denoted V_{sum}. The potential distribution V_d generated by the large dipole *d* is also computed using the multiple shell model. The Berg parameters for *d* are computed from Equation (3.17), by setting $k = 1$. In the strictest sense, *k* is not equal to 1, because the dipole *d* spans across three layers. However, since the model does not cover this special case, a value of $k = 1$ is assumed. The validity of this assumption is then tested in the following manner. The potential distributions V_d and V_{sum} are compared over a wide range of recording locations on the scalp. Differences between V_d and V_{sum} are negligible at most locations. Significant differences between V_d and V_{sum} are observed in the region surrounding the return electrode location. This experiment was then repeated using the homogeneous model, which produced similar results as seen before with the multiple shell model. Significant differences between the potentials V_d and V_{sum} still occurred in the regions surrounding the return electrode. The observation of these differences in both the homogeneous and multiple shell model suggests that that these differences are most likely due to the geometry of the head and/or the violation of the basic principle in the dipole model that the source and sink are close to each other, rather than due

to inaccuracies resulting from the assumption made in the multiple shell model (i.e. setting $k = 1$). The assumption of $k = 1$ in the computation of the Berg parameters (Equation 5.17) is thus reasonable for the multiple shell model.

3.4.2 The Inverse Problem

The inverse problem is solved by determining the set of dipole parameters that generate potentials which most closely match the potential distribution measured on the scalp surface in a cochlear implant subject. The forward multiple shell model is used to generate these potentials. The *search region* defines the source locations within the head model where dipoles are placed.

3.4.2.1 Defining the Search Region

Basically, the two forms of data to be analyzed include the monopolar potential data, which is generated as a result of stimulation applied between the remote reference electrode and an intracochlear electrode, and the bipolar potential data, in which stimulus current flows between two intracochlear electrode contacts. In this model, the following conventions are used to define the source and the sink for these two dipole conditions: (1) for monopolar data, the remote reference electrode represents the source, and the intracochlear electrode represents the sink, and (2) for bipolar data, each intracochlear electrode represents either the source or the sink.

For each monopolar stimulus condition, the orientation of the dipole rotates as the location of the stimulated electrode contact changes along the basilar membrane in the cochlea. The reference electrode, which is the source of the dipole in the monopolar mode, has a fixed location, while the location of the sink varies across stimulus conditions. The

spatial coordinates of the reference electrode (also referred to as return electrode) are measured using the 3-D digitizer. This is further verified using the model by *searching* in the vicinity of the recorded location of the return electrode for the source of the dipole that provides the best fit to the data. The search region is thus reduced to a single location corresponding to the location of the reference electrode.

In the bipolar mode, neither the source nor the sink has a fixed location; they constantly vary depending on the pair of electrode contacts being stimulated. Thus the search region is mostly undefined and bounded only by the limits of the spherical head. The search region is expressed as an nx3 matrix, where the three columns represent the X, Y, and Z coordinates, and each row represents a possible source location. Once the general region for the possible source location is identified, the search region is redefined and the process is repeated.

3.4.2.2 Estimating the Optimal Dipoles

After the search region is defined, optimal dipoles are generated at each location, as given in Equation (3.18). The potentials generated by the optimal dipoles are computed from Equation (3.16). The model-generated potentials are referenced to a specific location on the surface of the head, depending on the location of the reference recording electrode (negative) in the differential amplifier measurement.

3.4.2.3 Least Squares Fitting

The equivalent dipole is found as the optimal dipole with the least error. The error function is defined as the sum of squares of differences between the measured potential data and the model-generated data on a location-by-location basis across all recording positions.

Equation (3.19), which represents this linear least squares problem, is solved using the Least Squares Curve Fitting Optimization Toolbox in MatLab (The MathWorks Inc., Natick, MA, USA). The large scale optimization algorithm, which is a subspace trust region method based on the interior-reflective Newton method (Coleman and Li, 1996 and 1994), is used. This particular algorithm is chosen because it is robust in nature. Also, it allows bounded constraints to be set. These bounded constraints enable the search region to be defined within the boundary limits of the head surface. Figures 3.9, 3.10, and 3.11 represent the error measures plotted as a function of dipole location along X, Y, and Z axis respectively.

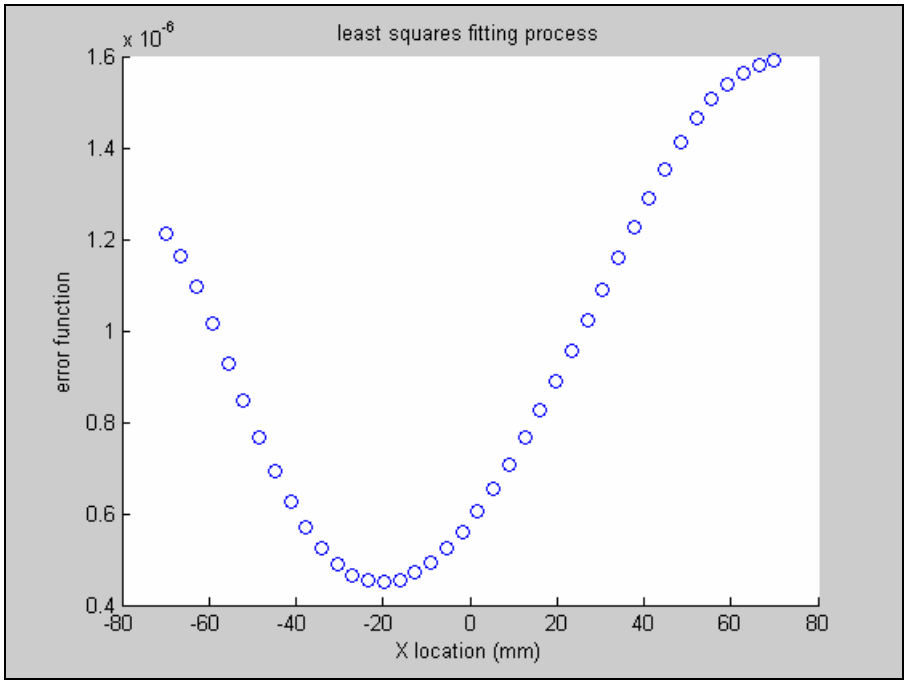

Figure 3.9: Least Squares fitting process – error vs. dipole X location

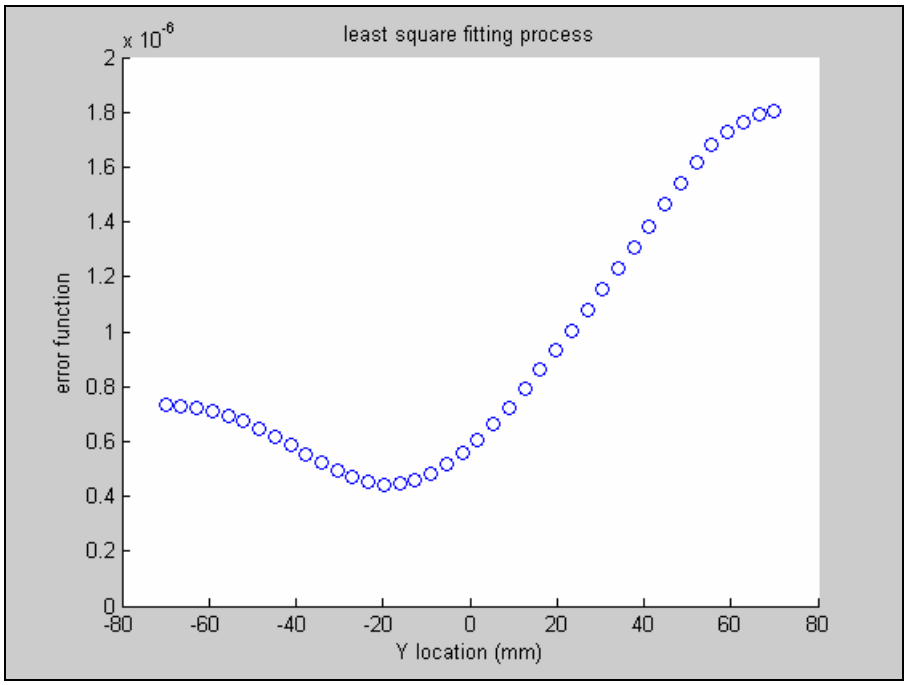

Figure 3.10: Least Squares fitting process – error vs. dipole's Y location

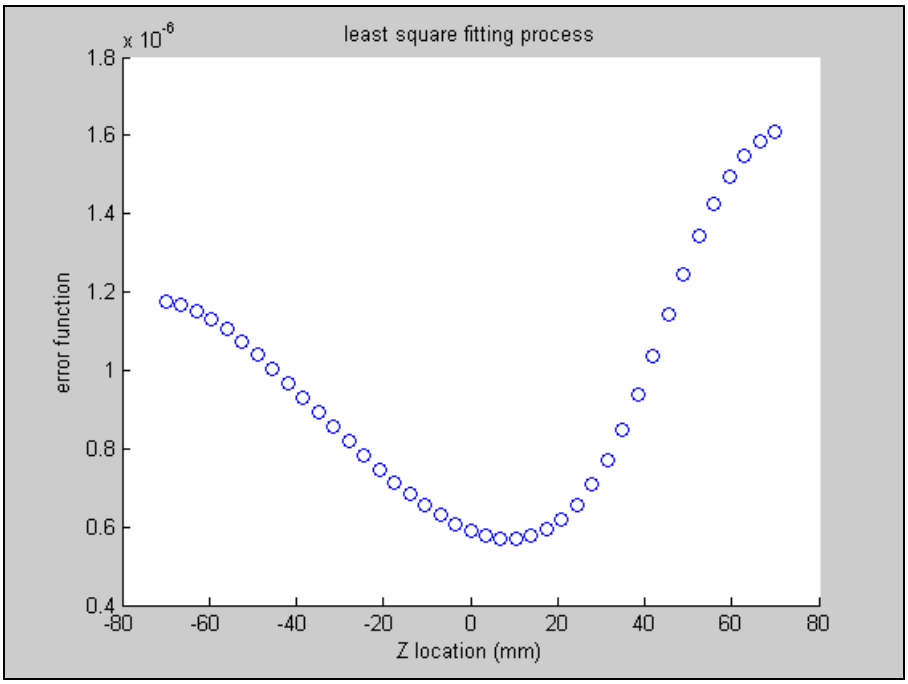

Figure 3.11: Least Squares fitting process – error vs. dipole's Z location

The Least Squares Curve Fitting model is defined such that the values chosen for the number of iterations and termination tolerance are conservative in nature. Figures 3.12 and 3.13 show the error function plotted as a function of the dipole location along the X axis for two different values of termination tolerance for the same set of data. The termination tolerance values in Figures 3.12 and 3.13 are set to be 0.6e-6 and 1e-9 respectively. It can be seen that a more conservative value (Figure 3.13) produces a smoother curve without any occurrences of local minima in comparison to the previous plot (Figure 3.12).

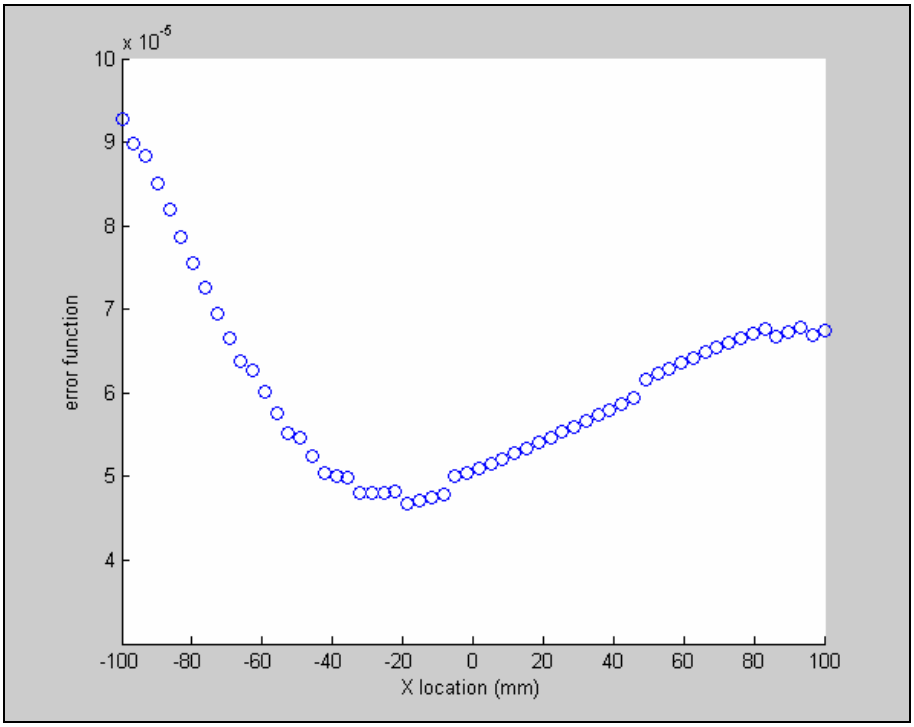

Figure 3.12: Least Square Fitting Process with a termination tolerance value = 0.6e-6

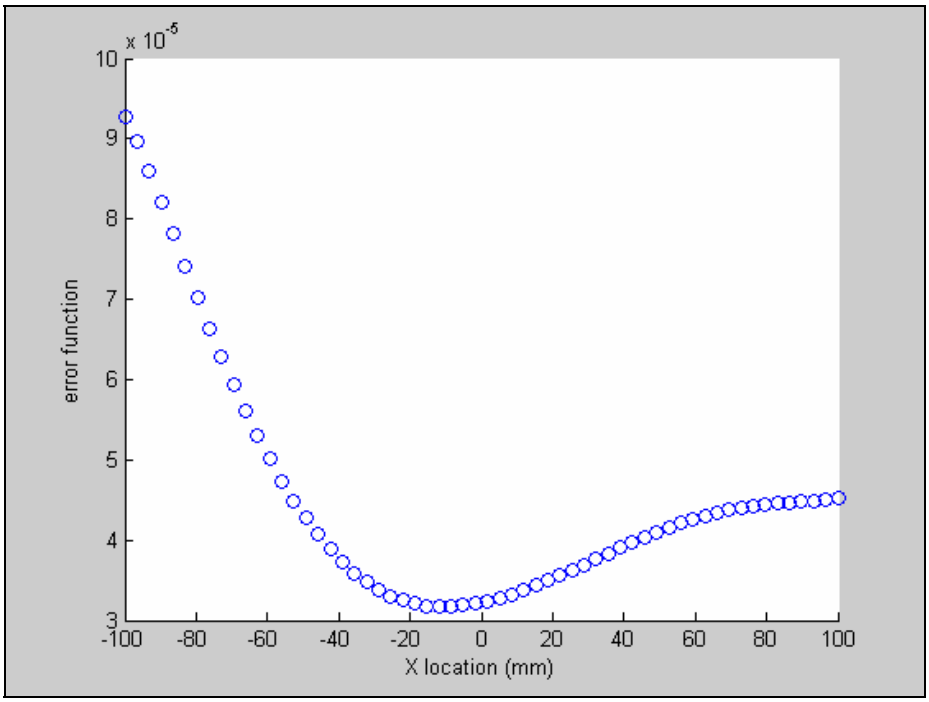

Figure 3.13: Least Square Fitting Process with termination tolerance value = 1e-9

4. METHODOLOGY – DATA COLLECTION

In this chapter, the procedures followed in the collection of data are described. A brief description of the subjects recruited is provided. The study protocol and the instrumentation used in collecting data are explained in detail. Data analyses methods used in this study are also presented.

4.1 Subjects

A total number of 9 subjects participated in this study, as shown in Table 4.1. This includes 6 subjects with cochlear implants, and 3 normal, non-implanted subjects. Informed consent was obtained from the subjects prior to the testing process. Copies of the informed consent forms are provided in Appendix A. This study was approved by the University of North Carolina at Chapel Hill (UNC-CH) Biomedical Institutional Review Board (Study #05-2243).

Only English-speaking adult subjects were recruited for this study. Subjects were not included or excluded from the study based on gender, ethnicity, or race. Subjects that were unable to sit still for ten minutes at a time were not recruited in this study. Prospective cochlear implant subjects were identified through the UNC-CH Ear, Nose, and Throat (ENT) clinic database and contacted by qualified personnel from the clinic. Non-implanted subjects were recruited and contacted directly by personal contact.

Table 4.1: Subjects

Subject	Type of device	No. of electrodes	M/F	Age	Stimuli phase width (μs)	Stimuli p-p amplitude (μA)
S1	Clarion HighRes 90K	16	M	80's	50	210
S2	Clarion HighRes 90K	16	F	20's	50	280
S3	Clarion HighRes CII	16 (10-12 inactive)	M	50's	32	207
S4	Clarion HighRes 90K	16	M	60's	32	140
S5	Clarion HighRes 90K	16	F	40's	32	56
S6	Nucleus Freedom CI24RE	22 (1-2 inactive)	M	20's	60	298 357
N1	Non-implanted	N/A	F	20's	N/A	20
N2	Non-implanted	N/A	M	50's	N/A	20
N3	Non-implanted	N/A	M	30's	N/A	20

4.2 Experimental Procedures

This section explains the general protocol followed in this study in obtaining the following measures:

1. Surface artifact potential measures from the scalp and face during intracochlear electrode stimulation in cochlear implant subjects.
2. Intracochlear electrical field measures using on-board telemetry capabilities from cochlear implant subjects.

3. Impedance measures due to externally-applied current at selected sites on the surface of the head in cochlear implant subjects and normal, non-implanted subjects.
4. Measures to determine the shape of the head in subjects.

4.2.1 Surface Potential Measures

Surface artifact potentials are recorded while the subject's implant device stimulates in a safe and comfortable manner. Data are collected during two sessions, during which the subject maintains a constant, relaxed postural position. Potential measures and the corresponding spatial coordinates are obtained from multiple sites on the face and scalp using a 3D-digitizing device to which an electrode probe is attached. A custom-designed, bio-potential amplifier is used to amplify the signal measured by the probe tip relative to a surface reference electrode placed on the back of the neck at the midline position. The instrumentation details of the various components used in the data collection process are explained in Section 4.3.

The general protocol is as follows. Reference points are first marked on each tragus, which is the small projection in front of the external auditory meatus, and at two midline locations on the apex of the head separated by 4 to 5 cm., denoted as "C_z front" and "C_z back", respectively. These landmarks are defined on the head to establish a reference frame by which recording site coordinates are related across sessions and head positions. Individual landmarks are marked by making a small (2-3 mm diameter) dot on the skin with an indelible marker. Due to the presence of body oils these marks are easily removed at the end of data collection with an alcohol wipe.

The stimulation is provided by the manufacturer's programming software which runs off a laptop and interfaces to the clinical programming interface (CPI) through a serial port.

This set-up, the block diagram of which is provided in Figure 4.1, is similar to that which is used during the clinical fitting of the system. The CPI connects to the speech processor which in turn transmits information to the subject's implant via the headpiece. The stimuli consist of biphasic pulses comprising both monopolar and bipolar electrode combinations. Stimulus levels and phase durations are fixed such that the subject does not hear sounds that are louder than a comfortable listening level. An external trigger signal that is synchronous with the presentation of the stimuli is generated by the CPI to facilitate recording and averaging of multiple stimulus trials by other hardware/software.

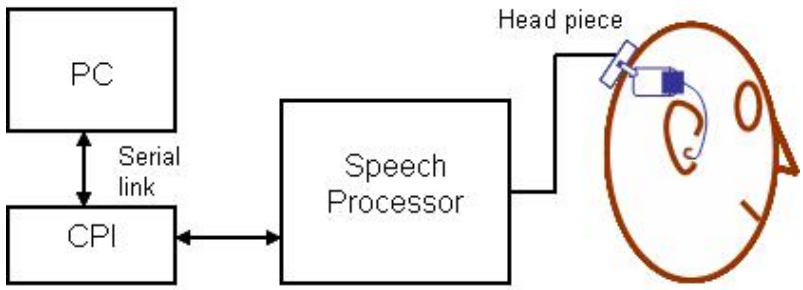

Figure 4.1: Stimulation set-up

The recording set-up is illustrated in Figure 4.2. Surface, paste-on recording electrodes are placed on the following locations after cleaning these regions with rubbing alcohol: back of the neck at the midline (negative/reference), collar bone contralateral to the implanted device (ground), and the mastoid ipsilateral to the implant (positive). Using the surface recording electrodes, the quality of the electrical potential is measured. The impedance of these recording locations is also checked to make sure that it is within limits.

The active (positive) surface recording electrode is then switched out for the recording electrode probe which features a blunt cotton wick that is continuously kept moistened by a saline-drip flow mechanism. The probe is electrically and mechanically designed to allow recording of potentials by simply touching the probe tip to the scalp without traditional scalp preparation such as cleaning or abrading the skin to reduce interface impedances.

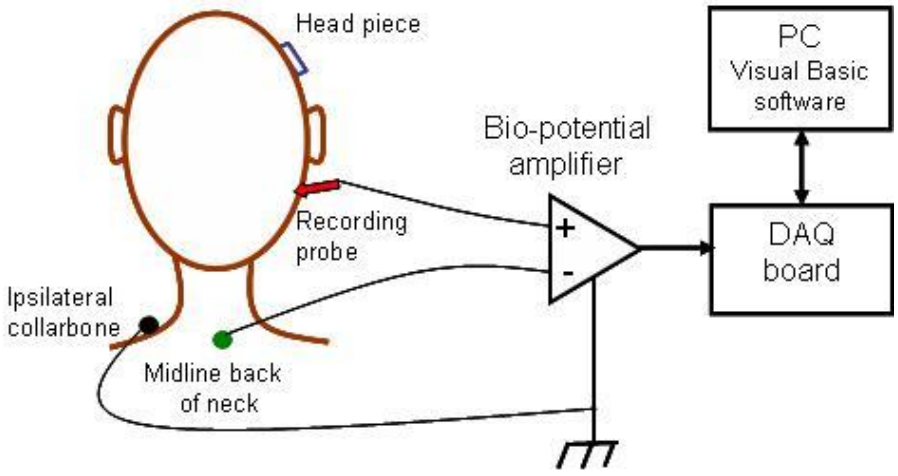

Figure 4.2: Recording set-up

A 3-D digitizer is used to record the spatial coordinates of the surface potential recording location. A full description of the digitizer system in included in Section 4.3.2. The digitizer is first powered on in the *home position* with the standard default tip in place. The home position is described in detail in Section 4.3. This enables the digitizer to self-calibrate. The default tip is then replaced by the custom electrode probe tip. The probe in conjunction with the 3D-digitizer enables rapid and accurate recording of surface potentials on a very fine spatial grid where potentials are changing rapidly.

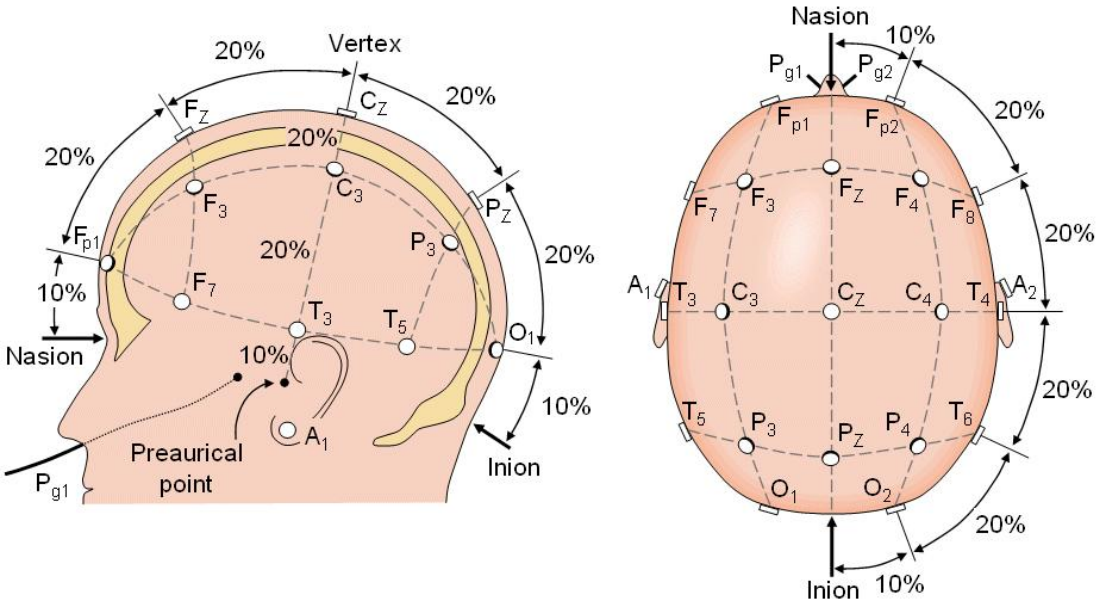

Figure 4.3: The International 10-20 System – left side and top side view (from Malmivuo and Plonsey, 1995; Figure 13.2)

The choice of locations on the scalp and face where potentials are measured is ad-hoc in nature and varies across subjects; however in general the *International 10-20 Recording System* (Chatrian, Lettich, & Nelson, 1985; Jasper, 1958; Oostenveld & Praamstra, 2001) is followed. The 10-20 System, which is represented in Figure 4.3, is a standardized electrode placement map primarily used in the analysis of electroencephalography (EEG) signals, which defines locations on the scalp surface at which surface potential measurements are made. The recording sites are located at 10% and 20% intervals on the top contour surface of the head. C_z marks the location at the center of the midline of the head. Locations on the left sagittal plane are odd-numbered while those on the right sagittal plane are even-numbered. *Fp*, *F*, *C*, *P*, *O*, and *T* signify the frontal pole, frontal, central, parietal, and occipital cortical areas respectively that correspond to the electrode locations. In addition to these standard sites located over the cranium, artifact potentials are also recorded for locations on the face,

neck, and in the vicinity of the ear. These sites include: locations in the forehead, eyebrow, cheek, and jaw line regions, tip of the nose, mastoid, ear lobe, edges of the pinna, and etc.

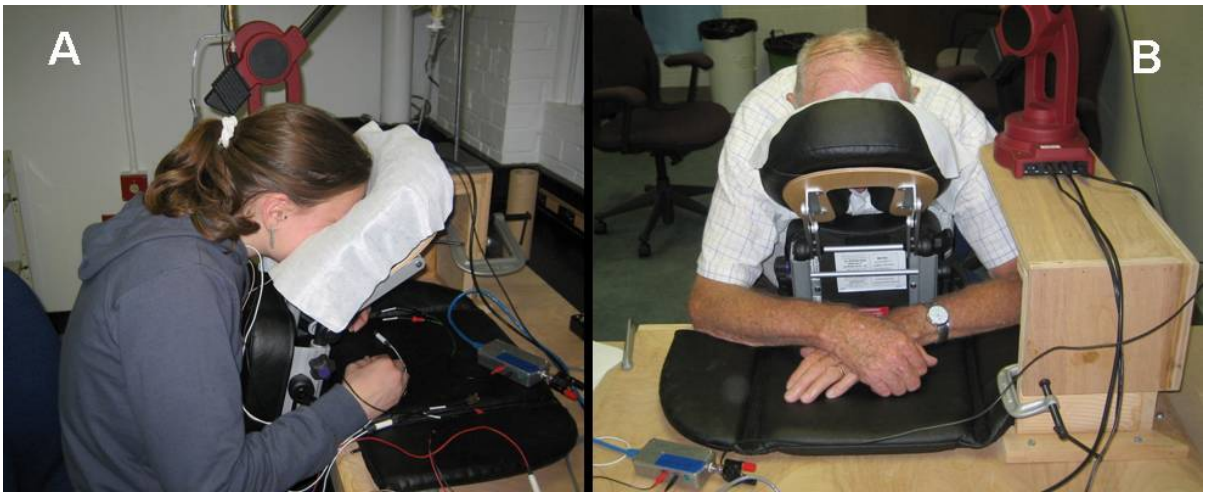

Figure 4.4: Face down position - (A) right side view of subject and (B) front side view of subject

Data collection is carried out in two basic sessions. First, the subject is placed in the face down position. The subject is aided in maintaining a stable head position by gently resting their face (face down) on a head support similar to that used in a therapeutic massage session, as shown in Figure 4.4 (A and B). Panel A in Figure 4.4 shows the right side view of a subject in the face down position. Panel B shows the front side view of another subject in the same position. The subjects are encouraged to relax their shoulders and place their arms on the padded arm rest in front of them. In this position, data are collected from the back and side of the head. The date collection process starts and ends with following four reference locations: C_z front, C_z back, left and right tragi. For each recording location on the

head, all experimental stimulus conditions are presented sequentially, and the corresponding electrical artifact signal and the x, y, and z location coordinates are recorded before moving on to another location on the head.

Figure 4.5: Face up position

The subject is allowed to relax and/or move about between sessions depending on the subject's choice. During the second session, the subject leans backwards into a headrest, as shown in Figure 4.5. This position enables the collection of data on the face. Again, data are collected from the four reference locations at the beginning and the end of the second session. If the subject wishes to take a break during a particular session, they can do so and the reference locations are again measured. The location of the left tragus reference is also visible in Figure 4.5.

The surface potential data is sampled synchronously at a high rate and averaged over 400 trials before being saved for off-line analysis. The resultant output file for each stimulus condition and location on the head consists of a single averaged frame that represents information across all the electrodes of the implanted device, as well as the spatial coordinates for the specific location.

4.2.2 Intracochlear Electrical Field Measures

Intracochlear electrical field measures are obtained by sending a known current through the stimulating electrode and a reference electrode. Using the on-board recording system of the implanted device, the potentials are recorded from all the electrodes on the implanted array including both stimulated and unstimulated contacts. Recorded data are then transmitted to the clinical interface by backward telemetry. The voltage measures are usually divided by the known injected current to obtain impedance values of the stimulate contacts and a relative normalized measured of potential spread across the unstimulated electrode contacts.

In this study, intracochlear electrical fields are measured in Clarion® CII and HighRes 90K devices (Advanced Bionics Corporation, ABC). The commercial term used for these measures is known as Electrical Field Imaging (EFI). Figure 4.6 shows the set-up for measuring these intracochlear electrical fields. The manufacturer's software used in this study to obtain these measures is the Advanced Bionics Electrical Field Imaging and Modeling (EFIM) Tool version 1.3.11 (Advanced Bionics, 2003), which runs off a laptop. The laptop is connected to the clinical programming interface (CPI) through a serial link. The configuration shown in Figure 4.6 is similar to that one that is used during the clinical fitting of the implant.

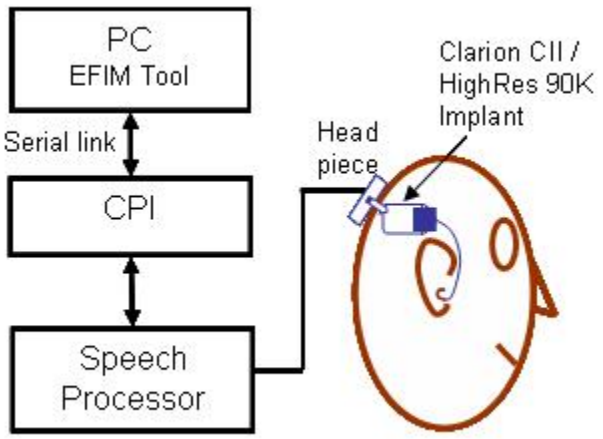

Figure 4.6: Intracochlear electrical field measures set-up

Both pulsatile and sinusoidal stimuli can be generated by the EFIM tool. Stimulus levels used in EFI measures are very small (typically 32 μamp peak) to maintain linearity of the on-board recording system and generally produce no detectable sound for the subject. The electrical field measures that are recorded at the stimulated contacts provide information regarding the electrode-interface impedances while those recorded at the unstimulated contacts determine the network impedances of the model. Details of the model have been described in Section 2.3.3. Upon generation of stimuli the tool first estimates the impedance to determine a suitable gain for the system.

4.2.3 Impedance Measures due to Scalp Stimulation

Impedance measures are obtained when known sinusoidal currents (20 μA p-p) of varying frequencies (100 Hz to 70 KHz) are applied externally via surface electrode contacts to the scalp and head. The peak current amplitudes used are five times or more below the recommended safety limits (100 μA) for 60 Hz leakage currents for non invasive patient-

connected equipment (ANSI/AAMI ES1, 1993). The stimuli are generated by a battery-powered, wide-bandwidth, custom-built, push-pull current source with optical isolation.

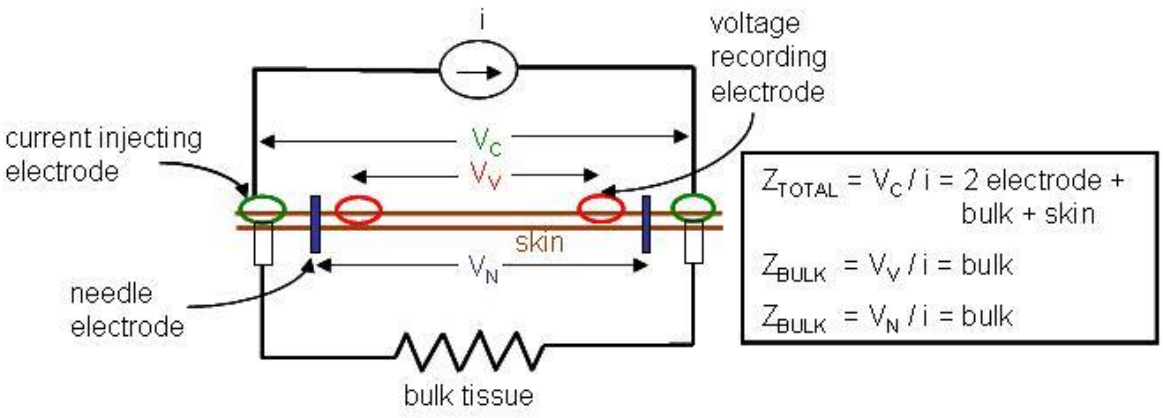

Figure 4.7: Impedance measures

A four-electrode method is used in which current is injected through two electrodes and the voltage is measured across two other electrodes that are placed very close to these injecting electrodes. This is shown in Figure 4.7. Electrodes are placed on opposite sides of the head to include the bulk head tissue in the impedance network. In the four-electrode configuration, current does not flow through the recording electrodes, so the total impedance measured approximates the impedance of the bulk-tissue alone.

4.2.3 Measures to Determine Subjects' Head Shape

The 3D digitizer is used to trace the shape of the subjects' head by recording the 3-D locations of various contours and landmarks on the head and face. Distances between the top of the head and the neck/chin, left and right ears, and the back of the head and the bridge of

the nose are measured to determine the approximate radius of the subject's head. These measures are used in scaling the size of the head models for dipole source localization.

4.3 Instrumentation

This section discusses the instrumentation details of the following main components used in the study: (1) electrode probe, (2) 3-D digitizer, (3) amplifier system, and (4) current source.

4.3.1 Recording Electrode Probe

To facilitate rapid and high quality recording of electrical artifact potentials on the scalp a specialized electrode probe is used. This probe allows recording of low-noise scalp potentials at discrete points on the scalp without having to prepare the recording sites in the traditional manner (e.g. scrubbing to remove oils and epidermis followed by electrode paste application) to obtain suitably low electrode impedances (<5 Kohms). The general features of the probe are shown in Figure 4.8 which describes an early implementation of the probe. The basic operational principle is that skin/electrode impedance should not influence potentials recorded on a surface electrode if the impedance of the recording system is sufficiently high to minimize current flow from the recording site into the recording system. As the recording current is reduced the voltage drop across the skin/electrode interface approaches zero. In the probe the recording current is minimized and the probe impedance is maximized by use of an active driven-guard surrounding a large surface area recording electrode that connects to the skin surface through a salt bridge formed by the surrounding electrode paste. Later implementations of the design to reduce its size so that the probe could mount on the tip of a 3D digitizer (see following section) involve use of a saline soaked wick

in lieu of the hypodermic syringe and electrode paste. The new design for the electrode probe is shown in Figure 4.9.

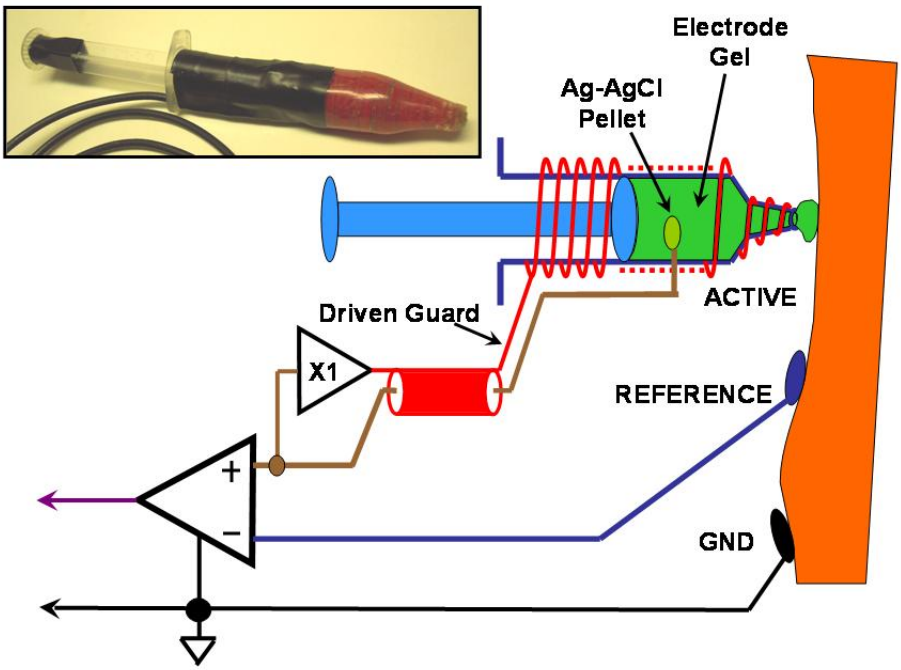

Figure 4.8: Electrode probe (early design)

Figure 4.9: Electrode probe (new design)

4.3.2 3-D Digitizer

A 3-D digitizing device is used to capture the spatial coordinates of any object. These devices are usually used for modeling purposes. In this study, the Microscribe 3-DX (Immersion Corporation, San Jose, CA) is used to record the spatial coordinates of the recording sites on the head, scalp, and neck of cochlear implant subjects at which surface artifact potentials are also measured. The Microscribe 3-DX is connected to the laptop through a serial port. The Microscribe Utility Software (version 5.0; Immersion Corporation, San Jose, CA) is used in conjunction with the custom-developed recording system to control the recording of the spatial coordinates. A foot pedal is attached to the system as a means to input spatial coordinate data at each recording site. Figure 4.10 is a photograph of the Microscribe 3DX. The base of the digitizer is bolted down to a rigid wooden surface.

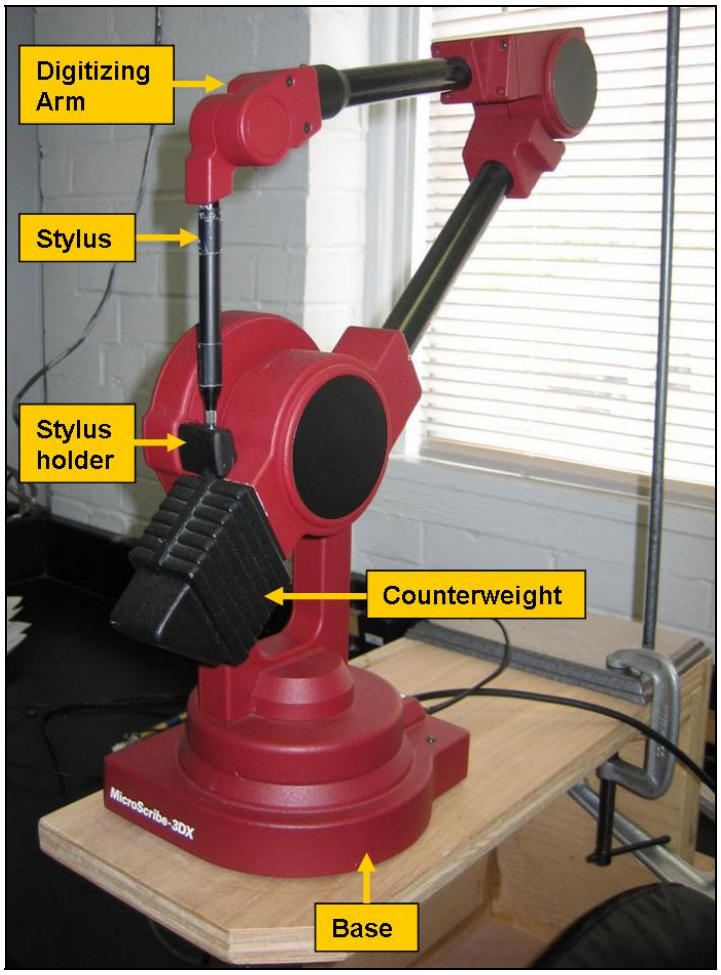

Figure 4.10: The Microscribe 3DX digitizer

The digitizer system consists of the digitizing arm with a stylus. Also shown in the figure at the base of the stylus is the default tip which completely rests in the stylus holder, perpendicular to the rigid wooden surface on which the digitizer is placed. The home position for the digitizer is represented in Figure 4.10. In this position, the counterweight lies flush against the stylus holder. The digitizer is always powered on in the home position with the default tip in place to ensure that the system is calibrated. Once calibrated, the default tip is replaced by the electrode probe, as shown in Figure 4.11.

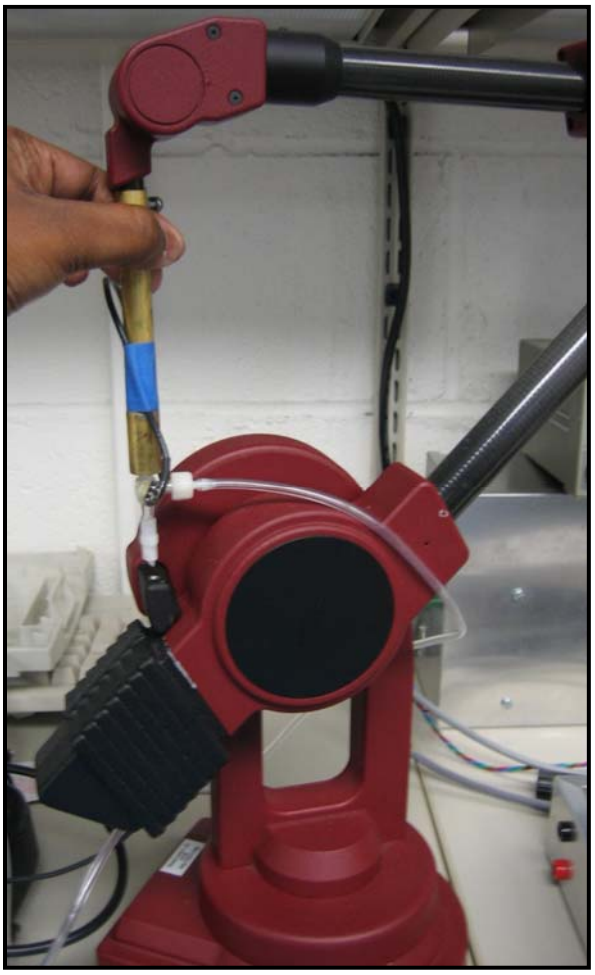

Figure 4.11: Electrode probe and digitizer

4.3.3 Amplifier System

A custom-designed, fast-recovery, wide-bandwidth, bio-potential amplifier and software system (Finley, Herrmann, & Eddington, 2004) is utilized to measure surface artifact potentials in cochlear implant subjects. The amplifier system consists of the following components: (1) a headstage, (2) a computer interface stage, and (3) a data acquisition card (DAQ) that runs off a laptop. These are shown in Figure 4.12.

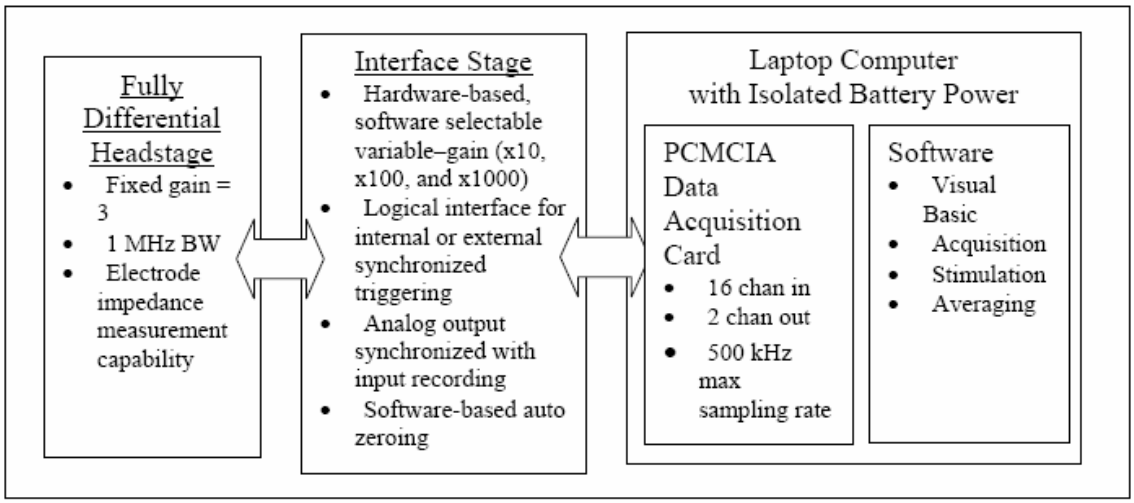

Figure 4.12: Amplifier system instrumentation

The headstage is composed of an instrumentation amplifier with a fixed gain of 2.7, configured in a differential recording mode in order to increase the common mode rejection ratio. Driven guards are used for the input leads from the subject to the amplifier to reduce noise injection into the system. The headstage is connected to the computer interface (also known as the PCMCIA interface), where the differential output is further amplified through cascaded gain stages with variable gain control. The PCMCIA interface generates external trigger pulses to synchronize the stream of output artifact data pulses. The output from the PCMCIA card is fed to the analog input channel(s) of the National Instruments DAQ (DAQCard-6062E, National Instruments Inc., Austin, TX, USA) at a sampling rate of 400 KHz. The amplifier, PCMCIA interface, and the laptop computer used during recording are all battery powered and electrically-isolated for subject safety.

Custom Visual Basic (VB Rev 6, Visual Studio, Microsoft Corporation, Redmond, WA, USA) software is utilized in controlling data acquisition and averaging. The software has the ability to generate appropriate stimuli, but this capability was not made use of in this study. Factors such as the gain, sampling rate of the system, buffer lengths for the recording output, number of trials for averaging, and etc. are specified using software control. The data are divided by the total gain of the system before saving for offline analysis or display, and are thus *referred to input*.

4.3.4 Current Source

A custom-designed, high-bandwidth current source was employed to inject 20 μA peak-to-peak sinusoidal currents across scalp electrode pairs to make impedance measurements. The design is battery-operated and optically-coupled to ensure subject safety. The operational bandwidth is approximately 350 kHz and voltage compliance is ± 12 volts.

4.4 Data Analyses Methods

In this section, the various data analyses methods are discussed. The spatial coordinates are first transformed from the *digitizer coordinate system* to the *head coordinate system* using an affine transformation routine, as explained in Section 3.3.1.1. Then the coordinates in the head coordinate system are projected to the surface of a sphere whose radius is approximately equal to the radius of the subject's head. Before analysis, the averaged surface potential frame is digitally-filtered using the signal processing tools in MatLab (The MathWorks Inc., Natick, MA, USA). In addition to the methods described below, dipole source localization methods are already presented in Chapter 3.

4.4.1 Global Dissimilarities

Global dissimilarity (GD) is a difference measure often used to find the differences between EEG topographic maps (Skrandies, 1990). In this study, GD metrics are computed to find the topographic changes between any two surface potential distributions, as explained below (Roth, Ford, Pfefferbaum, & Elbert, 1995). Each surface potential distribution is first normalized by dividing by the global field power (GFP). The GPF, which is the spatial standard deviation of the field distribution, is computed by calculating the root mean square of the potentials measured at all *n* locations. The global dissimilarity $GD_{X,Y}$ between any two electrode distributions X and Y is then computed as the root mean square of the differences between the two normalized maps X' and Y' based on all recording sites in the two maps. The following equations represent the computation of the global difference $GD_{X,Y}$ for the distributions X and Y:

$$GFP(X) = \left[\frac{1}{N} \sum_{n=1}^{N} X_n^2 \right]^{\frac{1}{2}} \tag{4.1}$$

$$X' = \frac{X}{GFP(X)} \tag{4.2}$$

$$GD_{X,Y} = \left[\frac{1}{N} \sum_{n=1}^{N} \left\{ (X' - Y')^2 \right\} \right]^{\frac{1}{2}} \tag{4.3}$$

where N = total number of recording locations

4.4.2 Clustering Methods

Clustering (Duda, Hart, & Stork, 2000) is a pattern recognition method in which similar objects are grouped together into clusters. Objects that are not within the same

cluster are less similar than objects within the same cluster. In this study, *hierarchical clustering* methods are used to classify potential distributions for all monopolar combinations and determine which of these distributions cluster together and form natural aggregations. The potential field due to each monopolar combination represents an object. The objects are classified into groups based on certain characteristics or *features.* Features are weighted or non-weighted depending on the levels of influence of each feature. Features and weighting factors are chosen based on existing knowledge regarding the system. The features are combined to compute a metric. An appropriate model then classifies the objects based on the value of this metric. The basic block diagram of a classifier system is shown in Figure 4.13. Example data sets may be provided to the classifier to train the classifier and effectively classify test data, in which case it is referred to as supervised learning. Clustering, on the other hand, is an *unsupervised* pattern recognition method in which no training is provided to the classifier.

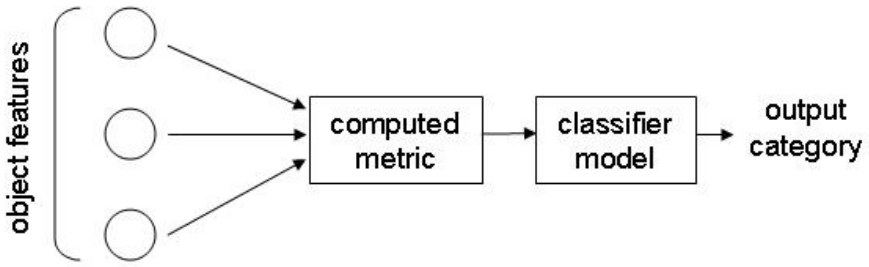

Figure 4.13: Block diagram of a classifier system

The features for each object in this problem are represented by the potentials measured at each recording site. These features are not weighted equally; locations on the

surface of the scalp and face where potentials are rapidly changing such as areas around the ipsilateral cheek and mastoid regions are weighted higher than regions surrounding the back of the head and near the neck where the potentials are small in magnitude and present no significant change in potential depending on the electrode that is being stimulated. The weighted Euclidean distance between the corresponding features is first computed for all objects. Clusters are then formed based on the average *linkage* algorithm, where clusters are linked based on the mean of the distances between the objects. The results of the clustering process are represented by a tree diagram known as a *dendrogram.*

5. RESULTS

This section presents the findings of this study. First, the relationship between the measured surface potentials and the current flow within and outside the cochlea is discussed. The impedance characteristics of the biological interface are then presented. Finally, the differences in current flow patterns across electrodes, and the alternate paths for current to exit the cochlea are discussed in detail.

5.1 Relationship between Scalp Surface Potentials and Stimulus Current Injected into the Cochlea

Specific Aim #1 tests the hypothesis that surface potentials measured on the scalp are influenced linearly by the flow of current within and outside the cochlea and throughout the volume of the head during device stimulation. The protocol followed in measuring these surface potentials is described in Section 4.2.1. Input stimuli consist of biphasic pulses with a phase duration of 50 μs that are delivered to the odd-numbered electrodes (even- numbered electrodes were not stimulated in this experiment) using a monopolar mode of stimulation. The amplitude level of the pulses is chosen such that the subject hears these sounds at a comfortable level. Surface potentials are measured when input stimuli are at 40%, 60%, and 100% of the comfortable level indicated by the subject. The raw data is filtered digitally and the mean peak-to-peak measures for each biphasic pulse are extracted. Table 5.1 shows the input stimuli levels and the output measured.

Table 5.1: Input and output

Input	Amplitude Level	Output
a	40%	A
b	60%	B
c	100%	C

A system satisfies the property of homogeneity if the outputs *A* and *B* generated by the inputs *a* and *b* respectively have a ratio equal to the ratio of the individual inputs*, i.e. A/B = a/b*. The peak-to-peak measures of the surface potentials obtained in response to input stimuli at the 40% and 60% levels are studied across all recording locations. The goal is to establish that changing the amplitude of the input stimuli does not change the topography of the resultant distribution.

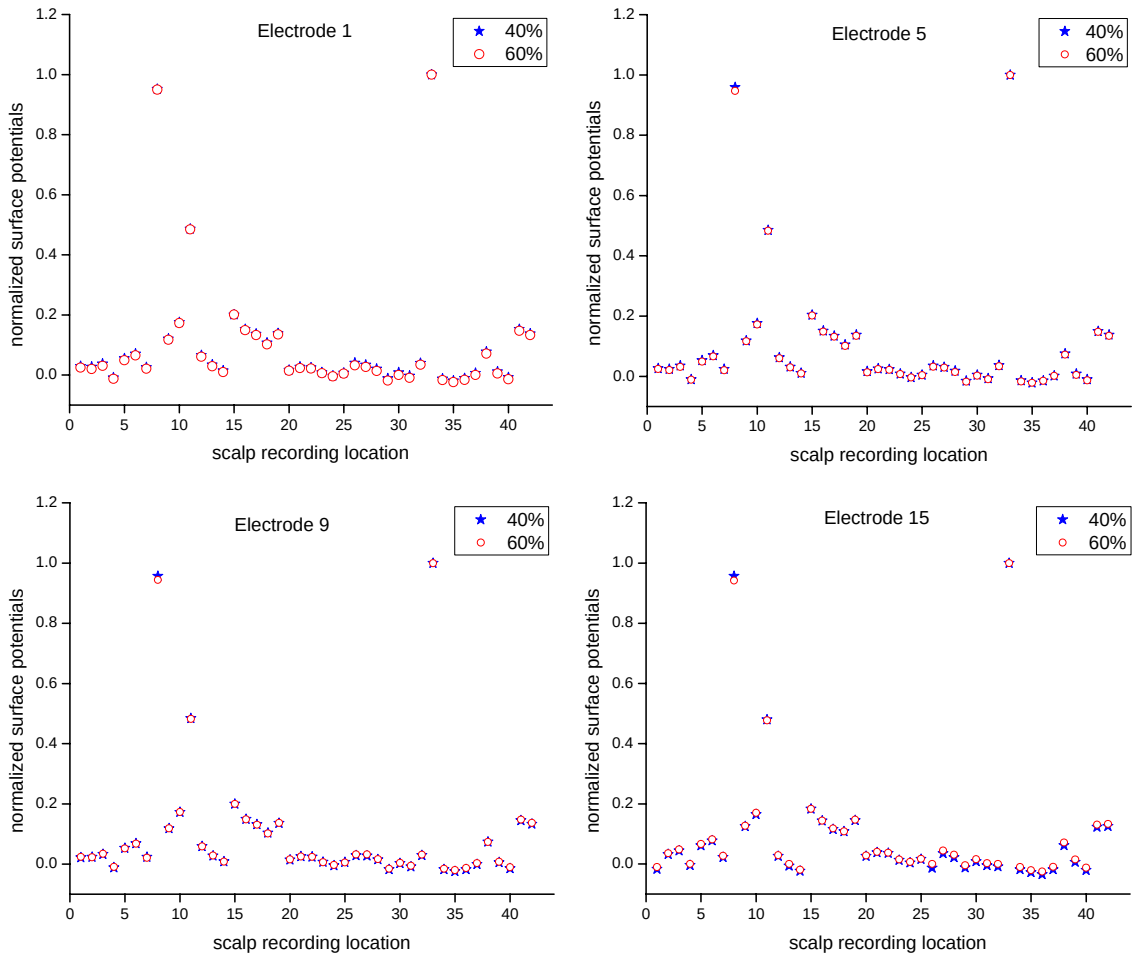

Figure 5.1: Normalized potential fields at the 40% and 60% levels - Electrodes 1, 5, 9, and 15

The peak-to-peak measures at the 40% and 60% level are normalized to the maximum value. This is done for each odd-numbered electrode group. The normalized distributions are then plotted as a function of recording locations in Figure 5.1. Note that some recording locations in the immediate vicinity of the implanted stimulator (8, 11, and 33) produce large surface potentials. The scalp recording locations for both conditions (40% and 60%) are identical. The plots shown are for electrodes 1, 5, 9, and 15. It can be seen that

the normalized surface potential distributions at the 40% and 60% levels have similar topography.

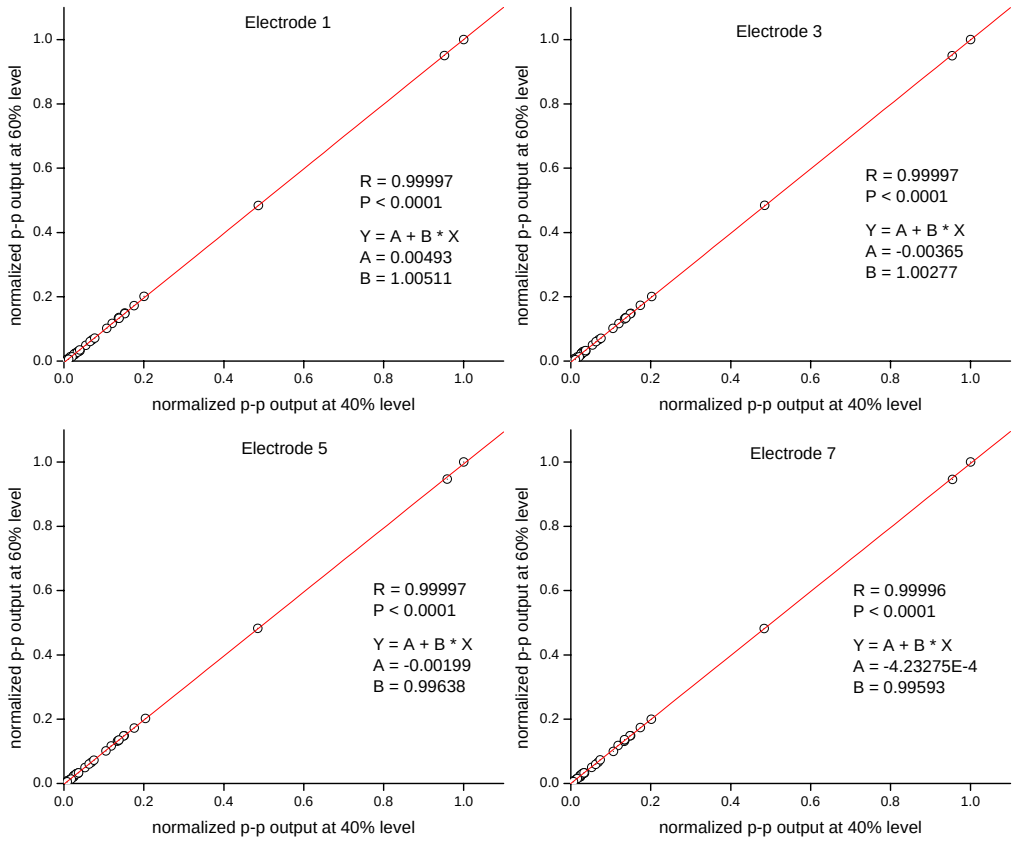

Figure 5.2: Scatter plot of normalized potentials at the 40% and 60% level – Electrodes 1, 3, 5, and 7

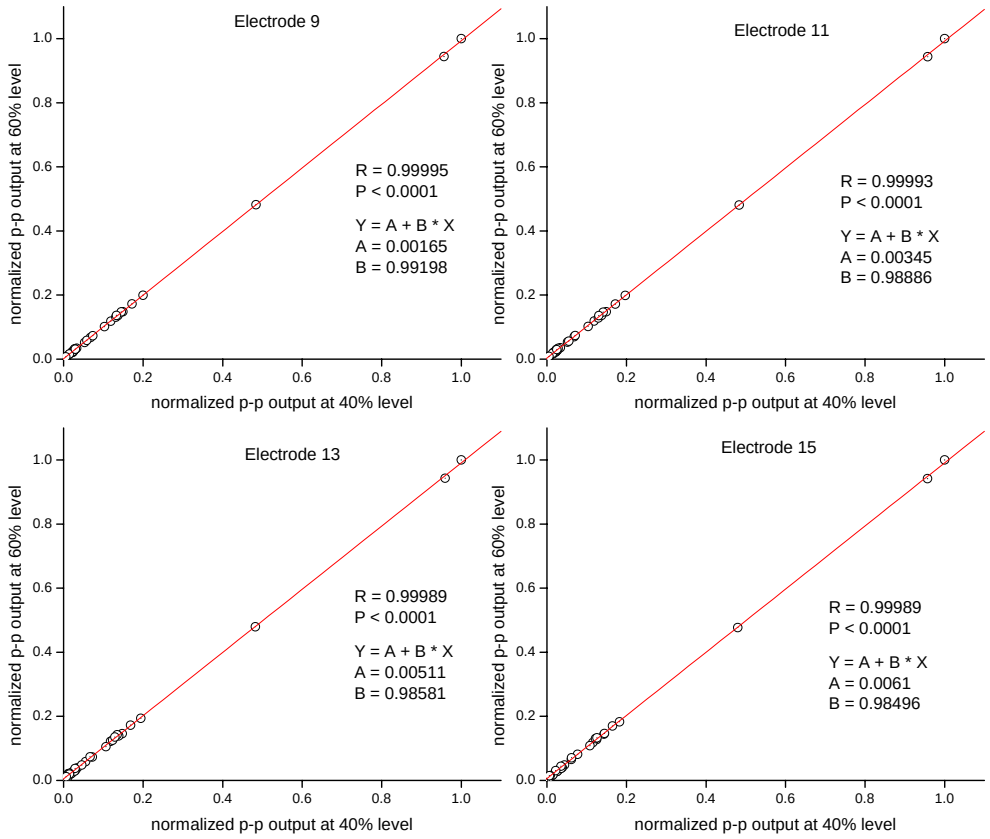

Figure 5.3: Scatter plot of normalized potentials at the 40% and 60% level – Electrodes 9, 11, 13, and 15

Figures 5.2 and 5.3 show the scatter plots between the normalized potentials at the 40% and 60% input stimuli levels for all odd-numbered electrodes. A regression line between the two input stimuli levels shows a significant linear correlation across all data sets (correlation coefficient square $R^2 \approx 1$, p value < 0.0001). These results indicate that varying the amplitude of the input stimuli changes only the amplitude and not the structure/topography of the potential distribution. Thus the system exhibits the principle of homogeneity.

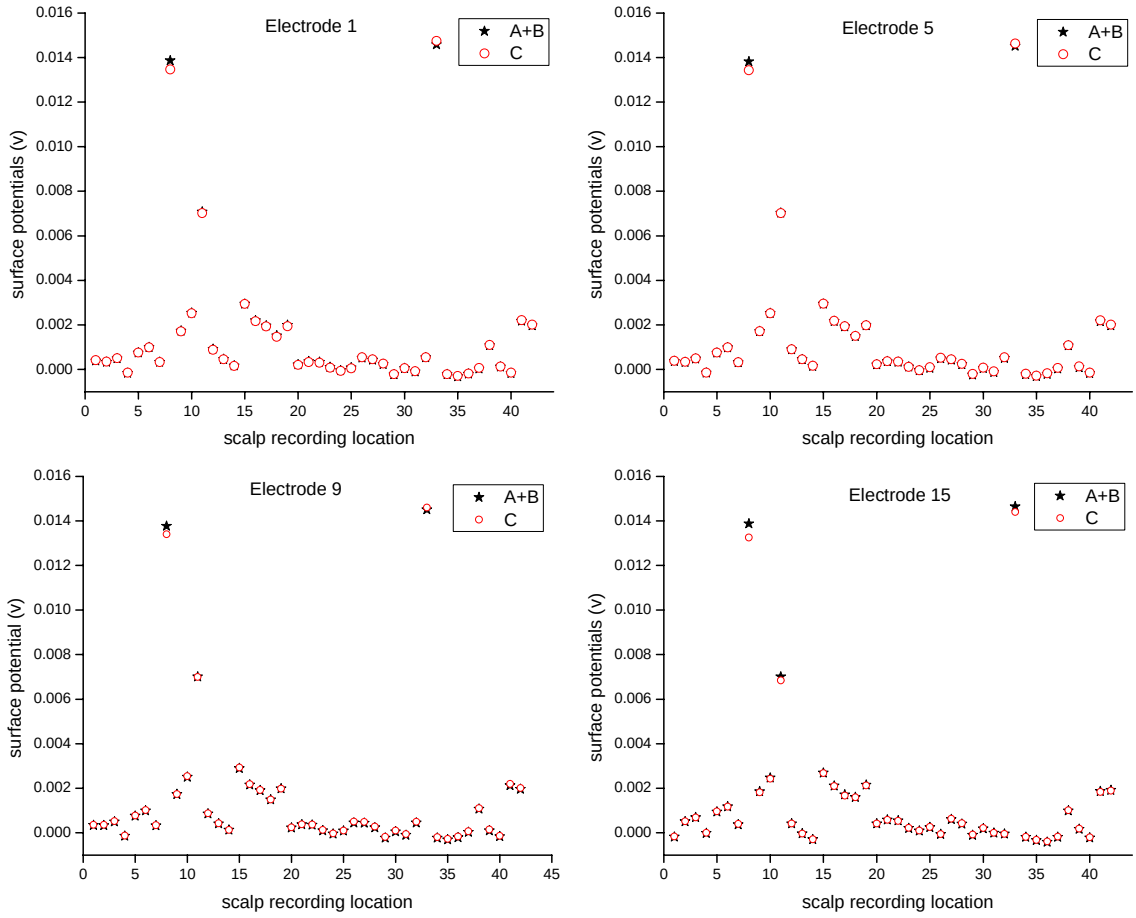

Figure 5.4: Field distributions C and (A+B) - Electrodes 1, 5, 9, and 15

For a system with inputs *a*, *b*, and *c* whose outputs are *A*, *B*, and *C* respectively, the additive property is tested by checking if $A + B = C$, where $c = a + b$. As seen in Table 5.1, the input stimuli at the 40%, 60%, and 100% levels are represented as *a*, *b*, and *c*. The surface potential distributions generated due to *a*, *b*, and *c* are represented as *A*, *B*, and *C* respectively. The surface potentials generated due to input stimuli at the 40% and 60% amplitude levels are summed across the corresponding recording locations. This summed potential distribution $(A + B)$ is then compared to the potential distribution measured when

the input stimulus is at a level that is 100% of the comfortable level (*C*). Figure 5.4 shows the potential distributions (*A* + *B*) and *C* plotted as a function of recording locations. The plots shown are for electrodes 1, 5, 9, and 11. The plots show that *A* + *B* = *C*. Further analysis is presented in Figures 5.5 and 5.6.

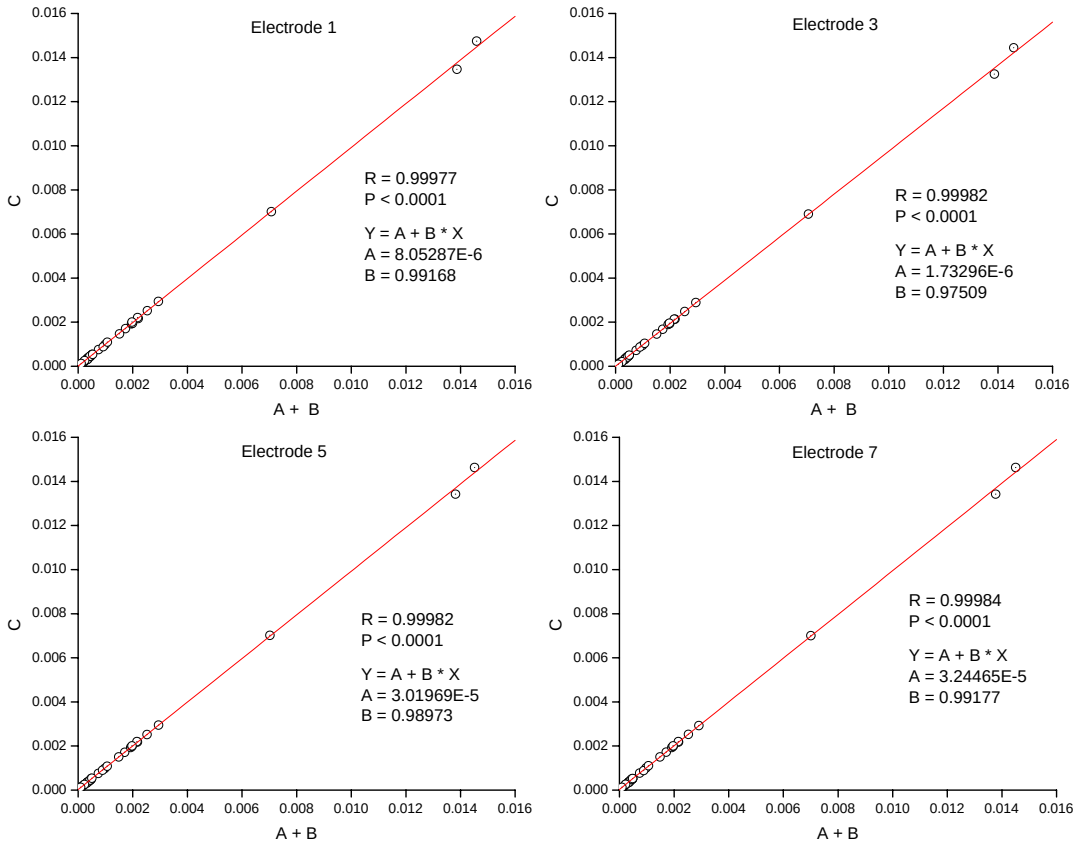

Figure 5.5: Scatter plot of (A + B) vs. C - Electrodes 1, 3, 5, and 7

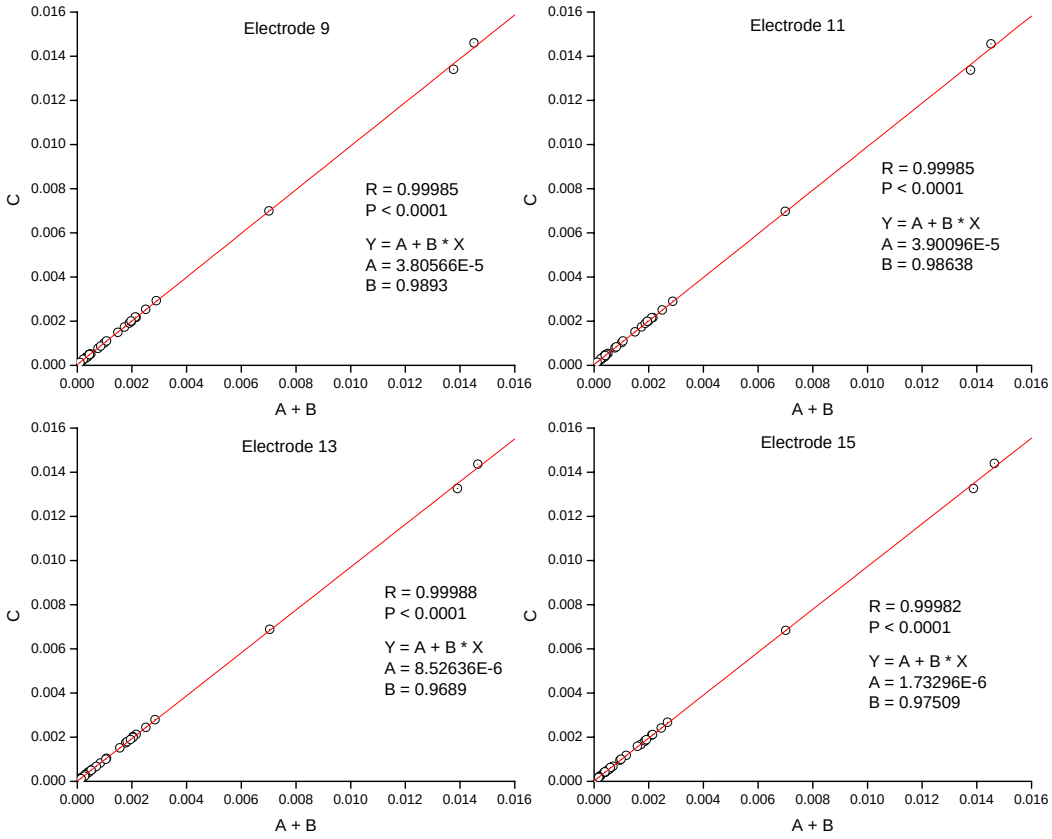

Figure 5.6: Scatter plot of (A + B) vs. C – Electrodes 9, 11, 13, and 15

Figures 5.5 and 5.6 represent the scatter plots of the potential distributions ($A + B$) and C for electrodes 1, 3, 5, 7, 9, 11, 13, and 15. Regression analysis shows a significant linear correlation between $(A + B)$ and C (correlation coefficient square $R^2 \approx 1$, p value < 0.0001). It is evident from Figures 5.4, 5.5, and 5.6 that the system satisfies the property of additivity. The system thus follows superposition theorem. Surface potentials measured on the scalp are thus influenced linearly by the flow of stimulus current within and around the cochlea during device stimulation.

5.2 Impedance Characteristics of the Bulk Head Tissue

Specific Aim #2 tests the hypothesis that the bulk head can be considered to be purely resistive in nature for the range of frequencies of stimulation delivered by modern cochlear implant systems. Section 4.2.3 explains the protocol followed in obtaining impedance measures from non-implanted subjects in order to test this hypothesis. Prior to performing these impedance experiments, a simulation study was performed to study the frequency spectrum of interest and spectral energy levels for input stimuli that are generated by modern cochlear implant devices. This simulation study is described below.

The phase widths of the input biphasic pulse stimuli used in the scalp potential experiments performed on cochlear implant subjects ranged from 30 – 60 μs. The spectral energies of biphasic pulse trains, whose phase widths are within the range specified above, are determined by obtaining the Fourier transform of the specified pulses. The Fourier transforms are obtained using MatLab (The Mathworks Inc., Natick, MA, USA). The results of the simulations are presented in Figure 5.7 for a pulse train containing 10 biphasic pulses each with a phase width of 50 μs. The peak is centered at a frequency of 10 KHz. Figure 5.8 shows a detailed version of the same plot that focuses on the spectral energy levels above -40 dB. Energy levels at and below -40 dB contribute less than 1% of the peak spectral line. The frequency spectrum of interest reduces to a range of frequencies from 10 – 100 KHz, as indicated in Figure 5.8.

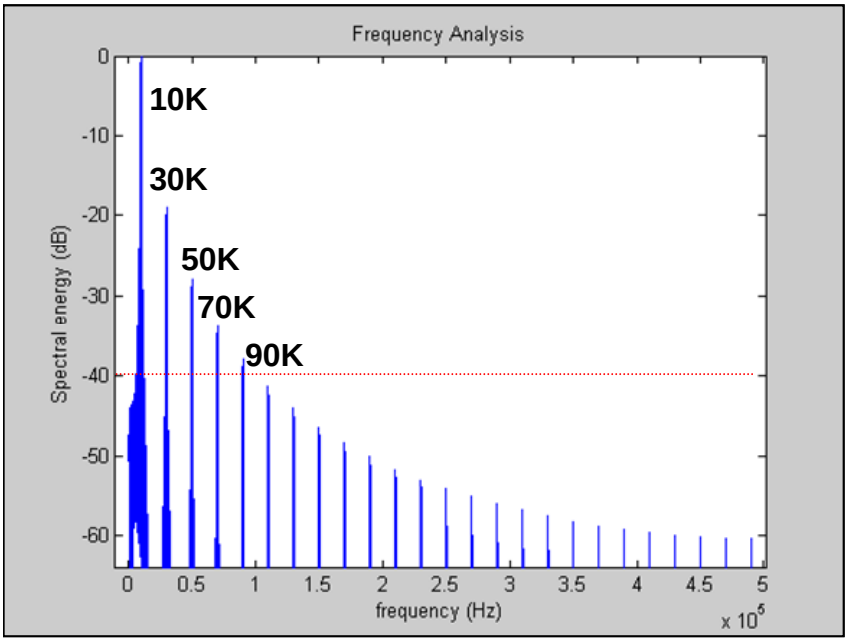

Figure 5.7: Spectral analysis of a biphasic pulse

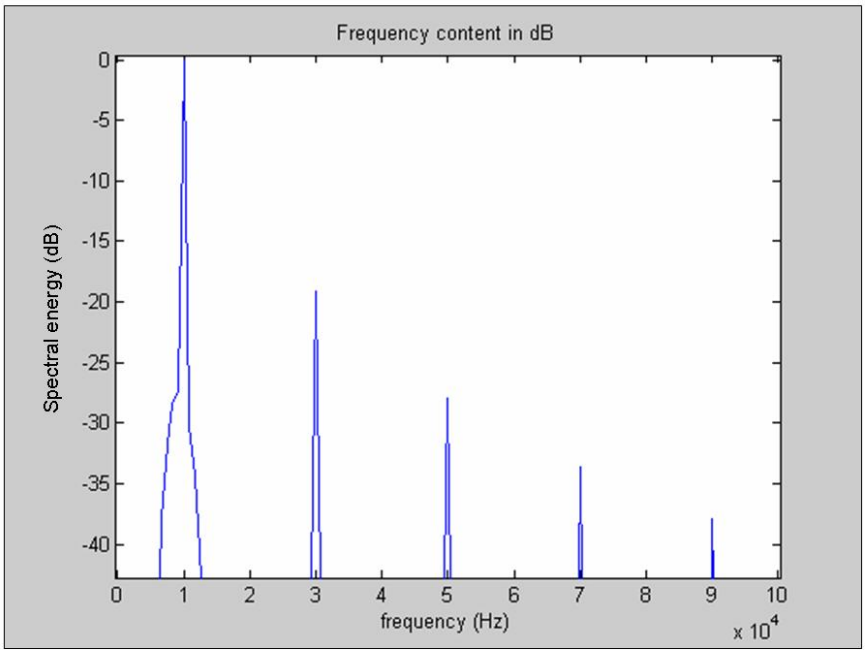

Figure 5.8: Spectral analysis of a biphasic pulse – frequency spectrum of interest

The stimuli used in the impedance experiments consist of a train of sine waves of varying frequencies in the range 100 Hz – 70 KHz. Reasonable waveforms could be generated at 70 KHz that enable the estimation of the RMS energy levels. Stimuli, however, could not be generated above a frequency of 70 KHz due to limitations posed by the sampling rate of the data acquisition system. The amplitude is fixed at 20 μA peak-to-peak. Stimuli are applied to the subject through paste-on surface electrodes placed on the forehead (positive) and nape/back of neck (negative). Recording electrodes are placed on the forehead (positive) and nape (negative) at a distance of 4 mm from the stimulating electrodes to measure the voltage on the surface of the head. The ground electrode for the recording amplifier is placed on either clavicle. The protocol and details regarding the instrumentation and set-up are provided earlier in Section 4.2.3. These voltage measures are then compared with voltages that are measured when stimulating and recording electrodes are placed at a distance of 2.5 cm from each other in the forehead region. The latter set of measures does not include the head tissue component.

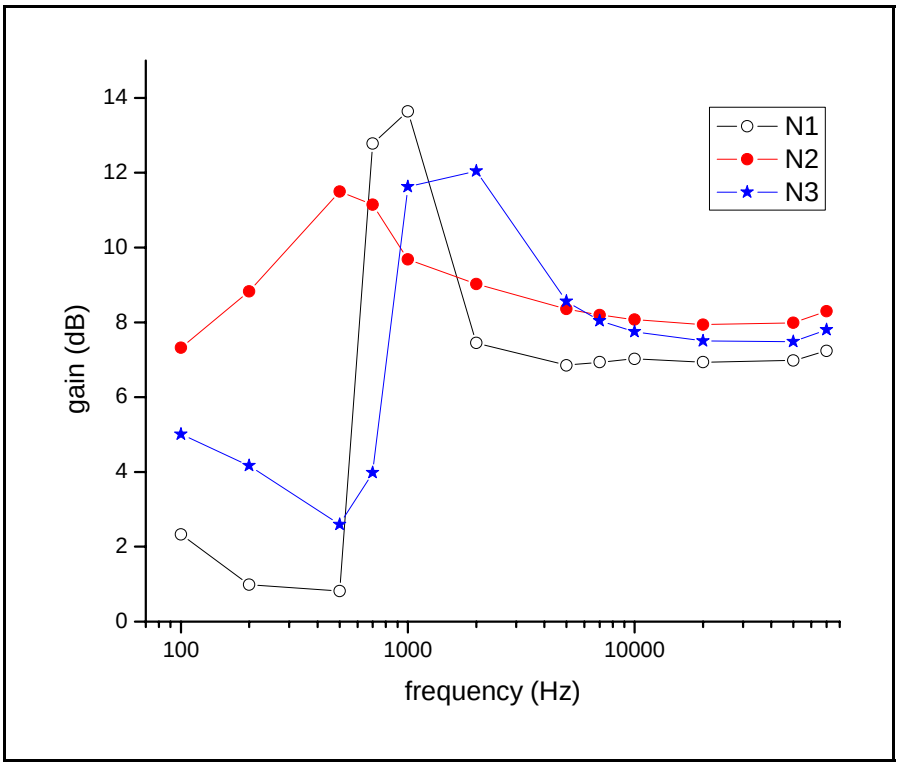

Figure 5.9: Frequency response – gain characteristics

The frequency response of the impedance characteristics of the bulk head tissue measured in three non-implanted subjects is presented in Figures 5.9 and 5.10. The gain holds steady in the high frequency region starting from 5 KHz. The phase characteristics are represented in Figure 5.10 for the same subjects. The phase shift is also steady in the high frequency region. The events seen in the gain and phase plots that occur in the lower frequency range up until 2 KHz are most likely due to the effects of muscle tissue (Reilly, 1998). Based on the earlier simulation study, the frequency range of interest is from 10 – 100 KHz. Both the phase and gain remain steady over this entire range, as seen in the figures. The low-frequency effects can thus be ignored and the head can be modeled as a resistive network over the specified range of frequencies.

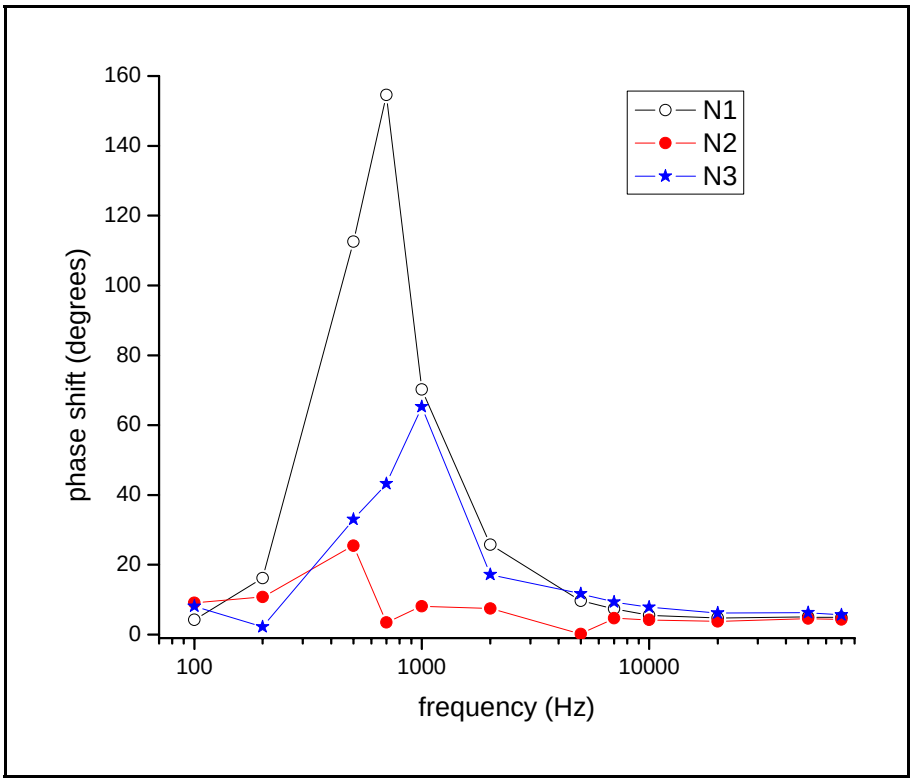

Figure 5.10: Phase plot

5.3 Differences in Current Flow Patterns across Electrodes

The major hypothesis of this study is that different pathways exist for current to flow either within or outside the cochlea, depending on the electrode(s) being stimulated and/or the mode of stimulation. Because surface potentials measured on the scalp are directly related to the stimulus current flow within and outside the cochlea (see Section 5.1), differences in current flow patterns are deduced by comparing the surface potential distributions for all electrode stimulus conditions.

Table 5.2 represents an example stimulus delivered to Subject S2. The stimuli consist of 32 pulses, including both monopolar and bipolar combinations. Pulses 16 – 31 represent the monopolar stimuli. Here, sequential stimulation is provided by each of the 16 intracochlear electrode contacts, relative to the return electrode. The current magnitude and phase width for all pulses are constant. These pulses are delivered to the subject's cochlea in an interleaved manner, using the *continuous interleaved sampling* strategy, which has been described in Section 2.2.

Table 5.2: Input stimuli set

Pulse #	Reference Electrode	Stimulating Electrode(s)	Current value (μA)	Phase duration (μs)
1	10	1	280	50
2	11	2	280	50
3	12	3	280	50
4	13	4	280	50
5	14	5	280	50
6	15	6	280	50
7	16	7	280	50
8	14	15	280	50
9	13	15	280	50
10	12	15	280	50
11	11	15	280	50
12	10	15	280	50
13	9	15	280	50
14	8	15	280	50
15	7	15	280	50
16 -31	return	1 -16	280	50
32	16	14	280	50

The top panel of Figure 5.11 shows a surface potential record measured in Subject S1. The data represented are measured at the left mastoid location behind the ear. Data are averaged across 400 trials. Here, the averaged value of the potentials is plotted in red, along with 95% confidence interval plots in blue. It is seen that the plots lie on top of each other. The bottom panel gives a detailed view of two of the pulses.

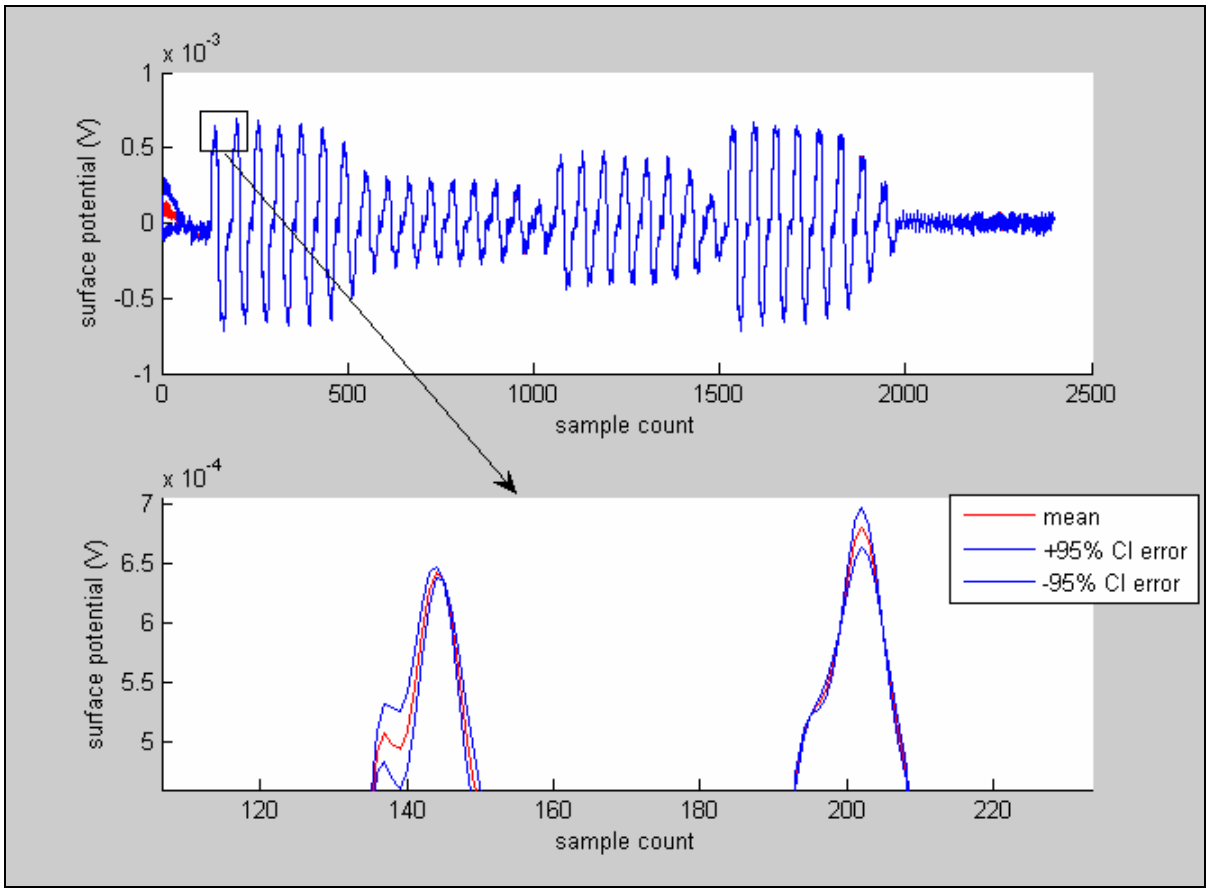

Figure 5.11: Surface potentials measured on the scalp

Data were collected from Subject S1 during several different occasions. Figure 5.12 shows the scatter plot of data measured at the left reference, "C_z front", and tip of the chin (midline) locations on two separate days (day 1 and day 2) in Subject S1. The potentials that are measured at identical locations on the scalp but on two separate occasions are normalized to the maximum value. A regression analysis of the data shows a significant linear correlation between surface potential data collected on the two separate days. Data measured at the left reference location shows the highest correlation (R = 0.99161) due to the fixed location of the left reference location at the left tragus during the recording sessions on both

days. Data collected at the "C_z front" and tip of the chin locations show lower correlation because the spatial coordinates for these recording locations can vary. These results indicate the surface potentials can be considered to be time invariant in nature.

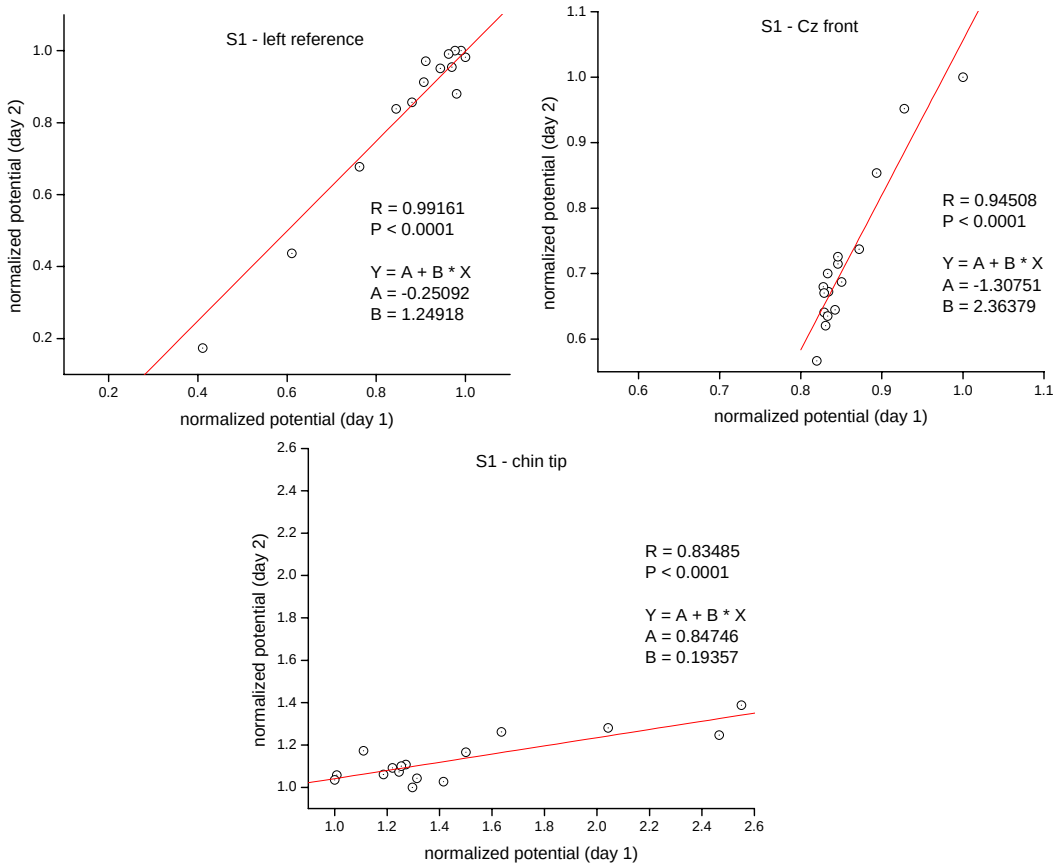

Figure 5.12: Normalized surface potentials – day 1 and day 2

The four plots shown in Figure 5.13 represent the filtered and averaged surface potentials (in volts) from Subject S2 measured at the following four recording locations: (1) left reference, (2) below ear lobe, (3) C_z, and (4) left cheek. These are generated in response

to the input stimuli described in the Table 5.2. The monopolar data is represented by 16 biphasic pulses, which are positive leading for the four recording locations that are shown. The monopolar frame begins at a time interval of 2.5 ms approximately, and consists of the first 16 biphasic pulses thereafter, as is marked in the first plot (left reference). Both the data that precede the monopolar frame and the single biphasic pulse that succeeds the monopolar data represent bipolar artifact potentials.

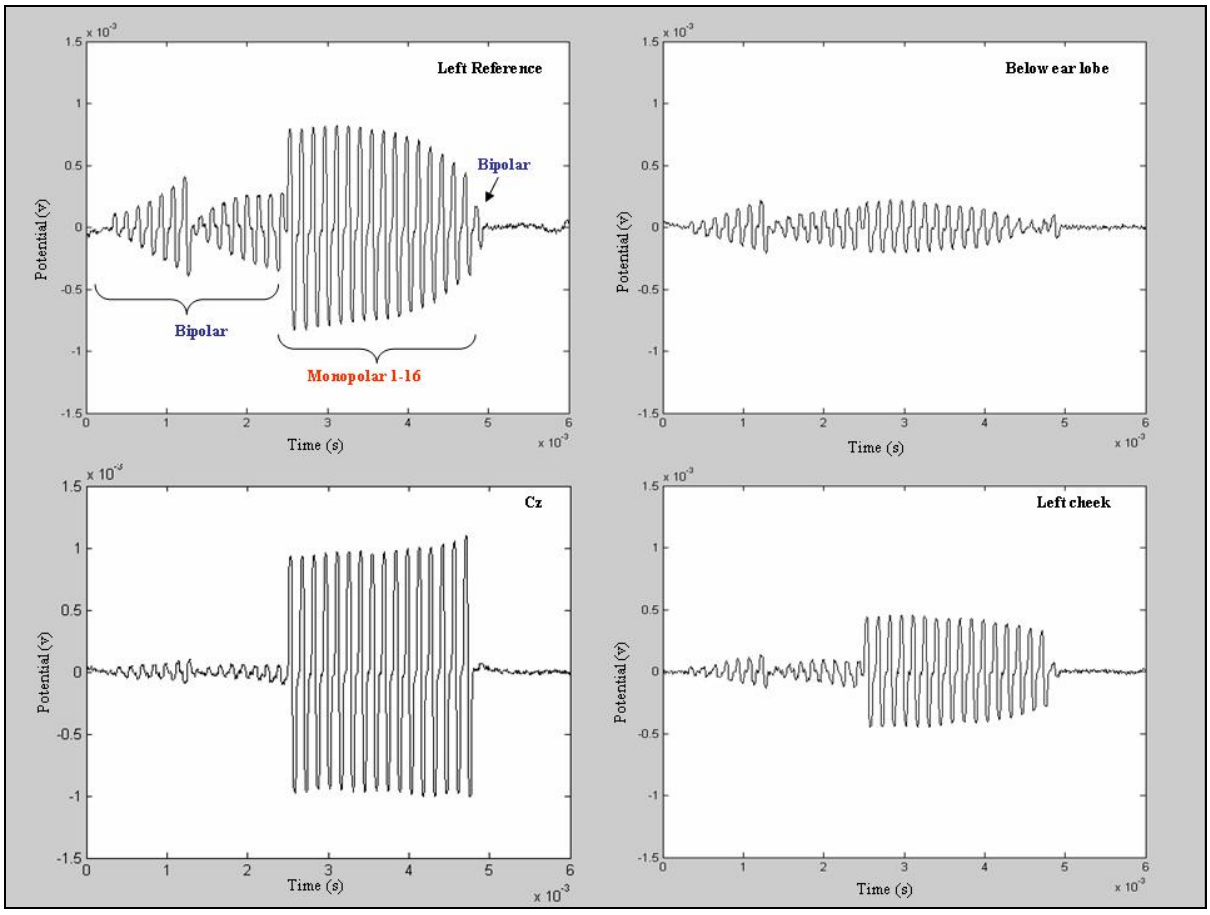

Figure 5.13: Surface potentials (S2)

The plots clearly indicate that the recorded scalp potential amplitudes differ as a function of stimulus electrode configuration and scalp recording location. The differences in amplitudes across recording locations are to be expected because current flows out from the generator source and then spreads throughout the entire surface of the head. This causes large potentials to be generated on the surface of the scalp in the vicinity of the implanted device. Smaller potentials appear on the side of the head contralateral to the implant.

The amplitude differences across different monopolar stimulus conditions convey significant information. The plots show definite trends in that apical electrode potentials are similar to each other whereas significant differences exist between apical and basal electrode surface potentials. These surface potentials are measured in response to current stimuli of constant magnitude, as shown in Table 5.2. The bipolar artifacts show phase inversions in addition to amplitude changes. Bipolar contacts, which generally mimic dipoles, create potential fields throughout the surface of the head whose maximum and minimum values lie on opposite sides of each other, separated by a zero potential line. The electrical fields rapidly change as the orientations of the bipolar contacts vary, and hence the phenomenon of polarity flipping is observed. The four recording locations in Figure 5.13 represent only a fraction of the 61 locations at which surface potentials were recorded in Subject S2.

5.3.1 Field Distributions

3-D topographic maps representing the electrical field distribution over the entire surface of the scalp and face are generated for the measured surface potentials. Figure 5.15 shows the field distribution plots for Subject S1. Figure 5.14 explains the orientation of the plots with respect to locations on the subject's head where potentials were recorded. The plot

represents the left-hand side view of the subjects head, with the subject's head tilted slightly upwards. Subject S1's cochlear implant is on the left side.

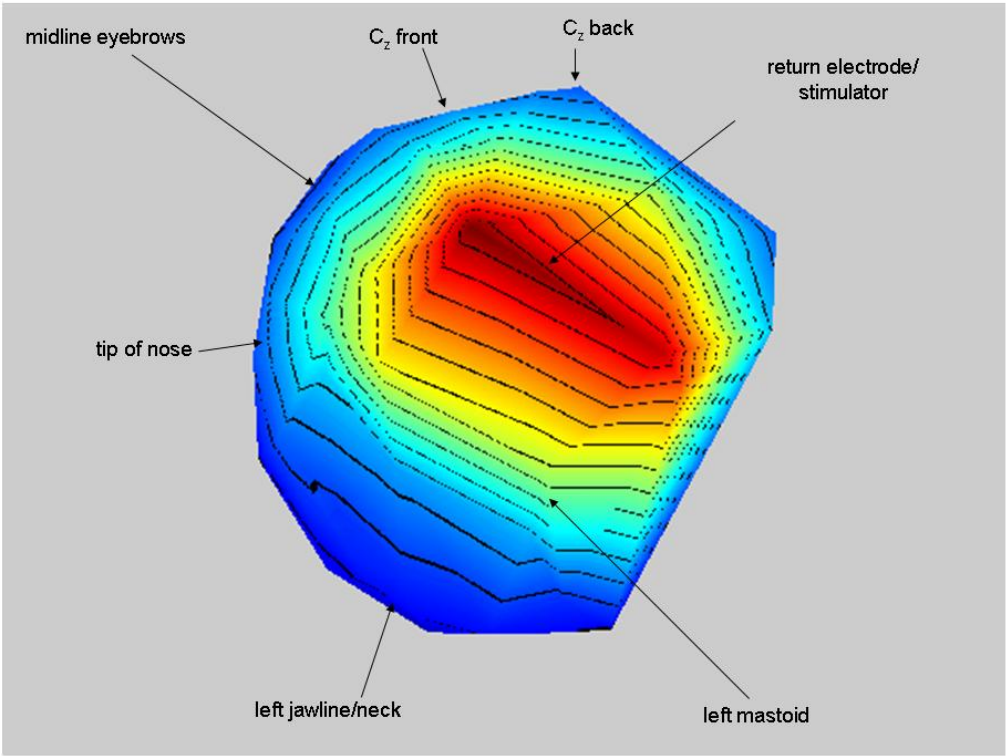

Figure 5.14: Plot showing recording locations for Subject S1

The field distribution plots for Subject S1 are shown in Figure 5.15. Each of the 16 sub-plots corresponds to the field distribution generated due to monopolar stimulation through the return electrode and a specific electrode contact, as numbered. The surface potentials are scaled by dividing the potentials by the global field power (GFP), as explained in Section 4.4.1. The spatial coordinates measured by the digitizer are transformed to the

head coordinate system, and are then projected to the surface of a sphere whose radius approximately equals the radius of the subject's head.

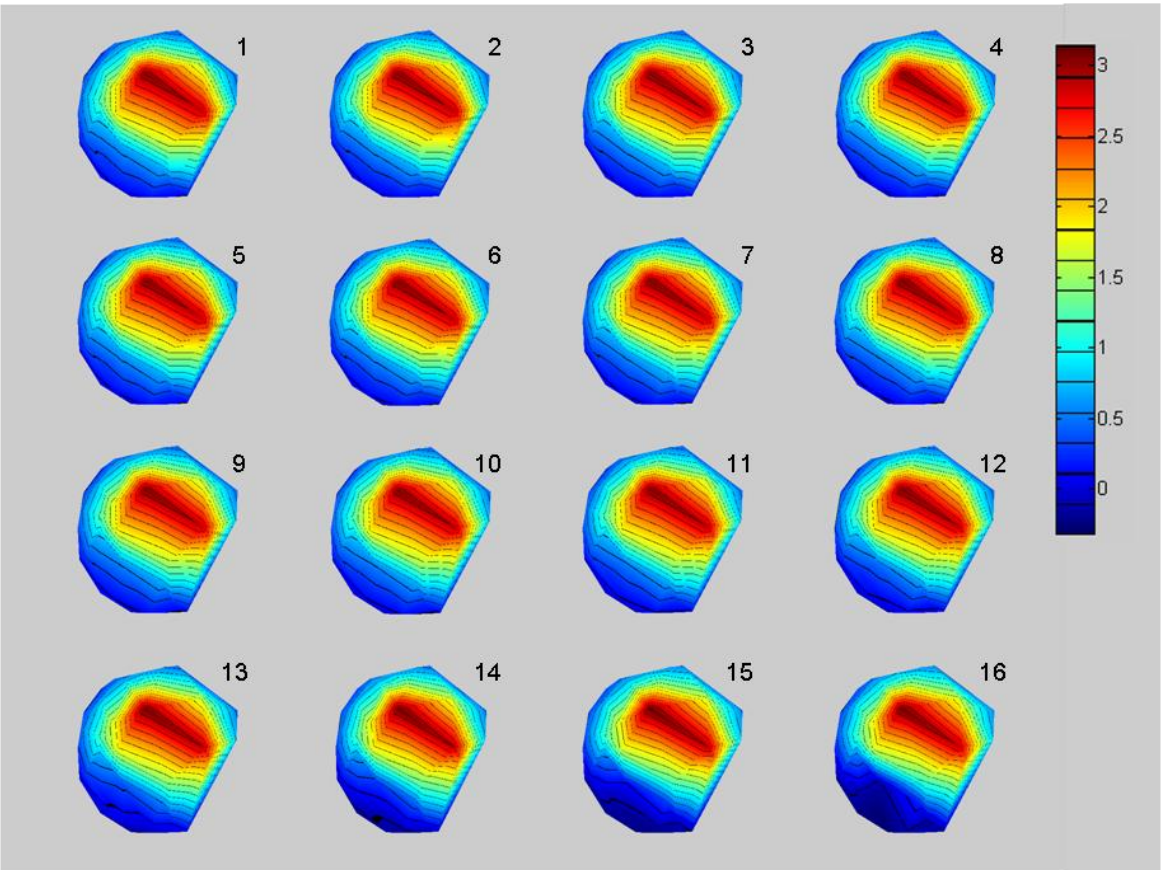

Figure 5.15: Scaled surface potential distribution (S1)

These plots, while detailed, do not convey adequate information regarding the changes in potentials across electrode conditions. More useful to plot are the differences in the potentials rather than absolute potentials for each electrode condition.

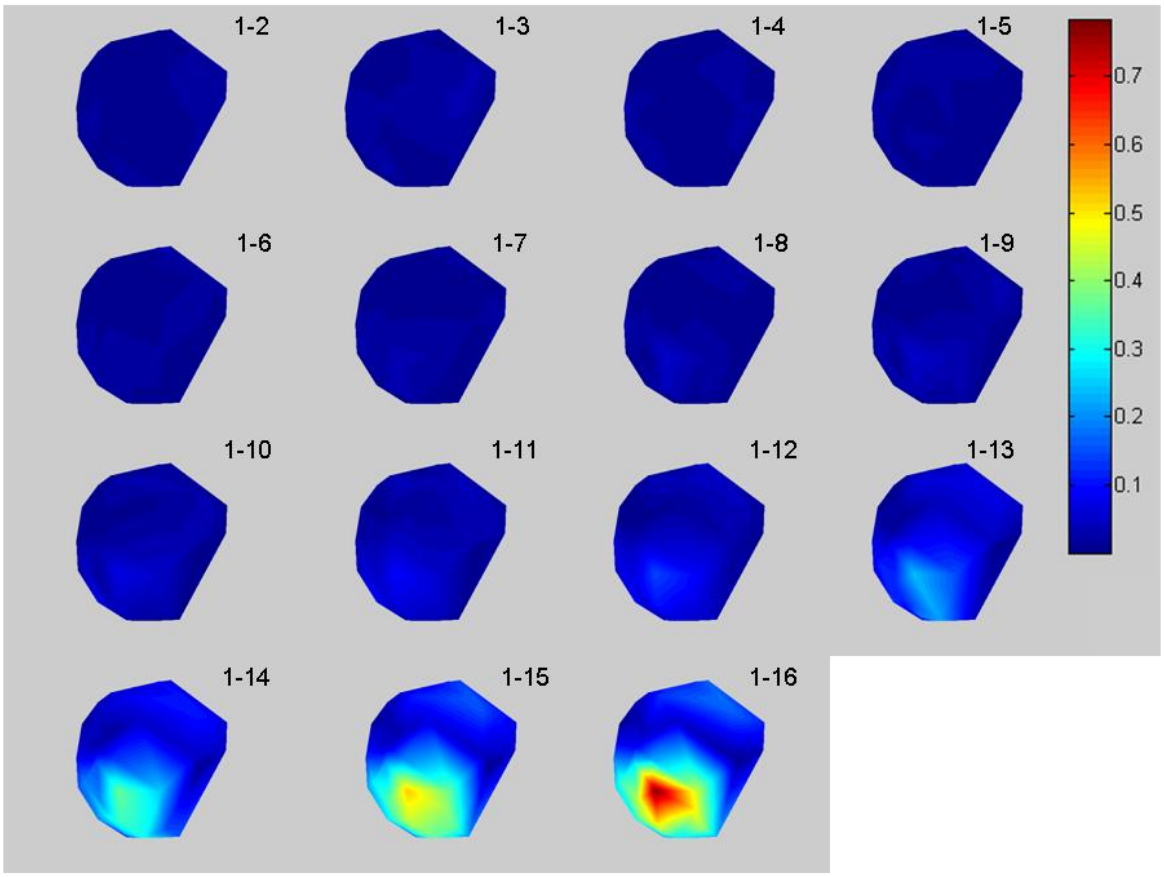

Figure 5.16: Changes in surface potentials relative to electrode 1 (S1)

The plots in Figure 5.16 represent the changes in potentials relative to an apical electrode (electrode 1). Potential differences between electrode 1 and electrodes 2-10 are small; this implies that surface potentials for electrodes 1-10 are similar. The changes in potentials appear to manifest from electrode 11 or 12 onwards.

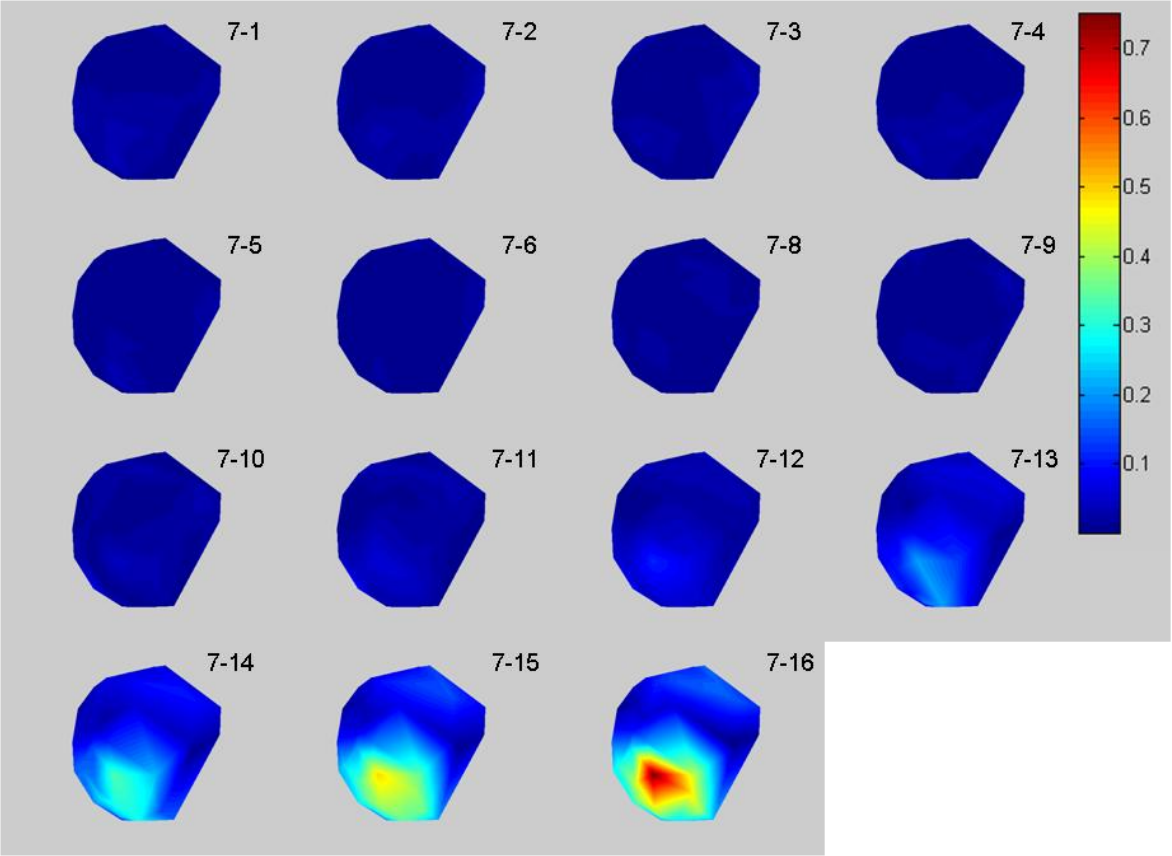

Figure 5.17: Changes in surface potentials relative to electrode 7 (S1)

Figure 5.17 shows the changes in potentials relative to a medial electrode (electrode 7) respectively. Again, the plots show that distributions for electrodes 1-10 are very similar and begin to depart around electrode 11 or 12. The regions on the surface of the head where these potentials seem to change the most appear to be around the ear and cheek region ipsilateral to the implant.

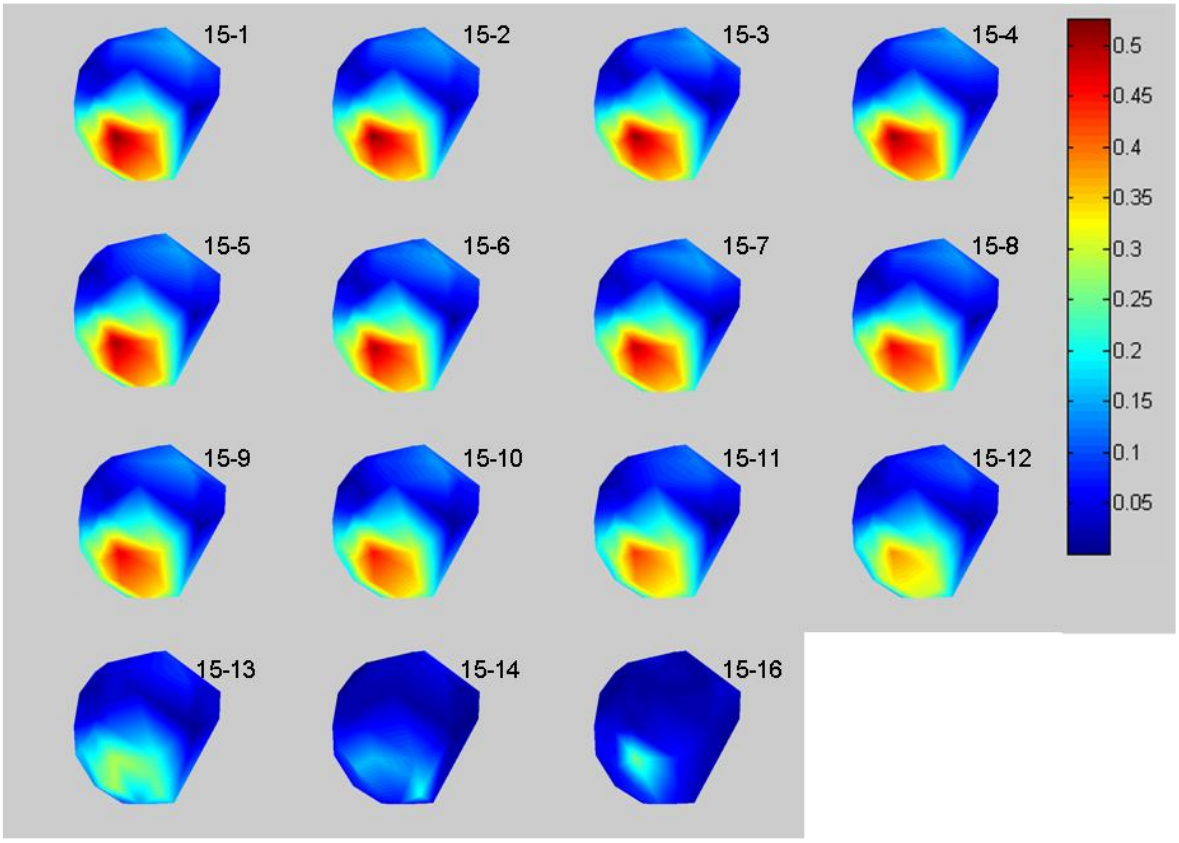

Figure 5.18: Changes in surface potentials relative to electrode 15 (S1)

Figure 5.18 represents the potential distributions for electrode 15 compared to electrodes 1-14 and 16. Here, the plots for apical and medial electrodes compared to electrode 15 are very different. The distribution for electrode 15 is closest to the distributions for electrodes 14 and 16.

Similar 3-D topographic maps representing the electrical field distribution over the entire surface of the scalp and face are plotted for Subject S6. An example is provided in Figure 5.19 to explain the orientation of the plots with respect to locations on the subject's

head where potentials were recorded. The plot represents the right-hand side view of the subjects head. Subject S6's cochlear implant is on the right side.

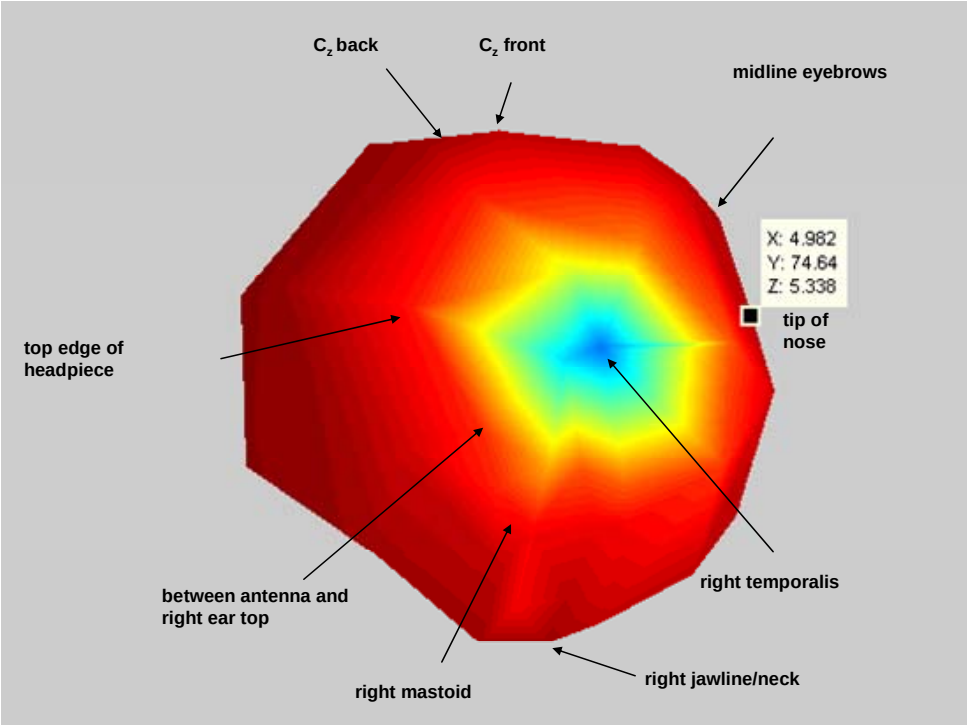

Figure 5.19: Plot showing recording locations for Subject S6

Nucleus devices can operate in the 3 monopolar modes with the following return electrode configurations: ECE1 (ball electrode located below the temporalis muscle), ECE2 (plate electrode on the case-band of the stimulator), and ECE1+2 (ball electrode and plate electrode tied together). Figure 5.20 represents the monopolar data for electrodes 3-22 referenced to the ball electrode located below the temporalis muscle. These data are scaled

by dividing by the global field power (GFP) as explained before. The "hot spot" i.e. the largest potential of the map is close to the temporalis muscle, whose location is marked in Figure 5.19.

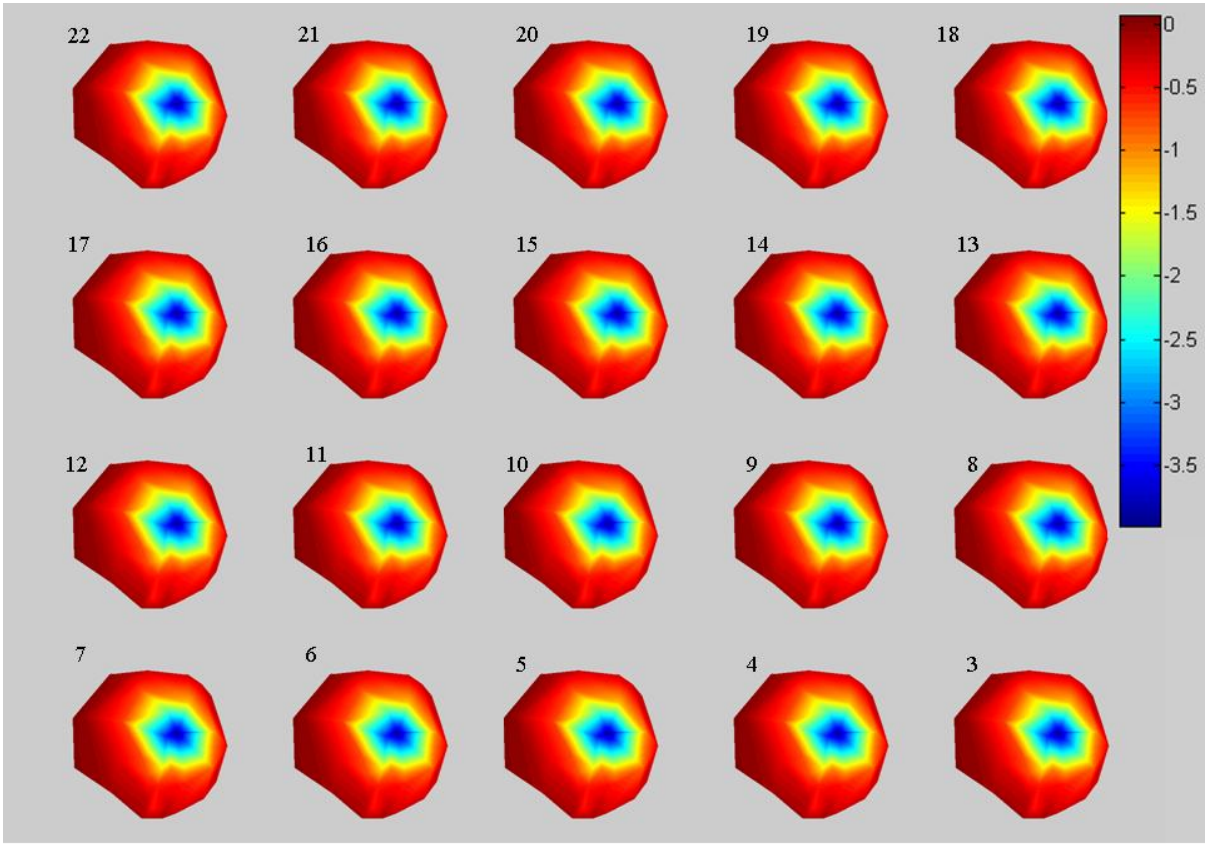

Figure 5.20: Scaled surface potential distribution (S6) - ball electrode

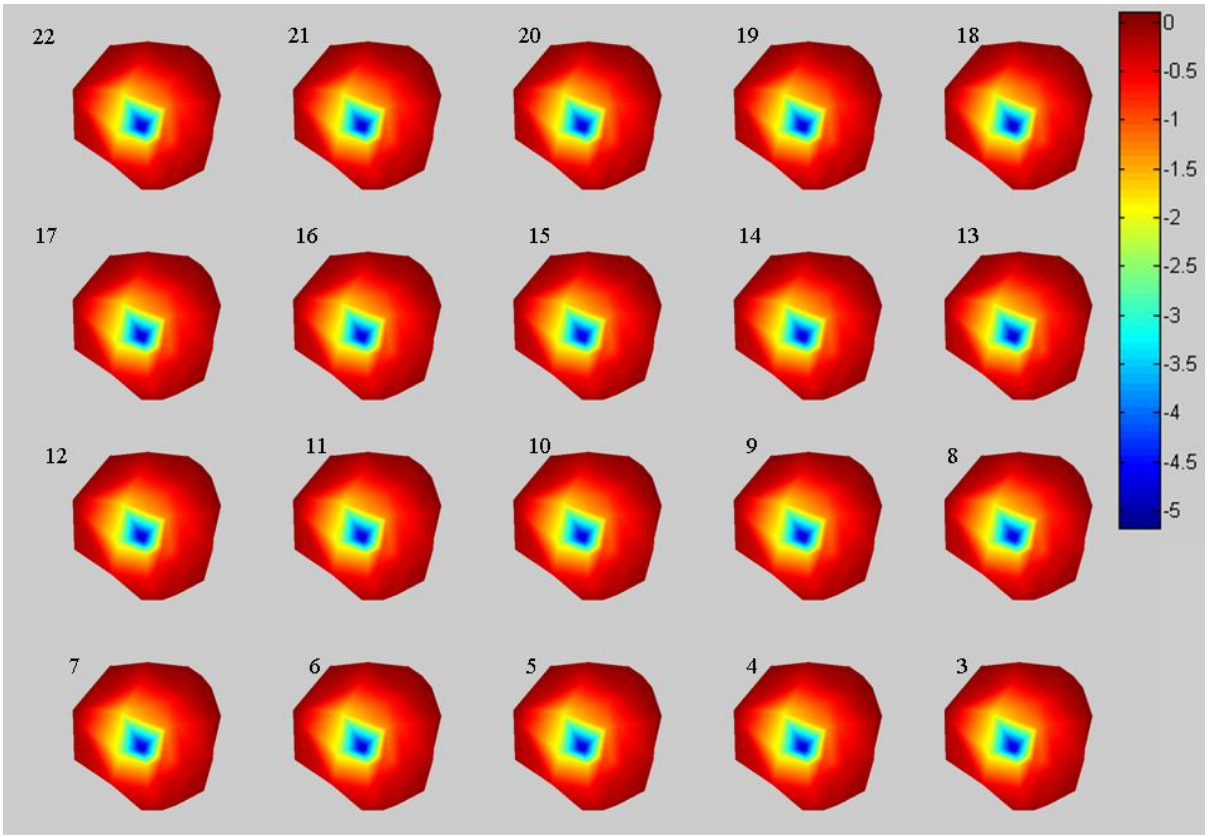

Figure 5.21: Scaled surface potential distribution (S6) – plate electrode

Figure 5.21 shows similar plots (obtained from the same subject) but with the device operating in the ECE2 mode, i.e. the monopolar contacts are referenced to the plate electrode. In Figure 5.22, the potential distributions are shown for the ECE1+2 condition, where the ball electrode and the plate electrode are tied together to represent the return electrode.

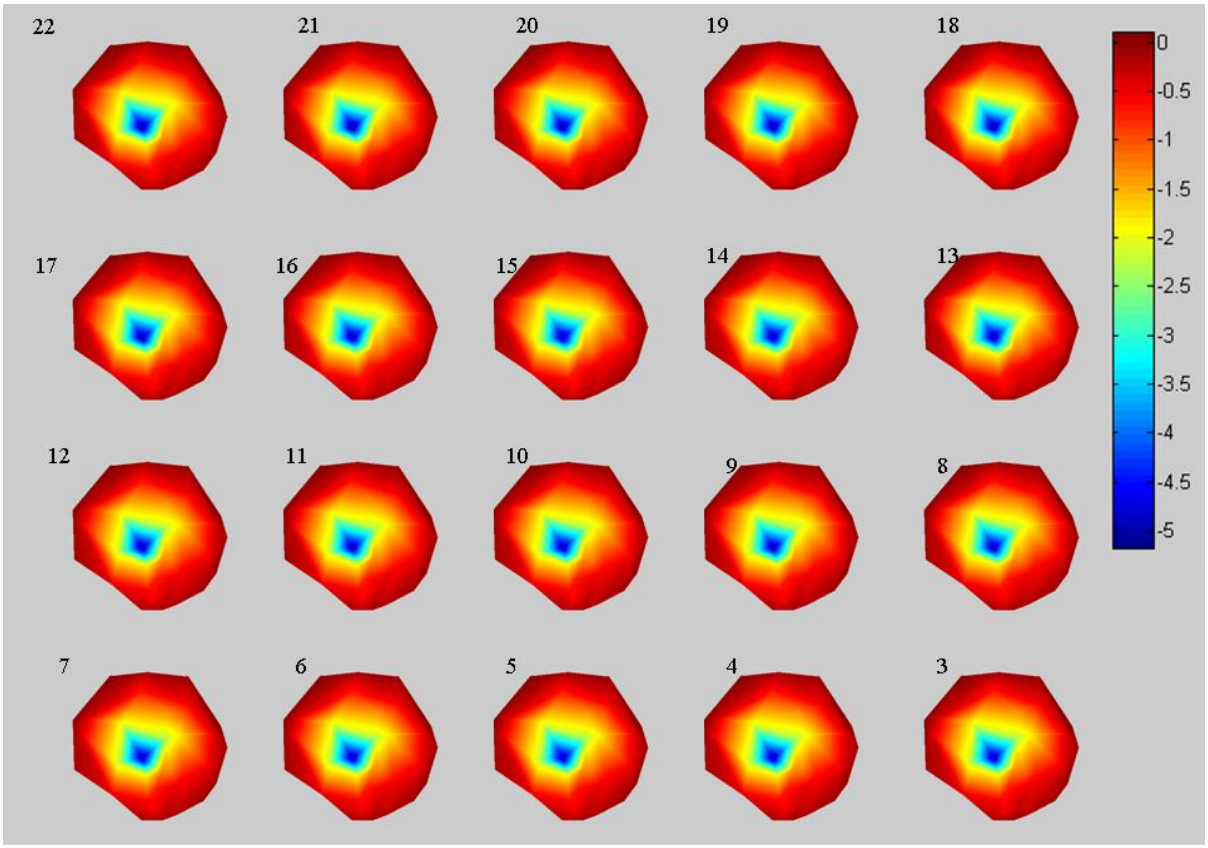

Figure 5.22: Scaled surface potential distribution (S6) – ball + plate electrode

Plots of monopolar distributions for electrodes 22, 15, 10, and 4 are generated for all the 3 monopolar stimulation modes. The color axes are set to the same limits for all figures. These plots show significant differences across the three monopolar conditions for the 4 electrode combinations shown. The field generated by the plate electrode contains the largest potential value near the implanted stimulator region. The potentials generated in the ECE1+2 mode of stimulation are influenced more by the plate electrode that they are by the ball electrode, when both the plate and ball electrode are tied together, as seen in Figure 5.23.

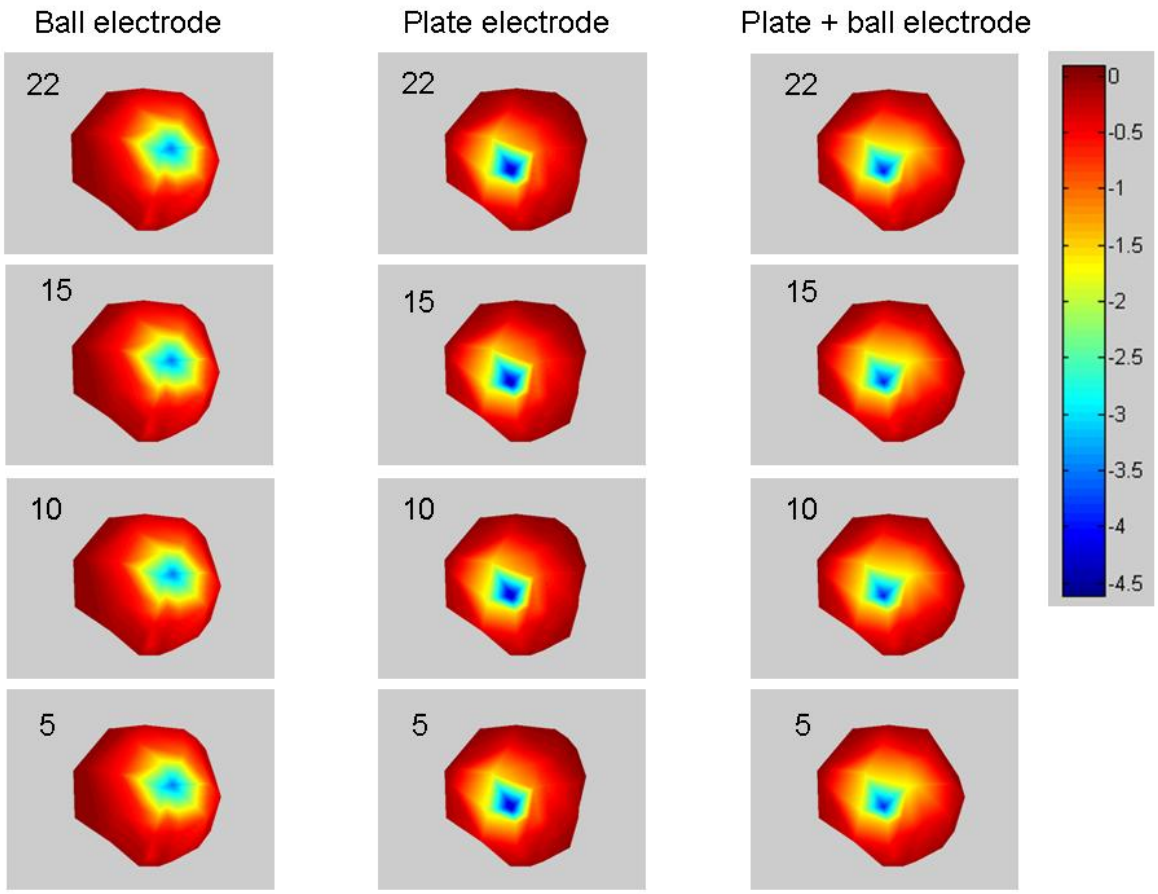

Figure 5.23: Comparing the 3 monopolar stimulation modes – Subject S6

5.3.2 Global Dissimilarities - Monopolar Data

Global Dissimilarity (GD), which is defined in Section 4.4.1, is a metric used to represent differences between surface potential distributions measured in cochlear implant subjects. This metric computes the topographic changes between any two surface maps independent of any amplitude differences. The peak-to-peak measures obtained from each subject are scaled such that the maximum amplitude of a particular distribution is of unit magnitude. This pre-processing is done to enable comparison across subjects. The GD value

between any two monopolar electrode conditions is computed from surface potentials that are measured across the entire surface of the head, scalp, and face in these subjects. The number of recording locations varies across subjects.

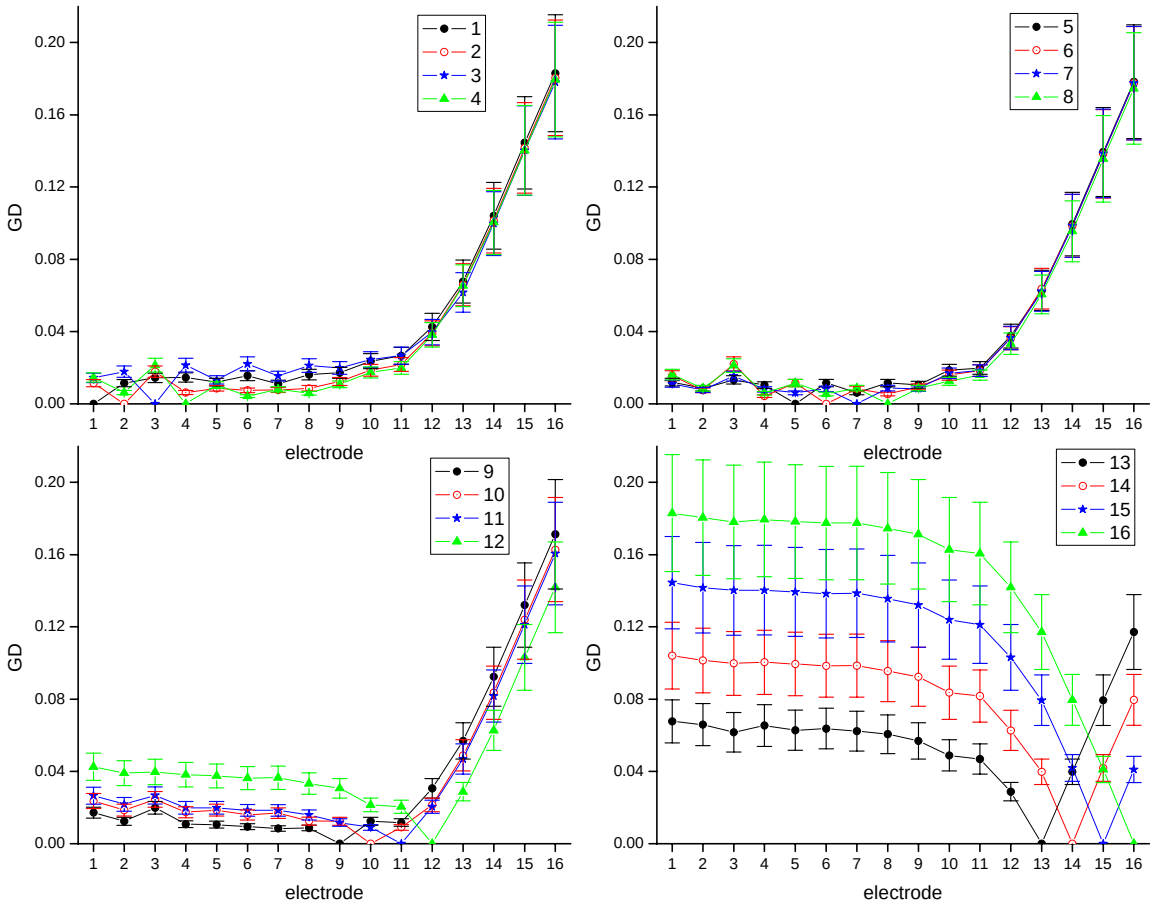

Figure 5.24: Global dissimilarities across all electrodes (S1)

Figures 5.24 and 5.25 represent the global dissimilarities across all monopolar electrode conditions in Subjects S1 and S2 respectively. The number of recording locations (*n*) for Subject S1 and Subject S2 are 32 and 39 respectively. Each sub-plot contains the

differences computed for a set of 4 electrodes (starting from apex to base) compared to all the other electrodes. The GD's are plotted on the y axis along with the standard error (SE) bars. The x axis represents electrode numbers. A global dissimilarity/difference value of zero indicates that there is no difference between the maps, which is the case when a map is compared with itself.

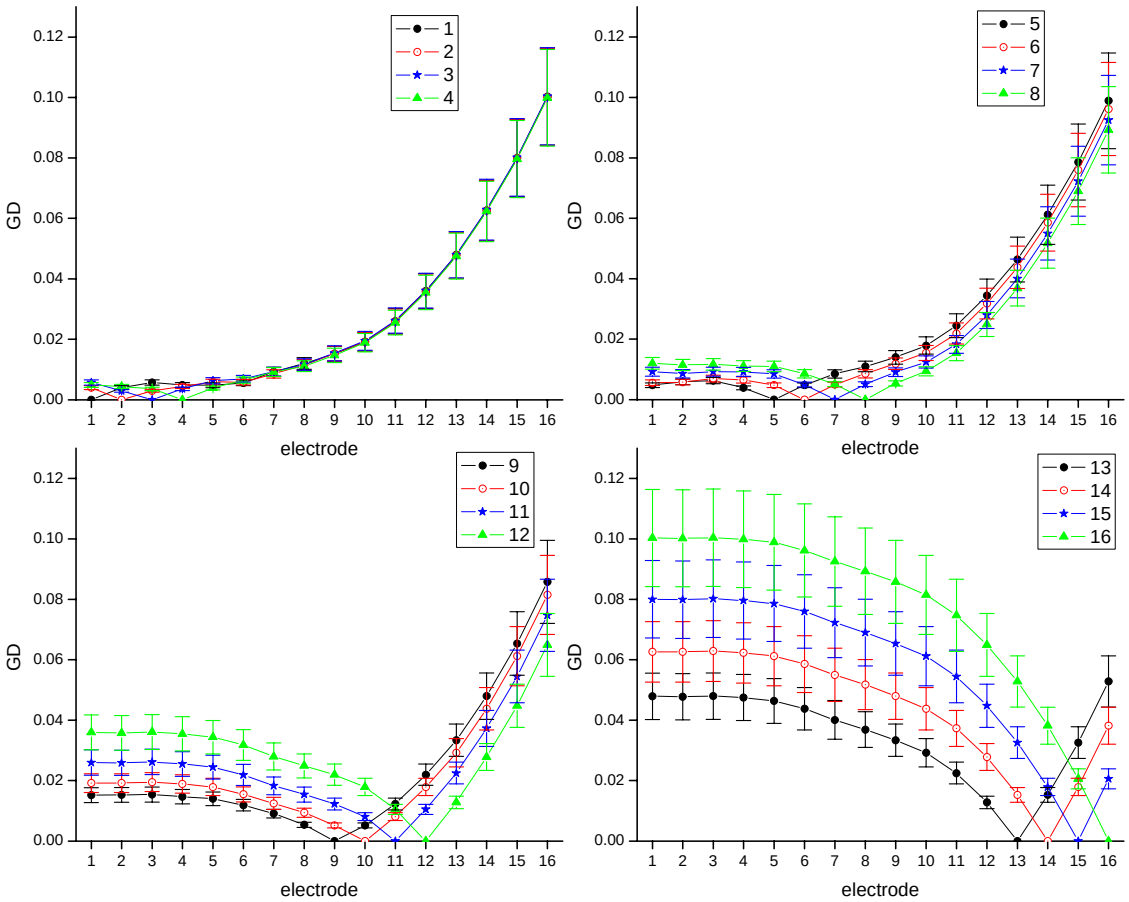

Figure 5.25: Global dissimilarities across all electrodes (S2)

Global dissimilarity for both subjects S1 and S2 show similar trends. When the maps for electrodes 1-4 are compared with the maps for all the other electrodes, small global differences are observed in the apical regions. These differences start to rapidly increase in the basal region. Electrodes 5-8 exhibit the same behavior. Larger differences in field structure are observed between distributions generated by electrodes 9-12 and those generated by the apical electrodes; however these large differences are approximately equal. The dissimilarities start to rapidly increase from electrode 12 onwards basally. Electrodes 13-16 exhibit larger GD's when compared to the apical electrodes. Again, these differences are large but remain steady across the apical region. The differences start to decrease closer to the basal region.

The vertical distances between any two standard error (SE) bars are a measure of significance; a gap of 1 (i.e. when the vertical distance between the SE bars equals the average value of the respective SE's) indicates statistically significant results at a level $P \approx 0.05$, while a gap of 2 (i.e. when the distance between the SE bars is twice the average value of the SE's) indicates that the result is highly significant at a level $P \approx 0.01$ (Cumming, Fiddler, & Vaux, 2007). The plots shown in Figures 5.24 and 5.25 clearly indicate that the distributions generated by stimulating apical electrode contacts are very different from those generated by stimulation of the basal electrodes. Furthermore, the error bars for the basal and apical electrodes are non-overlapping and thus these differences are highly significant. The differences between the apical electrodes, on the other hand, are small and statistically insignificant. In both subjects, significant differences exist in the distributions in the basal region. In Subject S1, the similarity in potential distributions for apical electrodes is observed for electrodes 1-11 whereas in Subject S2, distributions are

similar for electrodes 1-7. This may be related to the depth of insertion of the electrode array for each subject.

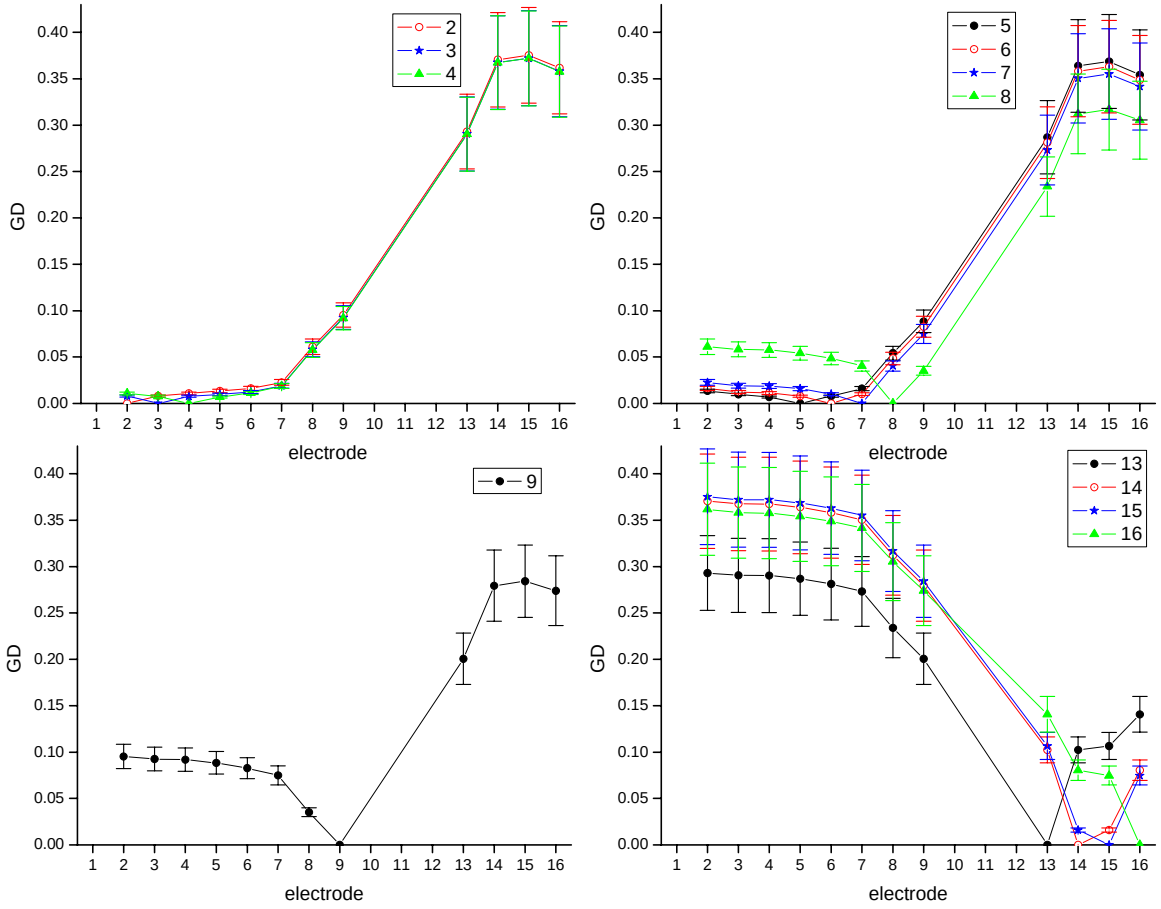

Figure 5.26: Global dissimilarities across all electrodes (S3)

Figure 5.26 presents the global dissimilarities computed for Subject S3. Data from electrode 1 is not presented since the input amplitude levels for electrode 1 are different from those for other electrodes, and hence would not enable meaningful comparison. Electrodes 10, 11, and 12 were clinically inactivated in this subject and hence could not be used in this

research study due to abnormally high electrode impedances which would force voltage compliance limits of the current sources. Apical electrodes up until electrode 7 have similar distributions. In general, the GD's computed across the active electrodes exhibit trends similar to those seen before. Also indicated by the plots is that basally-located electrode contacts 14, 15, and 16 generate potential patterns that are very similar to each other. Electrodes 5, 6, and 7 also exhibit this type of similarity. This is not observed in the previous subjects. The data presented in Figure 5.26 is based on surface potentials measured at 53 recording locations.

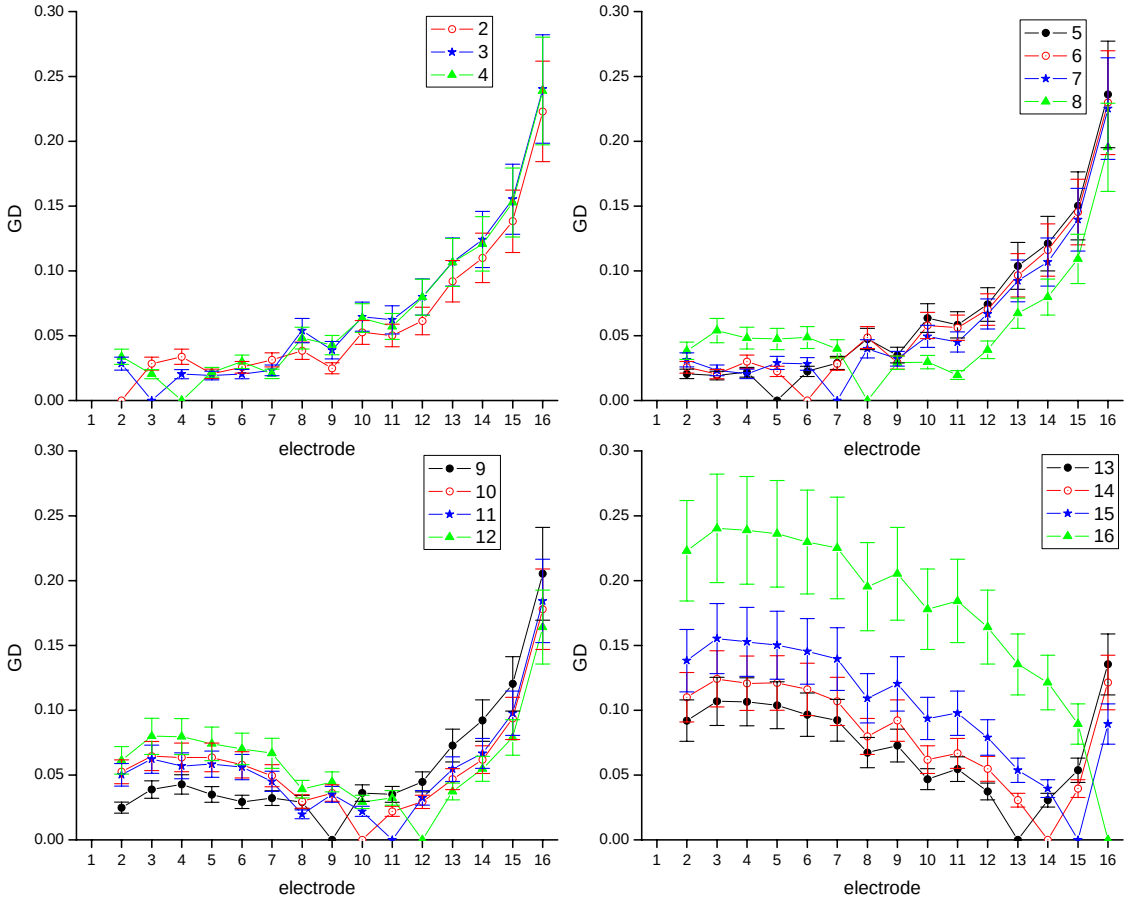

Figure 5.27: Global dissimilarities across all electrodes (S4)

The plots shown in Figures 5.27 and 5.28 represent the global dissimilarities across electrodes 2-16 in Subject S4 and Subject S5 respectively. Again, apical electrodes show similar distributions up until electrode 9 or 10 in both subjects. Basal electrode distributions are different from each other; however distributions generated by electrodes 13-15 appear to be more similar compared to the field generated by stimulating electrode 16. Data from electrode 1 is not included in these measures due to the fact that amplitude levels for electrode 1 are different from those for other electrodes, as explained previously. The number of recording locations in Subjects S4 and S5 are 33 and 24 respectively.

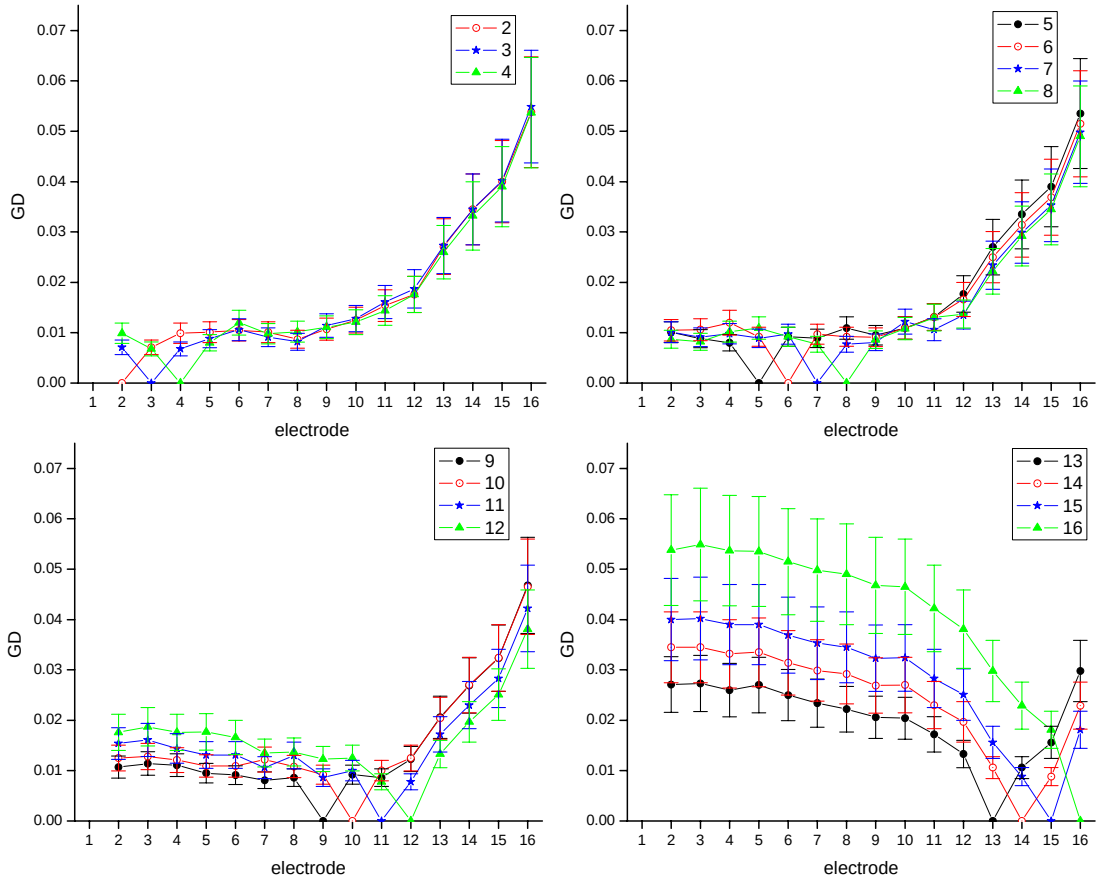

Figure 5.28: Global dissimilarities across all electrodes (S5)

The previous plots represented data from subjects with devices manufactured by Advanced Bionics Corporation. In these devices, electrode numbers *increase* from apex to base. Figure 5.29 represents the global dissimilarities for the data obtained from a Nucleus (Cochlear Corporation) subject. This subject has 20 active electrodes. The numbering scheme for electrodes is different in Nucleus devices. Here, smaller numbers indicate basal electrodes and larger numbers indicate apical electrodes. Thus electrode numbers *decrease* from apex to base. In Figure 5.29, the x axis represents electrodes from the apex to base (similar to the previously-presented data from Advanced Bionics Corporation devices); however the electrode numbers decrease. The two most basally-located electrodes (electrodes 1 and 2) that convey high-frequency information are turned off in Subject S6 due to high impedances associated with these electrode contacts.

Nucleus devices can operate in the 3 monopolar modes that are described earlier. These modes include the following return electrode configurations: ECE1 (ball electrode located below the temporalis muscle), ECE2 (plate electrode on the case-band of the stimulator), and ECE1+2 (ball electrode and plate electrode tied together). Figure 5.29 represents the global differences for monopolar data generated by electrodes 3-22 referenced to the ball electrode located below the temporalis muscle. The data are measured at 41 locations on the scalp, face, and neck regions for Subject S6. GD's computed for the Nucleus subject (S6) are similar to those observed in previous subjects.

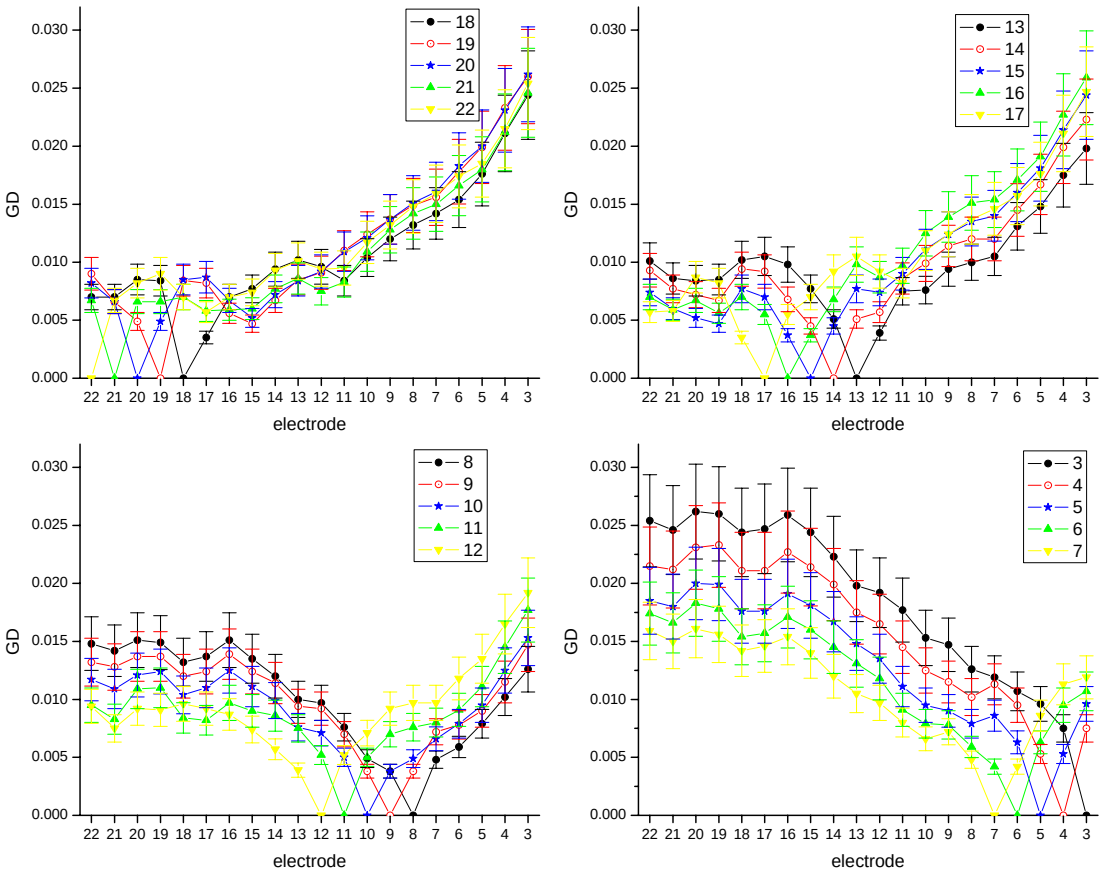

Figure 5.29: Global dissimilarities across all electrodes (S6)

In this study, each subject serves as their own control. The data presented indicate a significant difference in the potentials for apical versus basal distributions. Also, the distributions for apical electrodes are very similar. This pattern is consistent across all subjects as shown above. Certain differences, however, are observed across subjects. The number of apical electrodes that are very similar to each other varies across subjects. This may be related to the individual's anatomy and insertion depth of the electrode array. In most subjects, distributions in the basal region are different from each other with the exception of Subject S3. Also observed across subjects are the varying ranges of the GD

metric for all electrode combinations. As seen in the plots, the range of GD's for Subject S1 is twice as large as it is in Subject S2. This may be related to several factors such as the subject's electrical dynamic range, anatomy of the cochlea/surrounding temporal bone, size and shape of the head, and etc. Also, the protocol did not measure potentials at identical locations on the surface of the scalp and face across all subjects which may also be a contributing factor.

Additional data from Subject S1 is presented in Figure 5.30. GD's are computed between maps generated at the 60% and 100% stimuli levels for each odd-numbered electrode. The maps for each electrode are normalized to the maximum value of the amplitude. This is done for each electrode group. As seen in Section 5.1, varying the input stimuli did not change the topography of the field distribution, and the maps at the 60% and 100% level were found to be topographically similar. In theory, the GD's computed in Figure 5.30 should approximately equal zero because they are computed between maps that are topographically similar. However, the values computed lie approximately within the 0 - 0.02 range. This implies that computed GD values that lie between the range of 0 – 0.02 indicate similar topography in maps computed for the same subject and across identical recording locations. GD values within this range are seen for the same subject when apical maps are compared (see Figure 5.24). The recording locations for Figure 5.24 and 5.30 are also identical. This analysis shows once again how topographically-similar the apical maps are for this subject.

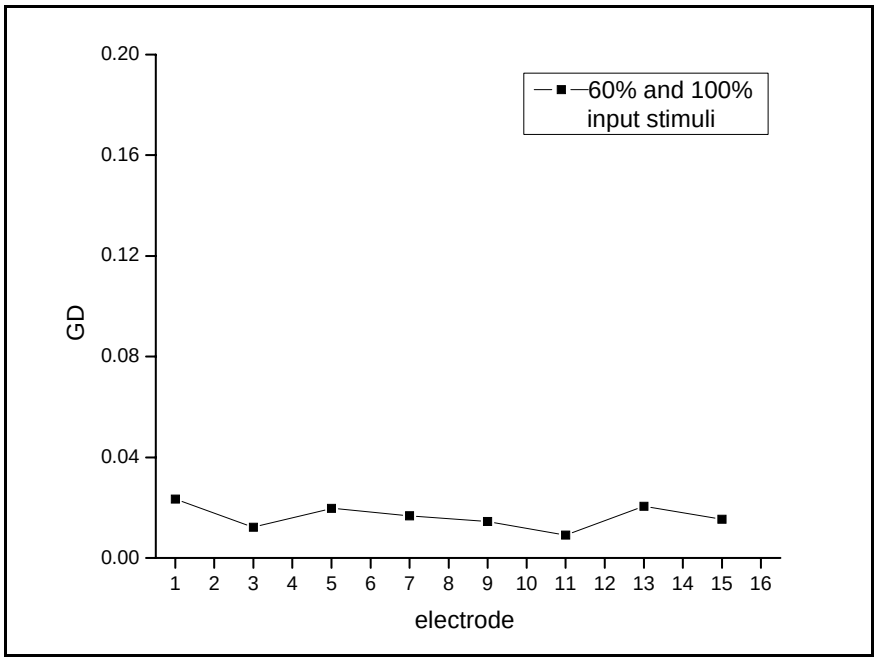

Figure 5.30: GD's between fields generated due to 60% and 100% stimuli levels

A summary plot showing the global differences between all monopolar stimulation modes for all the subjects tested is provided in Figure 5.31. Repeated measures that are obtained from Subject S1 on separate occasions ($S1_a$ and $S1_b$) are consistent with each other. $S6_a$, $S6_b$, and $S6_c$ represent the data from subject S6 collected in the ECE1 (ball electrode), ECE2 (plate electrode), and ECE1+2 (ball electrode + plate electrode) modes respectively.

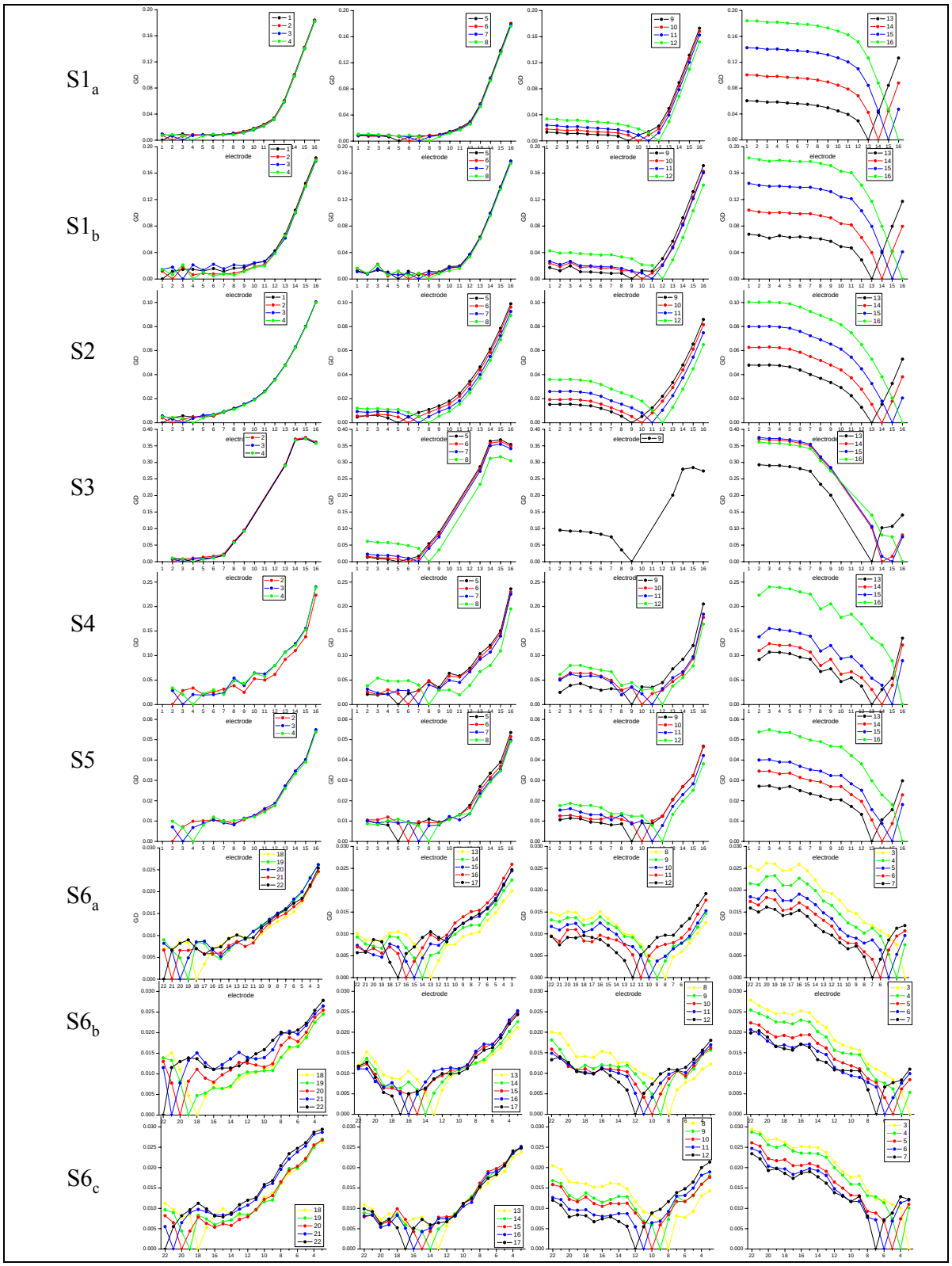

Figure 5.31: Summary plot of global differences

The global dissimilarity plots presented thus far are based on surface potential measures across all recording locations. The total number of recording locations for the subjects ranges from 24 – 53. Further analysis is performed on a select number of recording locations in Subject S1 and S2. A total of 10 recording sites are chosen for each subject based on where surface potentials change the most across monopolar stimulating electrode conditions. Figures 5.32 and 5.33 represent the GD maps for Subject S1 and Subject S2 respectively.

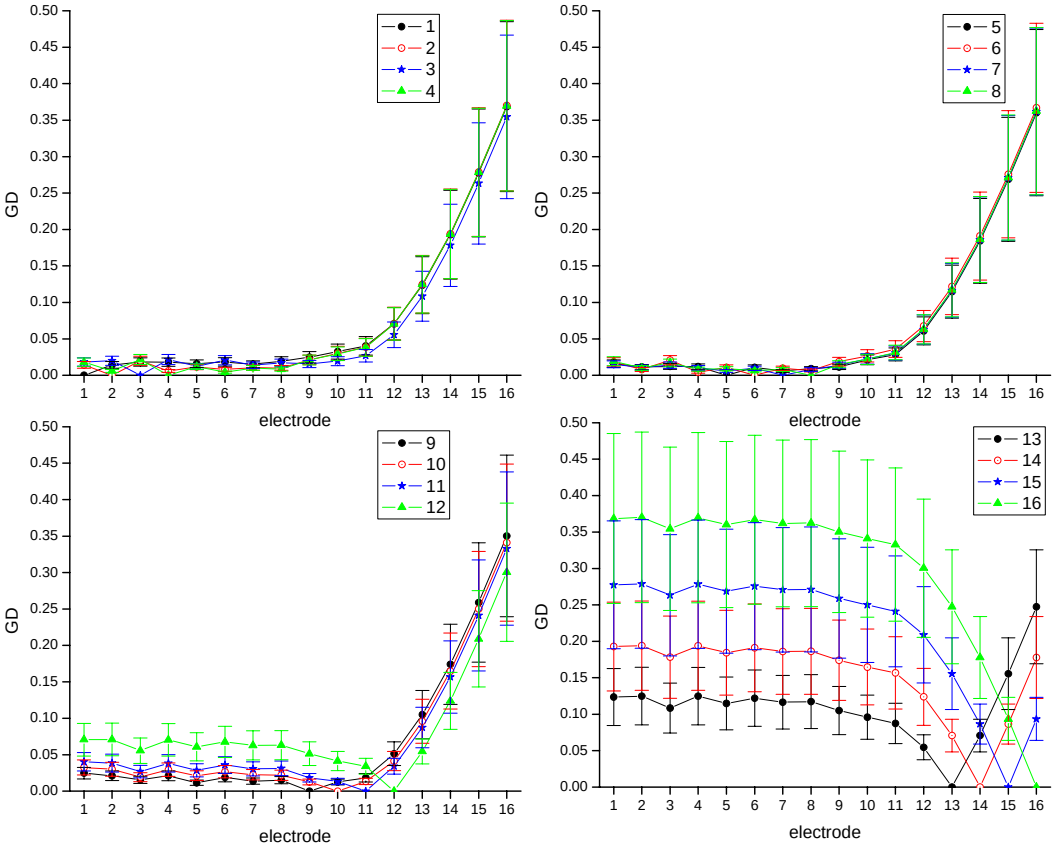

Figure 5.32: Global dissimilarities across all electrodes (S1) at a select number (10) of recording locations

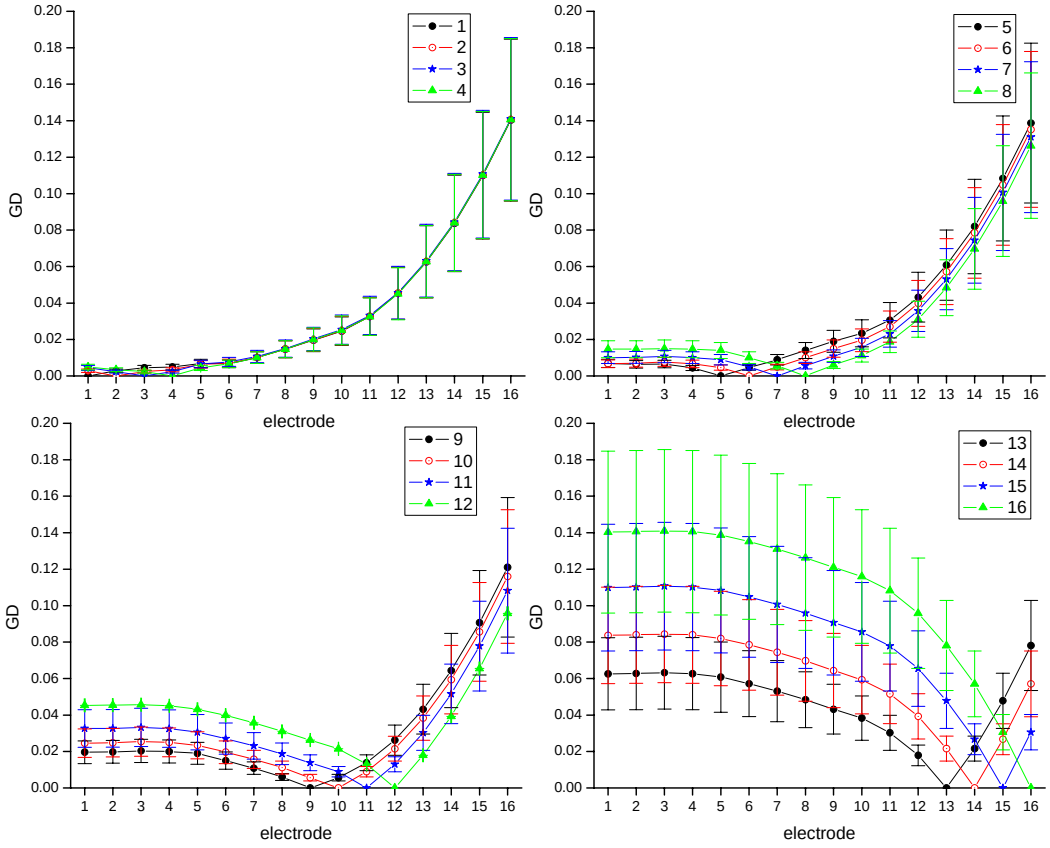

Figure 5.33: Global dissimilarities across all electrodes (S2) at a select number (10) of recording sites

The trends for the global dissimilarities remain the same even when the number of recording sites is reduced to 10 from 32 and 39 in Subjects S1 and S2 respectively. It appears, however, that the range of values for the GD metric approximately increases by a factor of two when global dissimilarities are computed at a reduced number of recording locations (10) that provide the most information regarding the changing surface potentials. These recording sites include the cheek, neck, and ear regions on the side ipsilateral to the

implant. Rapidly-changing potentials are also observed in the regions between the ipsilateral ear and "C_z back".

5.3.3 Global Dissimilarities - Bipolar Data

Surface potential data are recorded for various bipolar electrode combinations. In general, bipolar data in the apical region consists of very small potentials, and cannot be separated from the noise floor.

Results from the analysis of some bipolar data are presented in Figure 5.34. Here, bipolar combinations for electrodes 6-14 referenced to a basal electrode 15 are shown. The mapped GD's reflect small differences in the apical region compared to the basal region, which is in agreement with the results from the monopolar data shown previously. This observation is interesting because it shows that potential patterns show similar trends for a remote return electrode (case-band return electrode for the monopolar condition) as well as for an intracochlear return electrode (electrode 15 for the bipolar condition). This may suggest that current flow patterns are largely influenced by the intracochlear electrode contacts rather than by the location of the return electrode.

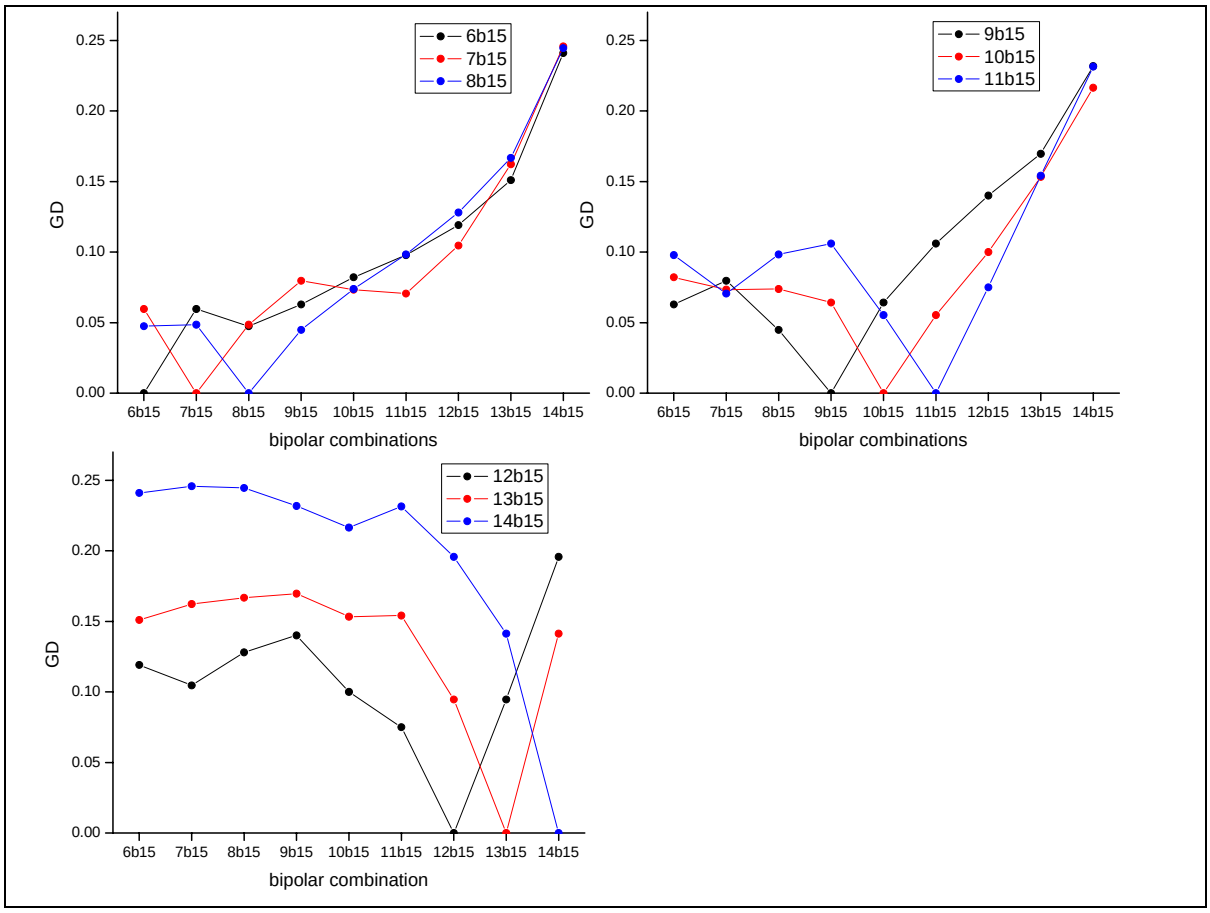

Figure 5.34: Global dissimilarities for bipolar combinations (S2)

During data collection, the reference (negative) recording electrode is generally placed at a remote site (the back of the neck midline) where the potentials are very small and negligible. This basically allows the differential recording to closely reflect the potential measured by the moving electrode probe (positive). Some earlier data collection procedures did not use this protocol and the reference electrode was placed at a non-remote site. *Average referencing* is used to remove the bias due to this. Average referencing is a process by which the mean across all recording locations is subtracted from each individual potential

value in a distribution. This is done across all electrode distributions in Subjects S3, S4, and S5.

5.3.4 Cluster Analysis

Hierarchical cluster analysis is carried out on the data sets described above as a further means to show differences and aggregations across different electrode distributions. Each electrode distribution represents a specific object/group. The features for each group are represented by the surface potentials measured at each recording location. The features are weighted such that locations on the scalp and face where potentials are constantly changing are ranked higher compared to other locations that convey little information about the changing electrical potential field. Objects are compared with each other based on differences between the corresponding weighted features. An *average linkage* algorithm then calculates the average of all the weighted differences. This metric is then used to form clusters between the groups. The full methodological approach for this cluster analysis is described in Section 4.4.2.

The results of this analysis are represented in the form of tree diagrams or dendrograms for all the subjects. Along the x axis, the strongest associations between objects are formed first, and the electrode numbers appear in that order along the x axis. The y axis represents the metric used in forming these associations. Figure 5.35 represents the dendrogram for Subject S1. Electrodes 4 and 6 most closely resemble each other and form the first association. Following this is an association between electrode 8 and electrodes 4 and 6, then electrodes 5 and 7 form an association. Electrode 2 groups together with electrodes 4, 6, and 8, and this association is then linked to electrodes 5 and 7 and so on. Further along the tree diagram, electrodes 12 and 13 aggregate followed by electrodes 14 and

15. Electrodes 12 and 13 then cluster together with the apical electrodes. Finally, electrode 16 joins electrodes 14 and 15, and these link with the rest of the electrodes. Basically, the tree diagram shows that electrodes 1-11 all form strong associations with each other immediately (indicated in red in the tree diagram).

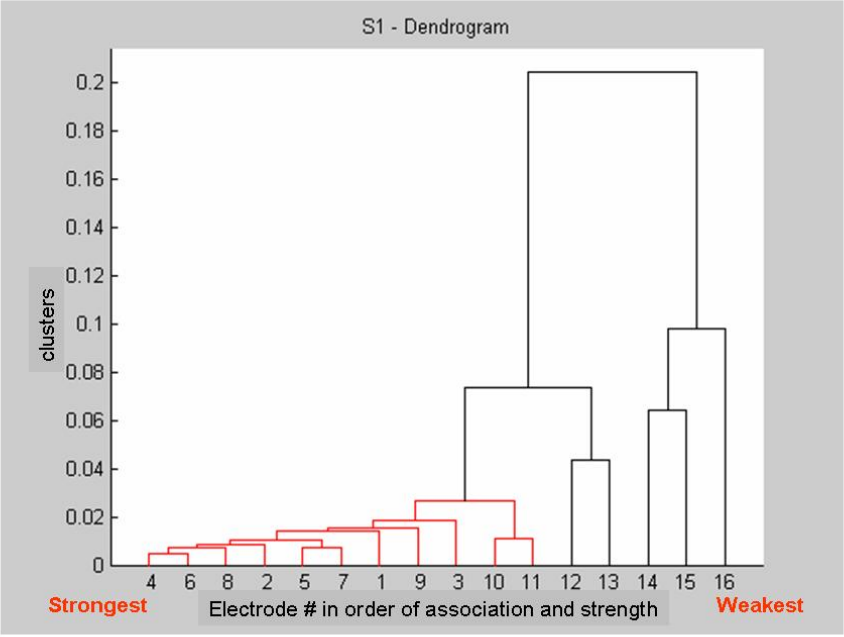

Figure 5.35: Dendrogram for Subject S1

Figures 5.36 and 5.37 represent tree diagrams for Subjects S2 and S3. The organizational structure of clusters within the apical group is different; however in general apical electrodes cluster together strongly and basal electrodes form weak associations. Subject S2's data form the following 4 distinct clusters: electrodes 1-6, then electrodes 7-10, followed by 11 and 12, and basal electrodes 13-16. Subject S3's data is unique in that differences between electrodes 14-16 are smaller than those observed in other subjects

(Figure 5.26). This is reflected in the tree diagram as well. Figure 5.38, which represents the dendrogram for Subject S4, shows how electrode 16 is highly dissimilar when compared to other basal electrodes. This observation, also made in previous GD plots, suggests that electrode 16 may not be within the cochlea. This phenomenon is observed in Subject S5's dendrogram in Figure 5.39 as well, but to a lesser extent. Data from the Nucleus subject, S6, with a different electrode array (in the monopolar ball electrode stimulation mode) are presented in Figure 5.40. Apical electrodes 14-22 form a rather large cluster. Electrodes 6-10 and 11-13 form clusters as well and aggregate. The high-frequency electrodes 3-5 in the base of the cochlea are most dissimilar compared to other electrodes.

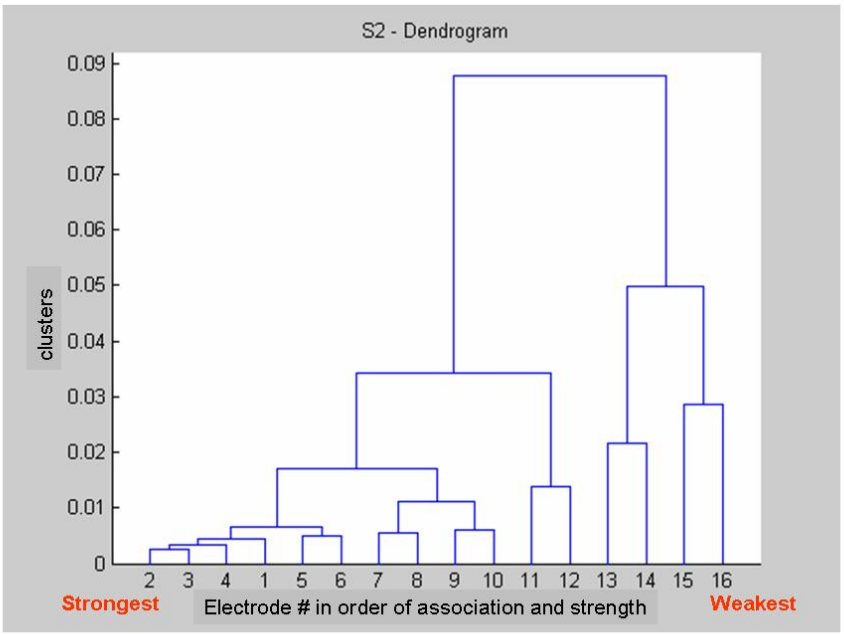

Figure 5.36: Dendrogram for Subject S2

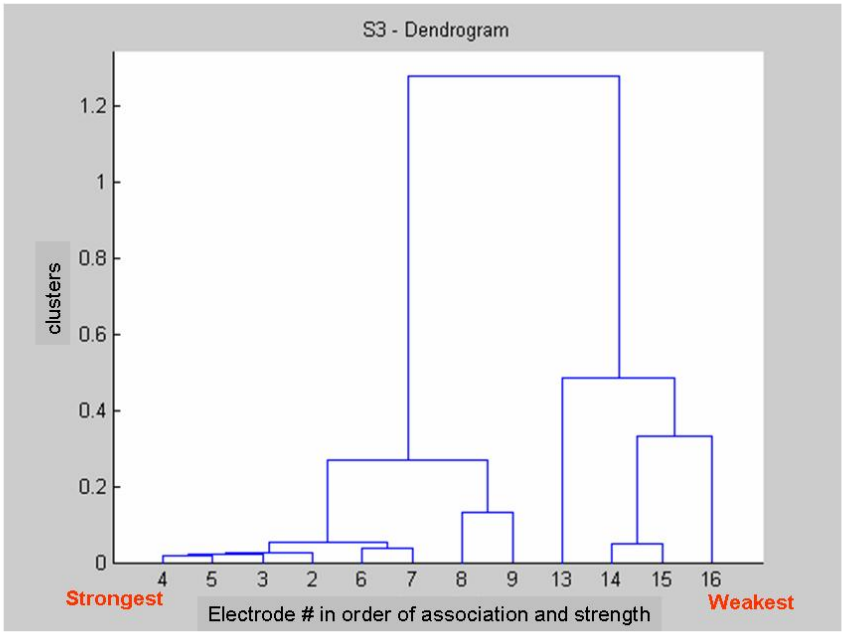

Figure 5.37: Dendrogram for Subject S3

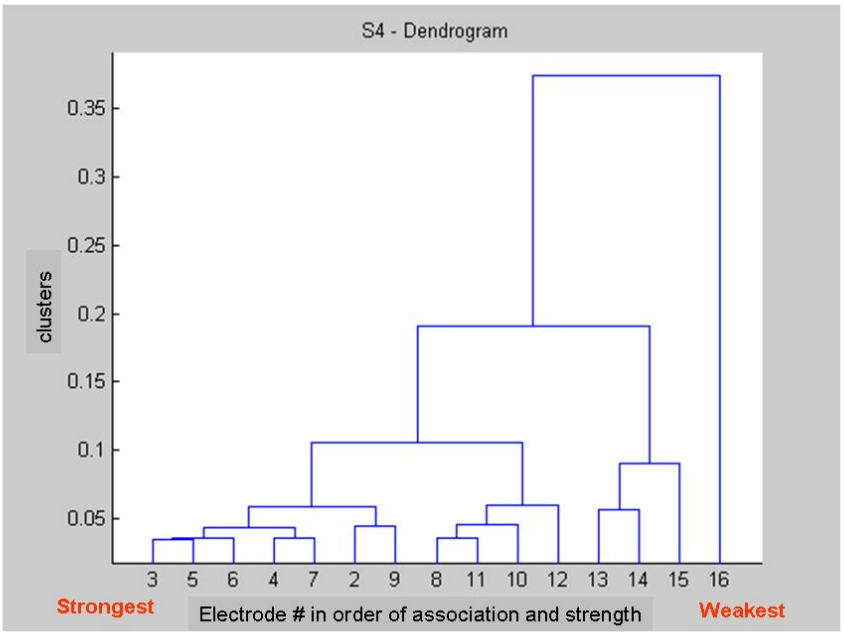

Figure 5.38: Dendrogram for Subject S4

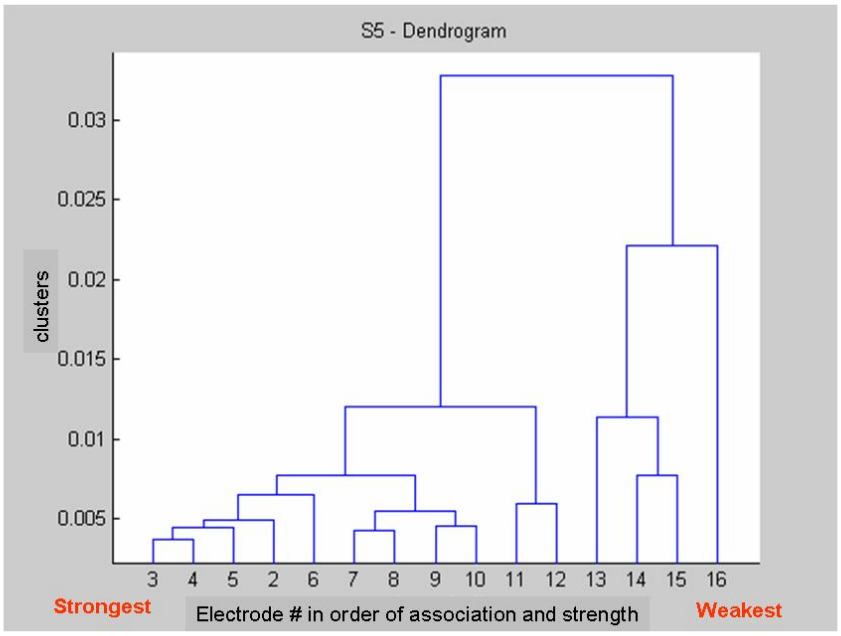

Figure 5.39: Dendrogram for Subject S5

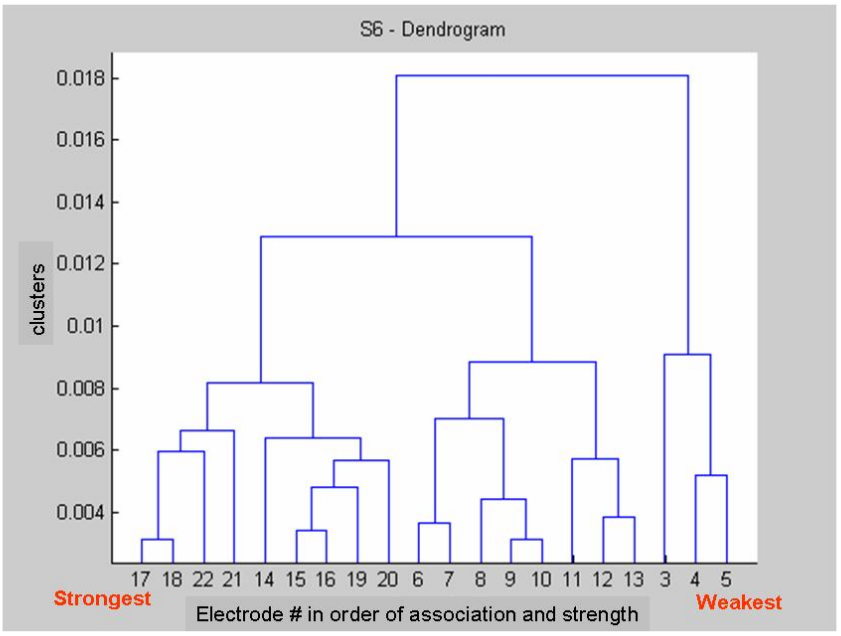

Figure 5.40: Dendrogram for Subject S6 – ball electrode mode

Section 5.3 presented different techniques that are employed in this study to analyze the surface potential distribution patterns in cochlear implant subjects. Differences between apical and basal distributions are observed across all subjects. If all current were to follow the same classical route (i.e. flow out into the modiolus and exit via the internal auditory meatus into the cranium), surface potential patterns measured on the scalp and face would be similar for all electrode contacts. The distinct differences seen in these patterns confirm the existence of different primary current pathways apical and basal electrode contacts. The similarity between apical distributions suggests a specific pathway for apical contacts, different from that of basal contacts. The following section explores in detail what these pathways may be.

5.4 Alternate Current Pathways

The theory and implementation of the inverse dipole source localization techniques have been explained in Chapter 3. The predicted dipoles for apical and basal surface potential distributions are compared and analyzed to provide information related to current pathways.

5.4.1 Dipole Source Localization

The goal of dipole source localization is to find the best-fitting generator source for the measured data. The forward model described in Section 3.2.2 is used to generate the simulated surface potential data. The measured data from cochlear implant subjects is then compared with the modeled data until the error measure between the two distributions is minimized. The inverse model basically *searches* for the equivalent dipole source within a

previously-defined search region. Details regarding the search region have been provided in Section 3.4.2.1.

The dipole is usually modeled as a source and a sink. In the bipolar mode of stimulation, the two intracochlear contacts represent the source and sink. Here, the source and sink are closely-spaced. In the monopolar mode of stimulation, the intracochlear stimulating electrode and the remote reference electrode form the dipole, in which the source and the sink are further apart. As explained in Section 3.4.2, during monopolar stimulation, the model defines the return electrode as the source of the dipole. The sink of the dipole is defined by the electrode contact on the array, depending on the monopolar stimulus condition. The sink changes as the location of the stimulated electrode contact changes within the basilar membrane. The inverse model then *searches* for the equivalent dipole source which is represented by the moment of the dipole that provides the closest fit to the data, based on prior information regarding the location of the source. The methodology for finding equivalent dipoles is described in Section 3.4.2.2. The dipole moment defines the amplitude and orientation of the dipole. Using vector algebra, the moment is added to the source to get the location of the sink. Using this approach, predicted dipole sinks are calculated for all monopolar conditions. The estimated dipole sinks provide information about where current may be flowing within the cochlea.

A computed tomography (CT) image obtained from the Washington University in St Louis, which provides a cross-sectional view through the cochlea, is shown in Figure 5.41. The transverse plane through which the cross sectional view is obtained is shown in Panel A. The following anatomical regions around the left cochlea are clearly marked in Panel B: (1) the dense bone surrounding the cochlea, (2) the internal auditory meatus, which is the bony

canal through which the bulk of the current is assumed to flow out from the cochlea, (3) the air cells, and (4) the temporal bone. The orientation of the cross sectional view is given by the head coordinate system, which is provided for reference in Panel C.

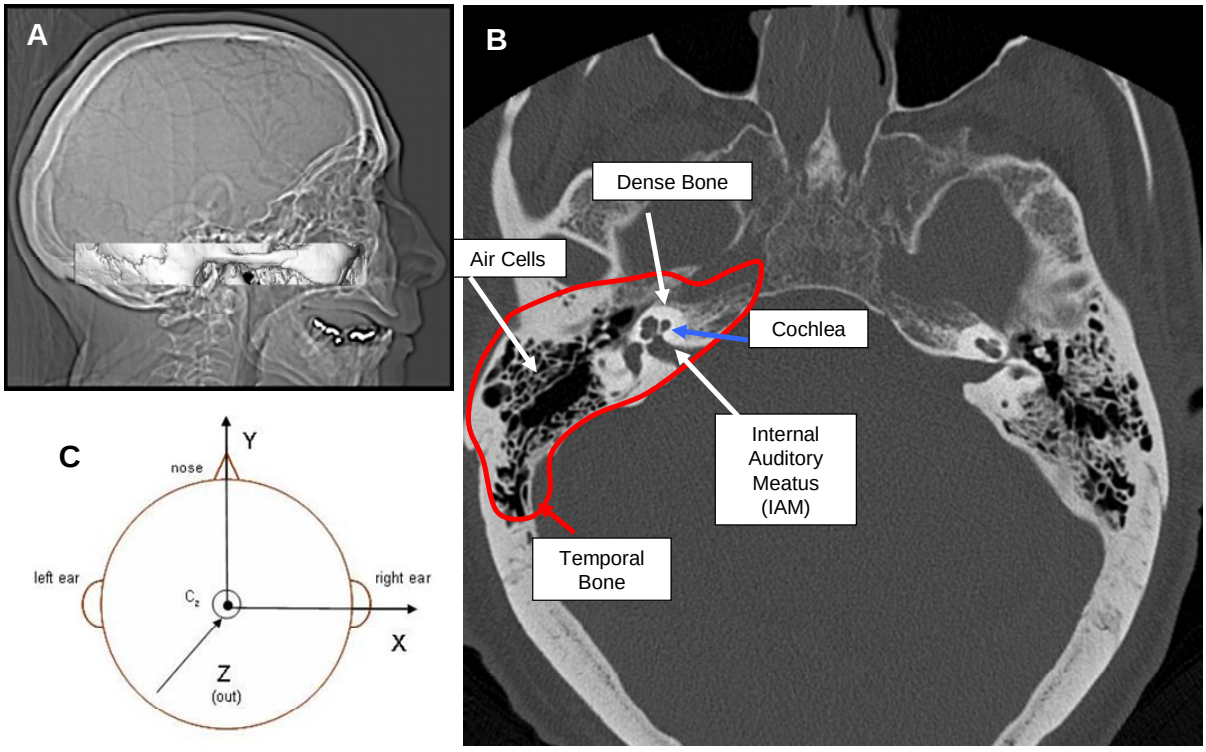

Figure 5.41: CT image – A: transverse section through the head, B – cross-sectional view through the left cochlea, and C: head coordinate system

The spatial locations for the reference electrode and intracochlear electrode contacts vary from subject to subject, but can be approximated based on existing CT imaging data. An estimate for the return electrode location on the case-band of the implanted stimulator

reference electrode location is determined during the experiment by obtaining the spatial coordinates of the headpiece over it. Section 3.4.1.2 describes the methodology involved in obtaining the spatial coordinates for the intracochlear electrode array in terms of the *head coordinate system*. Existing CT data for the intracochlear electrode contacts in a cochlear implant subject are transformed to the head coordinate system using the equations described in Section 3.4.1.2. The electrode array model in Figure 5.42, referenced to the head coordinate system (also shown in the figure), is obtained for a head radius of approximately 70 mm, and is based on existing CT data. The electrode array is within the left cochlea. The electrode contacts are numbered from 1-16 from apex to base. Figure 5.43 represents the same electrode model, but referenced to the *cochlea coordinate system.*

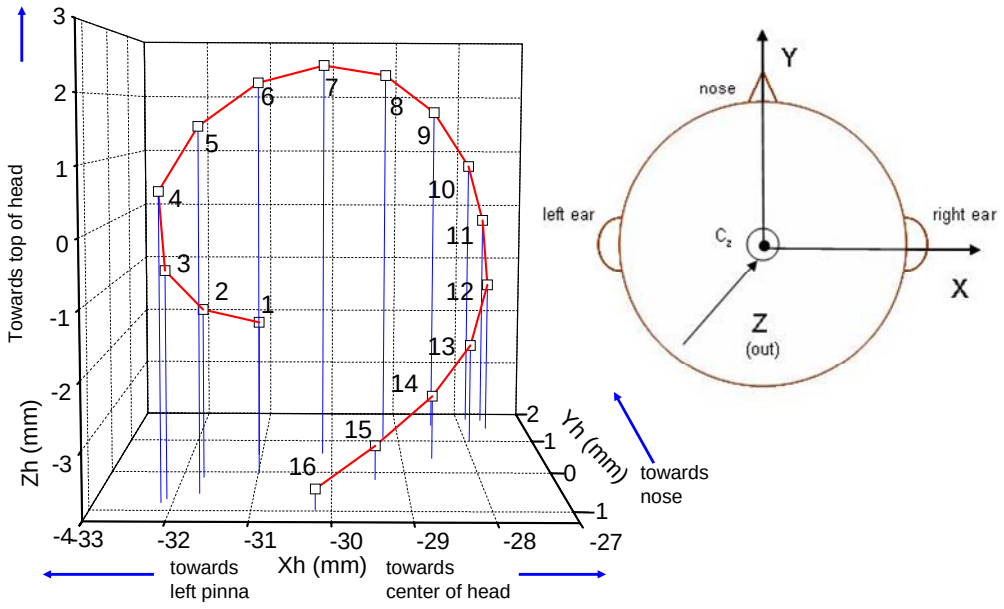

Figure 5.42: Left cochlea model – head coordinate system

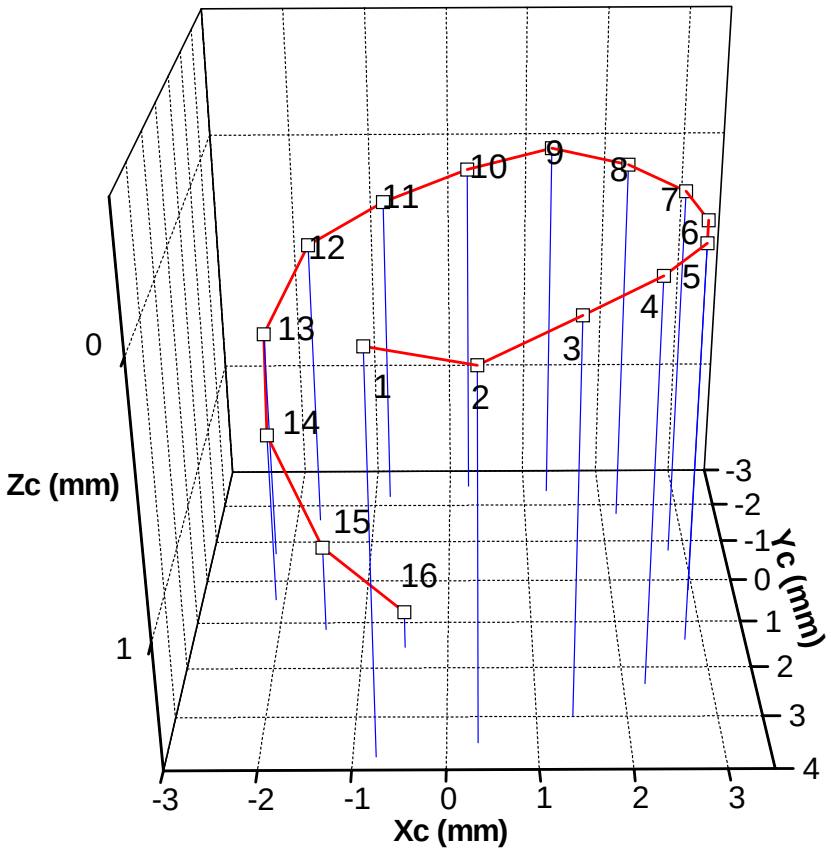

Figure 5.43: Left cochlea model – cochlea coordinate system

Surface artifact potentials measured in response to monopolar stimulation are analyzed using dipole source localizations methods. Based on prior information regarding its spatial coordinates, the location of the return electrode is fixed and made to lie between the bone and skin compartments of the multiple shell model. A total of 16 dipole moments are found in response to stimulation by each intracochlear electrode contact. The estimated dipole moments are added to the source (i.e. the location of the return electrode) to represent the spatial location of the dipole sink/electrode contact. Figure 5.44 represents the results

from this analysis for Subject S1. The plot is in the head coordinate system, and the orientation and limits of the axes are similar to those in Figure 5.42.

In general, the location and orientation of the electrode contacts with respect to the head and the cochlea line up accurately. The actual numbers, however, on the axes for Subject S1 are different when compared to the cochlea model. This is to be expected because the radius of Subject S1's head is larger compared to the model. Also, the anatomical location of the cochlea may vary from subject to subject. Furthermore, the spherical head model used only crudely represents the anatomy of the head.

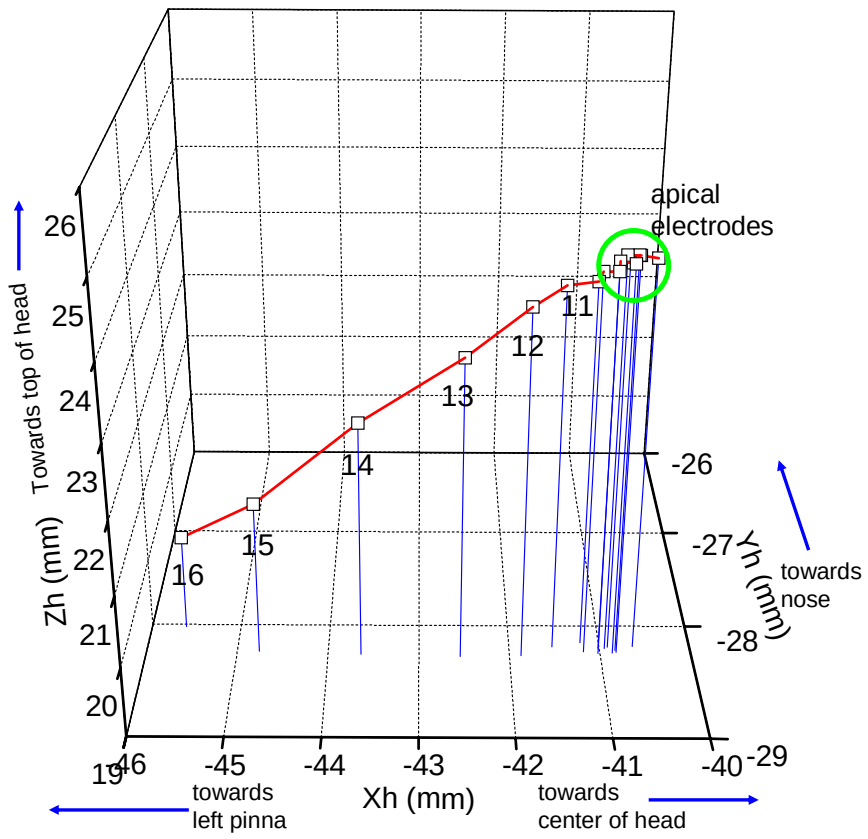

Figure 5.44: Dipole source localization results – Subject S1 (left cochlea)

In Figure 5.44, results indicate that the predicted dipoles for the apical contacts cluster together (shown by the green circle). The predicted dipoles for the basal contacts are located along the basal turn of the cochlea. The dipoles for the apical contacts, however, cluster together at a site that is further away from where the apical contacts are expected to lie. This location, which lies to the right of the cochlear apex, coincides with the internal auditory meatus of the left cochlea, and suggests that the current flow pathway for the apical contacts is primarily through the internal auditory meatus.

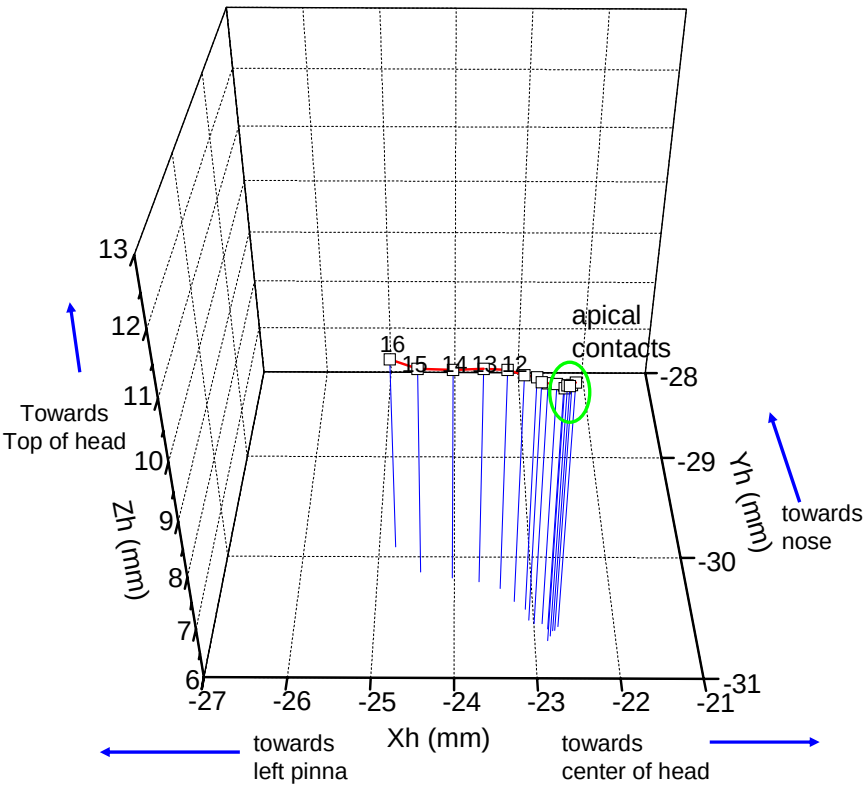

Figure 5.45: Dipole source localization results – Subject S2 (left cochlea)

A similar analysis of dipoles predicted for Subject S2's surface potential data is presented in Figure 5.45. These results are generally similar to those presented for Subject S1. A smaller number (6-7) of electrodes cluster together at the remote site when compared to Subject S1. This was observed earlier as well in Subject S2 where electrodes 1-6 had potential distributions that were very similar. Again, the location of the predicted dipoles for the apical contacts suggests a primary current flow pathway through the internal auditory meatus for these contacts, while the dipoles for the basal contacts appear to be a function of their location within the cochlea.

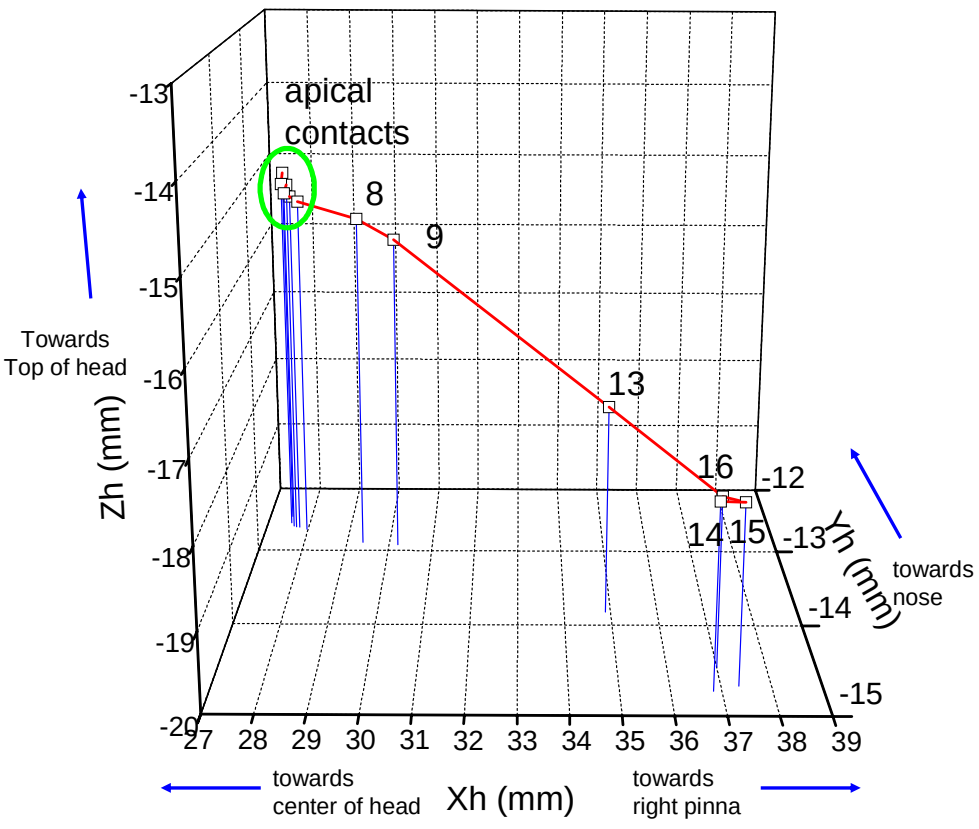

Figure 5.46: Dipole source localization results – Subject S3 (right cochlea)

Dipole source analysis for Subject S3, whose implant is on the right side, is shown in Figure 5.46. According to the electrode model, the apical contacts are expected to lie on the right side, closer to the right pinna. However, they cluster together at a location which coincides with the right internal auditory meatus. Results for Subjects S4 are shown in Figure 5.47. The measured surface potential distributions were different across stimulating electrode conditions in this subject (see Figure 5.27). However, the predicted dipoles all cluster together for this subject. This may suggest that the 4-shell model is crude, which in fact it is, and may not provide an accurate means of predicting dipoles.

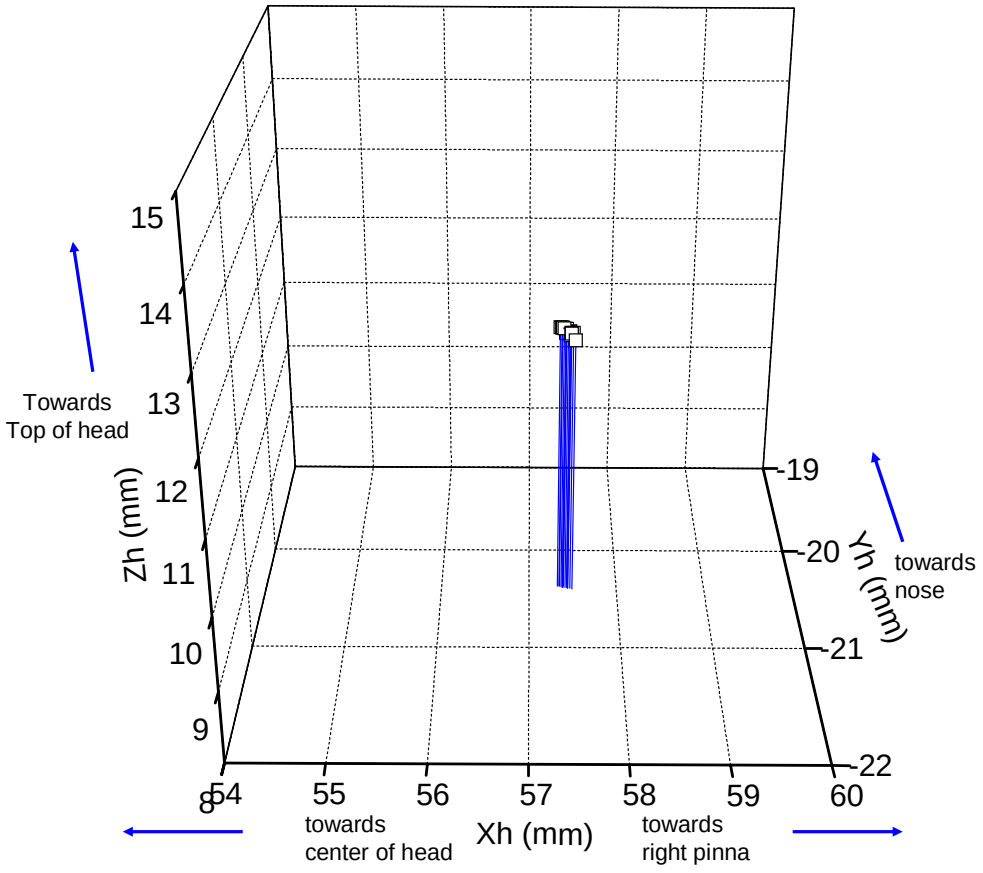

Figure 5.47: Dipole source localization results – Subject S4 (right cochlea)

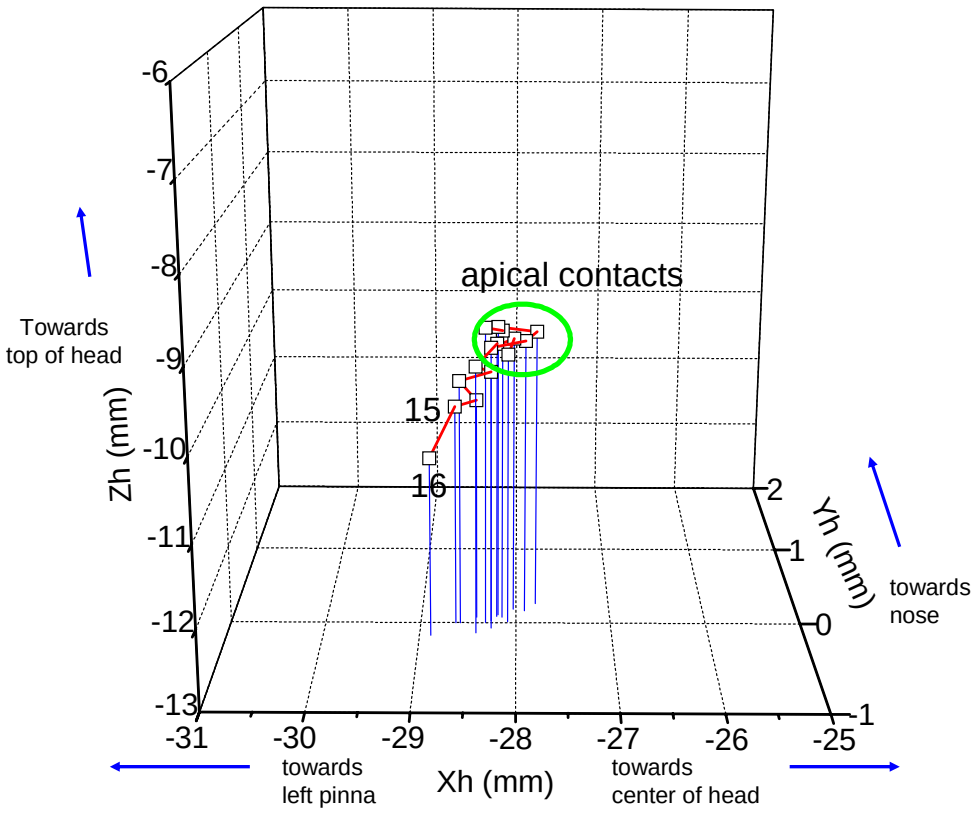

Figure 5.48: Dipole source localization results – Subject S5 (left cochlea)

Figure 5.48 presents the predicted dipoles for Subject S5. Again, the computed dipoles for both apical and basal contacts cluster together to a certain extent. However, the trends are similar to those observed in Subjects S1 and S2 in Figures 5.44 and 5.45 respectively. Figure 5.49 presents the results for Subject S6, a Nucleus subject, for the condition where the ball electrode is the return electrode for monopolar stimulation. The locations for the predicted dipoles appear to follow the locations defined by the electrode model, and do not suggest a preferential pathway through the internal auditory meatus for the apical contacts.

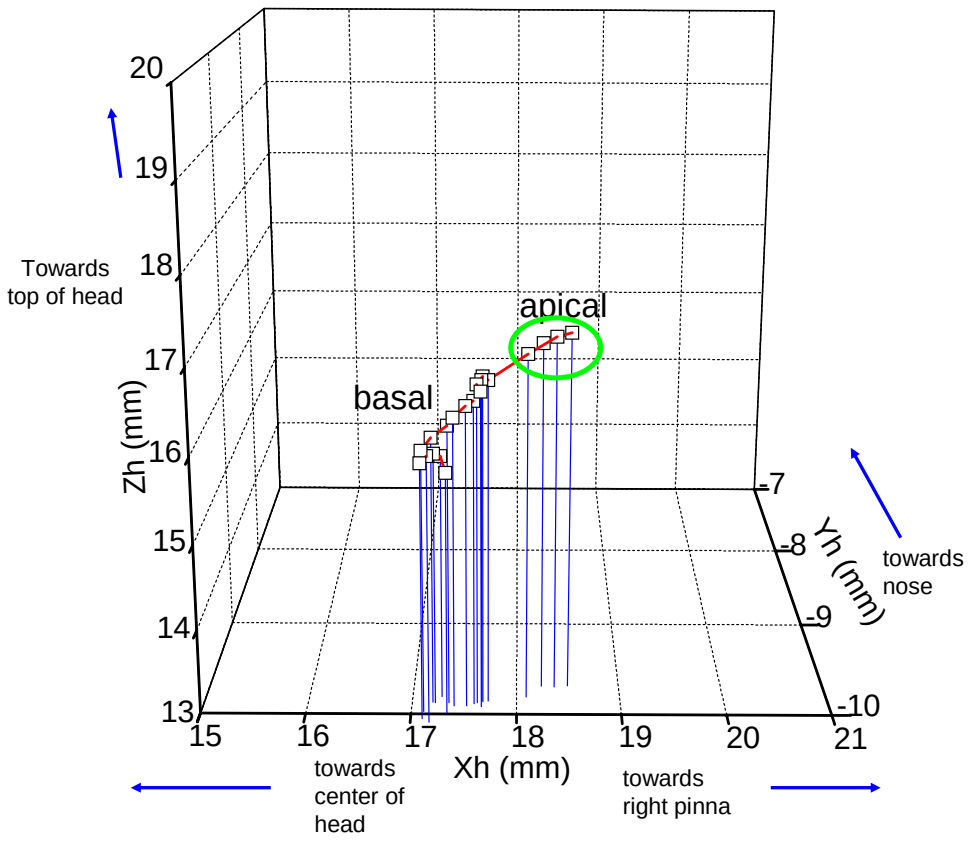

Figure 5.49: Dipole source localization results – Subject S6 (right cochlea)

The clustering of the apical contacts in almost all of the subjects provides further proof (in addition to results from Section 5.3) that there exists a distinct current pathway for these contacts, different from the pathway(s) for basal contacts. In addition, the predicted dipoles for these contacts are located at a remote site further away from where the apical contacts are expected to lie, in many of the subjects. This remote site lines up along the general area of the internal auditory meatus. This suggests that current generated by the apical contacts follows through the modiolar wall via the internal auditory meatus, which is the classical view. Stimulation of the basal contacts appears to result in current that flows

out more laterally out of the cochlea. The results from the inverse dipole are significant, especially considering the use of a very basic spherical head model for the analyses. Future work may include similar analyses using more realistic models, which may provide a more accurate means of estimating current flow within and outside the cochlea.

5.4.2 Intracochlear Electrical Field Measures

Intracochlear electrical field measures, also referred to as Electrical Field Imaging (EFI) are obtained in Subject S1. Input stimuli consist of biphasic pulses with an amplitude of 40 μA and a phase width of 66.4 μs. These current stimuli are sent to the subject's implant system through a single intracochlear electrode and the reference electrode. Potentials are recorded from the stimulated and unstimulated contacts of the intracochlear electrode array. These measures are repeated until all the individual intracochlear electrodes have been stimulated individually. The potential measures obtained are divided by the known current to represent impedance measures in ohms. These impedance measures are also referred to as *transimpedances*.

The top panel in Figure 5.50 represents the transimpedance measures obtained at the unstimulated contacts. The impedance curves for electrodes 3, 4, and 13 are marked. The center panel represents the impedances measured at the stimulated contacts. Impedances measured at the stimulated contacts are generally stable across all electrode contacts with the exception of electrodes 15 and 16 that have high impedance. The x axis represents electrodes numbered from the most apical (#1) to the most basal (#16) contact. The impedance of the curves peaks at the stimulated contacts (peak values represented in center panel). Notice that the impedance curves have a gradual and flat slope leading up to the peak amplitude. This is then followed by a steeper slope leading away from the peak value. The steeper gradient in

the basal region suggests that the apical region of the cochlea is less conductive that the basal region. The characteristics of these curves are similar to what is generally seen in subjects with similar devices and consistent with the patterns seen in the surface potential distributions as well.

These measures obtained in Subject S1 are then analyzed using the EFI model. Details of the model are presented in Section 2.2.3. The bottom panel in Figure 5.50 provides results from this modeling process. The peak value at electrode 2 corresponds to the model's prediction that a significant amount of current leaves the scala through a preferential pathway in the vicinity of electrode 2. This is inconsistent with the results obtained so far for Subject S1.

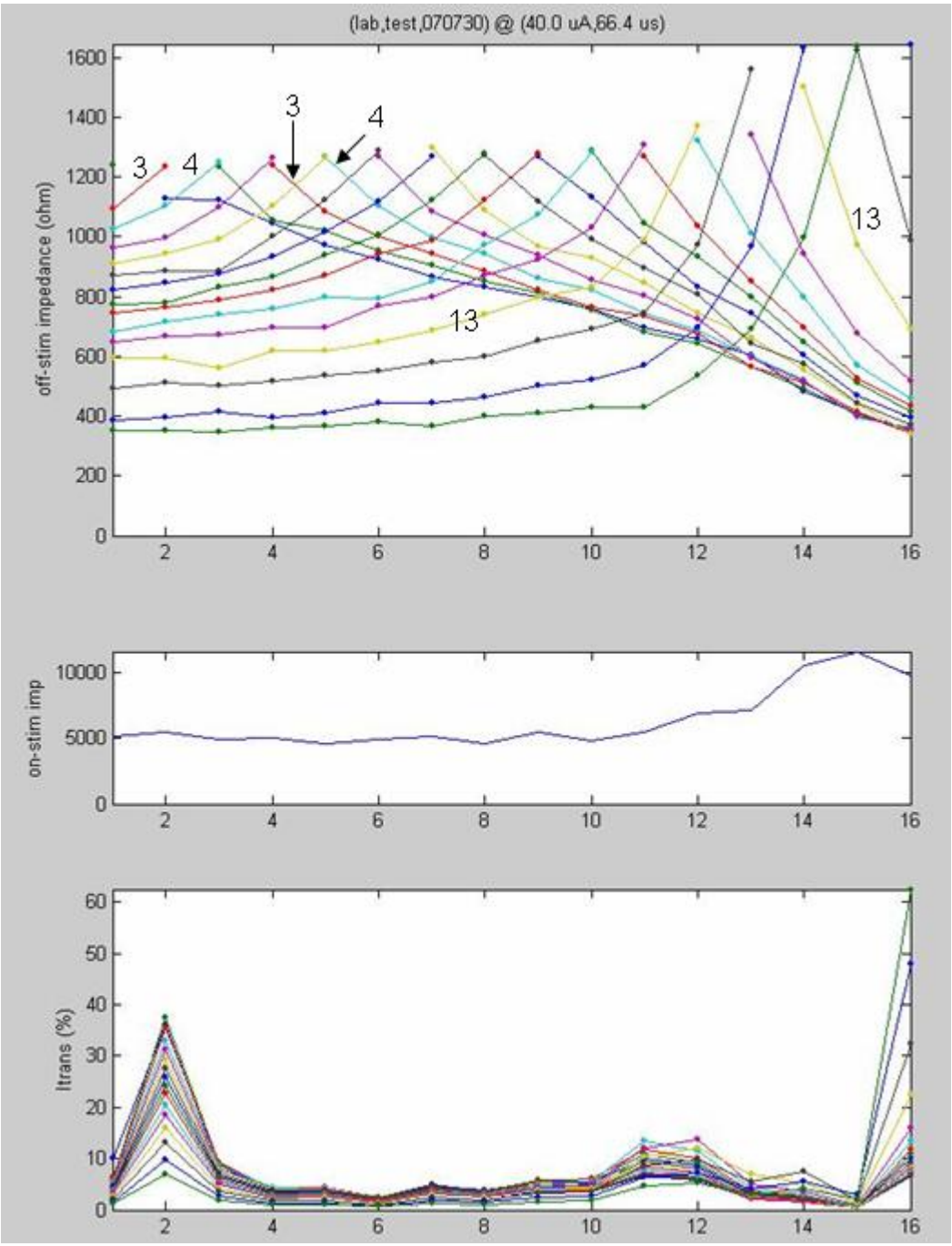

Figure 5.50: EFI maps in Subject S1

6. DISCUSSION AND CONCLUSIONS

This section provides a summary and discussion of the results obtained in this study. The challenges encountered and the general limitations of the approach used in the study are discussed. The potential applications that could develop from this study, topics for future investigation, and conclusions of this study are presented as well.

6.1 Significance of Results

6.1.2 Relationship between Scalp Surface Potentials and Stimulus Current Injected into the Cochlea

Scalp artifact potentials, which represent the *far field* of the stimulation delivered to the cochlea, are used to infer knowledge regarding current flow patterns within the cochlea. The relationship between the input stimuli and the measured scalp potentials was studied by injecting stimuli of varying amplitude levels into the cochlea and recording the resulting surface potential distribution on the scalp. This relationship was found to be linear in nature, and scalp potentials are thus directly related to stimulus current injected into the cochlea. The electrode-fluid interfaces are highly non-linear in nature (Geddes, 1997). The biphasic stimuli, however, are generated using a constant current source, which removes the non-linear effects due to the interface components. The recorded scalp artifacts thus consist of robust, square-shaped biphasic pulses, and this is reflected across all the subjects in this study.

6.1.2 Impedance Characteristics of the Bulk Head Tissue

An assumption made in earlier studies was that the inner ear represents a linear, resistive model. Prior work only verified this assumption up to a frequency of 12.5 KHz. This study successfully tested this assumption up to a frequency of 70 KHz. The assumption was verified and found to be true. The bulk head tissue can thus be modeled as a resistive network in the frequency range of interest between 10 – 70 KHz. The low frequency effects of the impedance characteristics can possibly be attributed to the behavior of muscle tissue (Reilly, 1998). The impedance characteristics of muscle are known to undergo large changes when low-frequency current is passed through, depending on the orientation of the muscle fibers in relation to the direction of current flowing through. When current travels in a direction that is perpendicular to the orientation of the muscle fibers, the resistance posed by the muscle fibers is large and necessitates the current to take a circuitous path. Current that flows in a direction parallel to the fibers, however, does not face the resistive effects of the muscle tissue. The spikes observed in the frequency response curves are thus likely due to the changes in impedance due to the path of current as it flows through the muscle tissue component of the head. At high frequencies, these effects are not observed because the resistivity of the cell membranes within the muscular tissue decreases. The variability of these effects across the three subjects is likely due to the % changes in muscle content.

6.1.3 Differences in Current Flow Patterns across Electrodes

Input stimuli consisting of biphasic pulses that are equal in amplitude across all monopolar electrode combinations were delivered to the cochlea. The resulting potential distribution patterns measured on the scalp were analyzed by the following techniques: (1) plotting of field distribution patterns, (2) computation of global differences between the

electrode distribution maps, and (3) clustering methods to group electrode data based on similar topography. The results from these three independent analysis techniques were completely consistent with each other. Results indicated that distinct differences exist between distribution patterns generated by stimulation of apical electrode contacts versus basal electrode contacts. Within apical electrodes, distributions were very similar. However basal distributions mostly varied from each other, with the exception of one subject where certain basal distributions were similar to each other. The apical electrodes grouped together during cluster analysis. The ranking order for the electrodes within the apex of the cochlea, however, varied across all subjects. This occurs due to noise because the values for the computed difference measure metric are very small in the apical region.

Surface potential data were also obtained from a Nucleus subject, who by nature of device design has two return electrodes that may be invoked either separately or together to provide a total of three return electrode configurations that differ in surface area and head location. The potential patterns generated in all 3 monopolar modes were studied. These data followed the same trends as observed previously in that distributions for apical and basal contacts were distinctly different from each other. The topography of the maps generated for each monopolar mode varied as a function of the location of the return electrode. In the ECE1 mode, where the return electrode is represented by a ball electrode placed within the temporalis muscle, the largest potentials were seen on the scalp close to the temporal region. The ECE2 mode, in which the plate electrode on the stimulator package represents the return electrode, presented largest potentials that were measured right on top of the implanted device. The potential patterns in the ECE1+2 mode, in which the ball electrode and the plate electrode are tied together, were found to be more influenced by the plate electrode than they

were by the ball electrode. This is likely due to the larger surface area of the plate electrode which produces a lower impedance electrode tissue interface and less voltage drop as current passes through it in addition to being distributed over a broader area.

Bipolar data were also analyzed and distributions for electrodes 6-14 referenced to electrode 15, which is a basally-located electrode contact, were studied in Subject S2. The mapped potentials showed small differences in the apical region compared to the basal region, even when the return electrode (electrode 15) was within the cochlea. Data thus suggest that irrespective of the location of the return electrode, apical electrode distributions are very similar to each other and different from basal electrode distributions. This finding is interesting in that it shows that current flow patterns within and around the cochlea are largely affected by intracochlear contacts rather than by the return electrode.

In general, it was very difficult to record bipolar data for apical electrode combinations due to small electrical field potentials appearing at the scalp recording locations. Bipolar data could only be generated when the distance between the apical electrode contacts was sufficiently large. The stimulation protocol was thus changed to include bipolar combinations of apical contacts referenced to a basal contact. It was also found that in order to record meaningful bipolar data, stimulus levels had to be at higher levels than those used for monopolar stimulation. Even with increased stimulus levels, it was impossible to obtain bipolar data when neighboring contacts within the apex of the cochlea were stimulated. The closest-spaced electrodes within the apical region that produced meaningful bipolar potentials were electrodes 19 and 22 in the Nucleus subject (where electrode 22 is the most apical electrode), and the largest potential recorded using this electrode combination was measured at the pinna. The potential at this location, when

referenced to the back of the neck, had a mean peak-to-peak value of approximately 40 μv. The monopolar potential at this location was approximately 1 mv peak-to-peak. This difficulty in recording bipolar potentials in the apical region was reported in a previous study (Mens et al, 1994a) as well, where bipolar potentials due to apical electrode combinations were buried in the noise floor. The fact that it is impossible to record the potentials generated by closely-spaced apical contacts deep within the cochlea suggests that the apex of the cochlea has a conductivity that is lower and different from the basal regions of the cochlea. This encourages a downward flow of current from the apex of the cochlea both through the central modiolar core and along the fluid-filled scalar compartments toward the base.

Though similar trends in the global dissimilarity measures were observed across all subjects as stated previously, large differences were seen in the levels of these GD measures across subjects. These differences are likely due to a combination of various factors. The anatomy and size of the head varied across subjects. Approximate head radii measured in this study ranged from 70 mm – 106 mm. In certain subjects, monopolar data showed phase inversions within a single frame of information. Polarity changes in the mean peak-to-peak amplitude measures would lead to large GD measures for these subjects. These differences could also arise due to varying recording locations across subjects. Some earlier data (Subject S5) did not cover the entire surface of the head and thus show small differences.

6.1.4 Alternate Current Pathways

Inverse dipole analysis techniques were used to compute dipole sources from measured surface potential data. The predicted dipoles varied in terms of location and orientation depending on the electrode being stimulated. If current were to flow through the modiolus and internal auditory meatus, and towards the cranium, measurements on the scalp

would then predict dipoles that would appear to cluster together at a single location outside the cochlea, due to the shunting effects of the cochlear bone. This phenomenon was seen in the dipoles calculated for apical contacts. The computed dipoles for basal contacts, however, were different from each other, and appeared to follow a monotonic function of their location in the basal region of the cochlea. These results suggest that stimulus current to the apical contacts has a primary return current pathway that is consistent with the classical pathway through the modiolar core, the internal auditory meatus, and towards the cranium (Clopton & Spelman, 1982; Spelman et al., 1982; von Békésy, 1951; von Békésy, 1960). In the case of basal contacts, however, current appears to flow out of the cochlea along additional pathways with proportionally less return current flowing through the internal meatus before spreading to the cranium. There are several possible alternative pathways. One is a basalward flow of current leaving the cochlea through the round window. This pathway for basal contacts is in agreement with the "basal pathway" suggested by Mens at al. (1994a), in which current flows out from the apical region, along the fluid-filled scalar compartments, and leaves the cochlea in the basal region in the vicinity of the round window. Mens et al. reached this conclusion in a study of implanted subjects without a medical history of otosclerosis. In contrast to the present study, Mens et al. made no predictions about different current pathways for apical and basal contacts. Mens et al.'s predictions were based on bipolar recordings at a single recording location. The present study, on the other hand, analyzed artifact potentials recorded over the entire surface of the head and includes monopolar-coupled stimulus configurations which may be expected to more strongly invoke alternative pathways for currents to a remote return electrode.

Mens et al's study also suggested a primary current pathway directly through the cochlear bone in subjects with otosclerosis. Bipolar potential distribution patterns measured in two subjects with otosclerosis were very different from patterns observed in the other 16 subjects that had no history of otosclerosis. Potentials in subjects with otosclerosis showed phase inversions that were not observed in subjects without otosclerosis. The measured bipolar data in Subjects S1, S2, and S6 in this current study showed phase inversions at various recording locations on the surface of the scalp and face. None of these subjects, however, had any known history of otosclerosis. These current patterns need to be studied in several other subjects with a known history of cochlear malformations before making any predictions.

An additional return pathway along the facial nerve was proposed by Vanpoucke et al in 2004. In this scenario current may exit the cochlea in the vicinity of the upper basal turn along the facial nerve and its bony canal as it passes anatomically close to the cochlea. This anatomical relationship varies across subjects so the functional significance of this proposed current pathway may differ across individuals. In any case, it is not uncommon for patients to experience extracochlear facial nerve stimulation when intracochlear electrodes in the upper basal turn are stimulated. This confounding electrical stimulation outcome may be due to current flow along this alternate conduction pathway out of the cochlea. The Antwerp group in collaboration with Advanced Bionics (Vanpoucke et al., 2004) developed a technique of measuring and modeling intracochlear electrical fields known as "electrical field imaging" (EFI) that borrows on the concepts underlying impedance tomogography. The intracochlear measures obtained in Subject S1 were analyzed using the Antwerp EFI model implemented in their data collection and modeling software package. The model results did

not suggest a significant role for the facial nerve pathway in this subject; however, it did make the prediction that a significant amount of current exits the scala tympani through the vicinity of Electrode 2 toward the cochlear core. This prediction is highly inconsistent with the findings of this study, and suggests that the Antwerp model may be flawed.

6.2 Problems Encountered

Several problems were encountered during the course of this study, especially in implementing the dipole source localization model. In general, a dipole is defined such that the source and the sink of the dipole lie very close to each other. Also, spherical head models are primarily developed for EEG source analysis problems where the bioelectric source that generates potentials on the surface of the head lies entirely within the cranial cavity i.e. within the innermost sphere in a shell model. The dipole model that is used to interpret monopolar surface artifact data, on the other hand, spans across several layers of the shell model. In a sense, this large dipole violates the basic principle of a dipole because the source and the sink are separated by a large distance and are placed within different layers of the multiple shell model. While the intracochlear electrode contacts within the cochlea can be modeled to lie within the innermost sphere, the return electrode on the case-band of the stimulator package lies within the bone compartment of the shell model. In order to fit this large dipole to the existing forward spherical head model, certain assumptions had to be made. These assumptions were then tested and found to be reasonably valid, as seen in Section 3.4.1.3.

There were some issues related to implementing the inverse model as well. Initially, the algorithm that searched for equivalent dipole sources within the head set no constraints on the *search region*. This resulted in dipoles being generated outside the limits of the head

in certain cases. This is a limitation of the inverse problem, in general, in that more than one solution may exist and more than one generator source may fit as the estimated generator source for a particular potential distribution. Placing restricted bounds on the *search region* eliminated this issue. Another problem faced during the least squares process of fitting the modeled data to the measured data was that in certain cases, the inverse computation resulted in finding a local minimum value instead of a global minimum value while searching for the equivalent dipole source. This issue was solved by picking a more conservative value for the termination tolerance function during the fitting process.

As discussed in Section 6.1.3, generation of bipolar data proved to be a difficult task. The stimulation protocol needed to be changed to include higher stimulus levels for bipolar data compared to stimulus levels used for monopolar data. This issue was further confounded by the limitations of the Advanced Bionics research software which does not provide the capability to control stimulus levels across different stimulation conditions. This requires bipolar and monopolar data to be separately recorded in these subjects, which proved to be a very time-consuming process. In spite of all the improvements and modifications made to the initial protocol, bipolar data are still difficult to record within the apex. Analysis of the bipolar data using simple spherical models proved to be difficult due to the nature of the small signals recorded in the bipolar data. The development and use of a more sensitive and realistic model of the head, in which details regarding the anatomy of the temporal bone and cochlea were provided, would better help to describe the bipolar data.

6.3 General Limitations of the Study

The study protocol did not involve measuring potentials at identical recording locations on the surface of the head across all subjects. Establishing identical recording

locations for all subjects may enable a closer comparison of the levels of global differences between electrode combinations across subjects. In addition, this may enable grouping data from all the subjects during the cluster analysis process. This approach, however, still does not completely remove the variability element in these measures due to the variable location of the return electrode across subjects based on placement of the stimulator package during surgery.

A second limitation of this study is that data were collected on a somewhat coarse grid resolution in certain regions of the head where the field patterns change rapidly. This limitation can be addressed by repeating these measures on a larger group of subjects with a finer grid of scalp recording positions to find the complete set of recording locations on the scalp, face, and neck that provide the most useful information regarding these changing potentials.

Another limitation of this study is that it uses a very basic spherical model to analyze surface potential data. The spherical model makes the basic assumption that the head is a sphere, which in fact it is not. In addition, the spherical head model does not include the detailed anatomy of the basal skull plate including the temporal bone and the cochlea. In spite of its crude nature, however, the spherical model performs very well in predicting dipoles that in fact appear in the general vicinity of where they are expected to lie. It is expected that a more detailed model would improve the accuracy of the results. A recent comparison of localization accuracy in predicting sources for EEG data using a realistically shaped boundary-element head model and a spherical head model (Cuffin et al., 2001), however, surprisingly only showed a marginal increase of localization accuracy in using the realistic model (10.5 mm) when compared to the spherical model (10.6 mm). This finding is

consistent with the relative success of the shell-based model in the present study in making spatial predictions consistent with the hypothesized current flow mechanisms to explain the experimental data. More realistic models of the head and temporal bone will likely provide more insight into possible current flow pathways active during stimulation in the basal cochlea.

Finally, the source localization process is labor-intensive and tedious in nature and requires defining and re-defining the search region several times before the best source location is found for the dipole.

6.4 Future Work and Applications

Potential improvements to this study include finding locations on the surface of the head, face, and neck in cochlear implant subjects that would provide the most useful information regarding current flow patterns. These locations could then be used across all subjects. Future work may also involve using realistic models such as finite-element models to analyze surface potential data, instead of the basic spherical models that were used in this study. Finally, knowledge of location within the cochlea where the electrode contacts are placed would aid in testing the accuracy of the dipole source localization process.

The approach used in this study could eventually be used in developing a clinical tool that measures surface potentials on a few, select locations on the surface of the head to help estimate current flow patterns in cochlear implant subjects and/or classify subjects based on these patterns. The development of a clinical tool such as this would involve prior testing of surface potential patterns in cochlear implant subjects with normal cochleae as well as known abnormalities in the cochlea such as otosclerosis (cochlear bone becomes spongiform in nature) and Mondini malformation (incomplete formation of the cochlea) etc. This prior

testing would enable knowledge of current flow patterns consistent with normal and abnormal cochleae, and this information could be used as training data for the classification system. In addition, the dipole localization process could also be used to estimate the location of the electrode contacts for subjects in which such existing data were not available already. Finally, knowledge gained from this study could help improve speech processing techniques and electrode designs to provide more useful information for cochlear implant users.

6.5 Conclusions

Based upon current knowledge, this is the first study of its kind that successfully measured surface artifact potential distributions on the entire surface of the head (including the regions on the face, head, and neck regions) in cochlear implant subjects. The study used these surface potential measures to test certain assumptions regarding current flow within and around the cochlea. Results indicate that distinct differences in current flow pathways exist for apical and basal contacts within the cochlea. Stimulation of the apical contacts results in a primary path of current flow through the classical auditory meatus pathway, while current flow in the basal region appears to flow out laterally. These results are significant in that they contradict the classical school of thought that all current flows through the internal auditory meatus. New information gained from this study could directly impact the design and development of future cochlear implant systems.

APPENDIX

The Appendix contains the subject informed consent forms for the IRB-approved surface potential study for the following subjects:

1. Adult cochlear implant subjects
2. Adult non-implanted subjects

University of North Carolina-Chapel Hill
Consent to Participate in a Research Study
Adult Cochlear Implant Subjects
Biomedical Form

IRB Study # 05-2243
Consent Form Version Date: 11/06/2006

Title of Study: Scalp Potentials Generated by Cochlear Implants

Principal Investigator: Punita Christopher, MS
UNC-Chapel Hill Department: Joint Dept. of Biomedical Engineering, UNC-CH and NCSU and Dept. of Otolaryngology/Head and Neck Surgery, School of Medicine, UNC-CH
UNC-Chapel Hill Phone number: (919) 966-6763
Email Address: pchris@unc.edu
Co-Investigators: Charles Finley, PhD
Craig Buchman, MD, FACS
Emily Buss, PhD
Marcia Clark, MS, CCC-A
Harold Pillsbury, MD, FACS
Carol Pillsbury, MS, CCC-A

Faculty Advisor: Charles Finley, PhD
Funding Source: Internal laboratory funds

Study Contact telephone number: (919) 966-6763
Study Contact email: pchris@unc.edu **or** charles_finley@med.unc.edu

---

What are some general things you should know about research studies?
You are being asked to take part in a research study. To join the study is voluntary. You may refuse to join, or you may withdraw your consent to be in the study, for any reason.

Research studies are designed to obtain new knowledge that may help other people in the future. You may not receive any direct benefit from being in the research study. There also may be risks to being in research studies.

Deciding not to be in the study or leaving the study before it is done will not affect your relationship with the researcher, your health care provider, or the University of North Carolina-Chapel Hill. If you are a patient with an illness, you do not have to be in the research study in order to receive health care.

Details about this study are discussed below. It is important that you understand this information so that you can make an informed choice about being in this research study.

You will be given a copy of this consent form. You should ask the researchers named above, or staff members who may assist them, any questions you have about this study at any time.

What is the purpose of this study?

The purpose of this research study is to better understand where electrical current flows within and outside the inner ear during stimulation by a cochlear implant. In this study, we will record potentials on your scalp and face that are generated by your cochlear implant. Every cochlear implant generates these potentials. We are using them to learn more about how cochlear implant devices function differently in individual subjects. You are being asked to be in the study because you have a cochlear implant device.

Are there any reasons you should not be in this study?

You should not be in this study if you cannot sit still for a period of 10 minutes while we make sensitive measurements. The total test session will last about two hours.

How many people will take part in this study?

If you decide to be in this study, you will be one of approximately 12 people in this research study.

How long will your part in this study last?

The study will consist of multiple short sessions that will last approximately 10 minutes each. The total test time will be about two hours. There are no follow-up sessions.

What will happen if you take part in the study?

In this study, surface electrodes will be attached on your head and skin to enable us to obtain certain measures. This will require us to clean the skin with rubbing alcohol before attaching the electrodes. When we stimulate your device, we will ask you how loud it is. Otherwise, you will sit quietly during the testing.

Next, we will obtain the following measures:

1. We will use an electrode probe and surface electrodes to measure potentials from your scalp and face, while your cochlear implant device is stimulating.
2. Using surface electrodes on the scalp, we will also measure the voltages on the scalp in response to the very small currents that are applied through surface electrodes.
3. During stimulation of the device, we will also obtain potential measures from the implanted electrode array in your ear. Not all cochlear implant systems have this capability and if yours does not, this test will not be conducted.
   Based on our records, your device does ____ does not ____ have this capability.
4. We will obtain measures to determine the shape of your head.

What are the possible benefits from being in this study?

Research is designed to benefit society by gaining new knowledge. There is no direct benefit to you for participating in this study. The benefit to you from being in this study may be a long-term benefit of a deeper understanding of how the cochlear implant functions.

What are the possible risks or discomforts involved with being in this study?

The risks from this study are no greater than what you experience while wearing your cochlear implant device. These include:

1. Over stimulation by the implant device: To prevent this we will make sure that the stimulus levels will be set well below the most comfortable loudness level.
2. Fatigue due to the testing protocol: We will minimize this by seating you as comfortably as possible and allowing breaks at intervals during the data collection session.
3. Skin reaction due to the electrode paste and tape: We will use non-reactive pastes and/or saline and hypoallergenic medical tape. Please indicate to us if you have had any past allergic reaction to such materials.
   I have ___ have not ___ had an allergic response in the past.
4. Tissue damage/shock: The external current stimulus will be very small in magnitude. In addition, there may be uncommon or previously unknown risks that might occur. You should report any problems to the researchers immediately.

What if we learn about new findings or information during the study?

You will be given any new information gained during the course of the study that might affect your willingness to continue your participation. We will also share new findings with fellow researchers, your clinical caregivers, and the implant manufacturing company engineers.

How will your privacy be protected?

No subjects will be identified in any report or publication about this study. Although every effort will be made to keep research records private, there may be times when federal or state law requires the disclosure of such records, including personal information. This is very unlikely, but if disclosure is ever required, UNC-Chapel Hill will take steps allowable by law to protect the privacy of personal information. In some cases, your information in this research study could be reviewed by representatives of the University, research sponsors, or government agencies for purposes such as quality control or safety.

Data will be coded such that is cannot be identified as from a particular subject. The master list will be secured and kept in a locked cabinet with access limited to the PI and the faculty advisor. Full head photographs will be made of you at points during our work. We use these photographs to record positions of recording and stimulating electrode location and the position of your cochlear implant beneath your scalp. At the end of your visit, each photograph will be edited to remove identifying information. This is typically done by blanking out eyes, noses, and lips. The original photographs will then be destroyed. You may participate in this process if you wish.

What will happen if you are injured by this research?
All research involves a chance that something bad might happen to you. This may include the risk of personal injury. In spite of all safety measures, you might develop a reaction or injury from being in this study. If such problems occur, the researchers will help you get medical care, but any costs for the medical care will be billed to you and/or your insurance company. The University of North Carolina at Chapel Hill has not set aside funds to pay you for any such reactions or injuries, or for the related medical care. However, by signing this form, you do not give up any of your legal rights.

What if you want to stop before your part in the study is complete?
You can withdraw from this study at any time, without penalty. The investigators also have the right to stop your participation at any time. This could be because you have had an unexpected reaction, or have failed to follow instructions, or because the entire study has been stopped.

Will you receive anything for being in this study?
You will be receiving $20 for taking part in this study.

Will it cost you anything to be in this study?
You will have no expenses other than transportation. We will pay for the parking fees.

What if you are a UNC student?
You may choose not to be in the study or to stop being in the study before it is over at any time. This will not affect your class standing or grades at UNC-Chapel Hill. You will not be offered or receive any special consideration if you take part in this research.

What if you are a UNC employee?
Taking part in this research is not a part of your University duties, and refusing will not affect your job. You will not be offered or receive any special job-related consideration if you take part in this research.

Who is sponsoring this study?
This research is funded by internal laboratory funds.

What if you have questions about this study?
You have the right to ask, and have answered, any questions you may have about this research. If you have questions, or if a research-related injury occurs, you should contact the researchers listed on the first page of this form.

What if you have questions about your rights as a research subject?
All research on human volunteers is reviewed by a committee that works to protect your rights and welfare. If you have questions or concerns about your rights as a research subject you may contact, anonymously if you wish, the Institutional Review Board at 919-966-3113 or by email to IRB_subjects@unc.edu.
- -

Subject's Agreement:
I have read the information provided above. I have asked all the questions I have at this time. I voluntarily agree to participate in this research study.

_______________________________________ __________________
Signature of Research Subject Date

____
Printed Name of Research Subject

_______________________________________ __________________
Signature of Person Obtaining Consent Date

____
Printed Name of Person Obtaining Consent

University of North Carolina-Chapel Hill
Consent to Participate in a Research Study
Adult Non-implanted Subjects
Biomedical Form

IRB Study # 05-2243
Consent Form Version Date: 11/06/2006

Title of Study: Scalp Potentials Generated by Cochlear Implants

Principal Investigator: Punita Christopher, MS
UNC-Chapel Hill Department: Joint Dept. of Biomedical Engineering, UNC-CH and NCSU and Dept. of Otolaryngology/Head and Neck Surgery, School of Medicine, UNC-CH
UNC-Chapel Hill Phone number: (919) 966-6763
Email Address: pchris@unc.edu
Co-Investigators: Charles Finley, PhD
Craig Buchman, MD, FACS
Emily Buss, PhD
Marcia Clark, MS, CCC-A
Harold Pillsbury, MD, FACS
Carol Pillsbury, MS, CCC-A

Faculty Advisor: Charles Finley, PhD
Funding Source: Internal laboratory funds

Study Contact telephone number: (919) 966-6763
Study Contact email: pchris@unc.edu **or** charles_finley@med.unc.edu

---

What are some general things you should know about research studies?
You are being asked to take part in a research study. To join the study is voluntary. You may refuse to join, or you may withdraw your consent to be in the study, for any reason.

Research studies are designed to obtain new knowledge that may help other people in the future. You may not receive any direct benefit from being in the research study. There also may be risks to being in research studies.

Deciding not to be in the study or leaving the study before it is done will not affect your relationship with the researcher, your health care provider, or the University of North Carolina-Chapel Hill. If you are a patient with an illness, you do not have to be in the research study in order to receive health care.

Details about this study are discussed below. It is important that you understand this information so that you can make an informed choice about being in this research study.

You will be given a copy of this consent form. You should ask the researchers named above, or staff members who may assist them, any questions you have about this study at any time.

What is the purpose of this study?

The purpose of this research study is to better understand where electrical current flows within and outside the inner ear during stimulation by a cochlear implant. A cochlear implant is a medical device implanted in patients with severe or profound hearing loss in order to restore some functional hearing. To learn more about the functioning of cochlear implant devices, we need to study the electrical characteristics of the skin, tissue, electrode, head etc. in both implanted and non-implanted subjects. You are being asked to be in the study because you have not been implanted with a cochlear implant.

Are there any reasons you should not be in this study?

You should not be in this study if you cannot sit still for a period of 10 minutes while we make sensitive measurements. The total test session will last about two hours.

How many people will take part in this study?

If you decide to be in this study, you will be one of approximately 12 people in this research study.

How long will your part in this study last?

The study will consist of multiple short sessions that will last approximately 10 minutes each. The total test time will be about two hours. There are no follow-up sessions.

What will happen if you take part in the study?

In this study, surface electrodes will be attached on your head and skin to enable us to obtain certain measures. This will require us to clean the skin with rubbing alcohol before attaching the electrodes.

Next, we will obtain the following measures:

1. We will apply very small currents through surface electrodes on the scalp and skin, and measure the resulting respective voltages on the head and skin.
2. In some subjects, we will use subcutaneous needle electrodes instead of surface electrodes to measure the voltage under the skin surface in the forearm region. This work will be conducted under the direct supervision of a collaborating physician or designated resident.
   We will ___ will not ___ obtain these measures from your skin.
3. We will obtain measures to determine the shape of your head.

What are the possible benefits from being in this study?

Research is designed to benefit society by gaining new knowledge. You will not benefit

personally from being in this research study. This study will nevertheless benefit the cochlear implant field at large by providing a deeper understanding of how these devices function.

What are the possible risks or discomforts involved with being in this study?

The following are the possible risks:

1. Skin reaction due to the electrode paste and tape: We will use non-reactive pastes and/or saline and hypoallergenic medical tape. Please indicate to us if you have had any past allergic reaction to such materials.
   I have ___ have not ___ had an allergic response in the past.
2. Tissue damage/shock: The external current applied will be very small in magnitude.

If we apply subcutaneous needle electrodes to your forearm, you will experience the same risks as in a hypodermic needle injection, and these risks include:

1. Discomfort due to insertion
2. Infection: We use disposable sterilized needles and clean your skin prior to injection.
3. Irritation and soreness in the local forearm skin region

In addition, there may be uncommon or previously unknown risks that might occur. You should report any problems to the researchers.

What if we learn about new findings or information during the study?

You will be given any new information gained during the course of the study that might affect your willingness to continue your participation.

How will your privacy be protected?

No subjects will be identified in any report or publication about this study. Although every effort will be made to keep research records private, there may be times when federal or state law requires the disclosure of such records, including personal information. This is very unlikely, but if disclosure is ever required, UNC-Chapel Hill will take steps allowable by law to protect the privacy of personal information. In some cases, your information in this research study could be reviewed by representatives of the University, research sponsors, or government agencies for purposes such as quality control or safety.

Data will be coded such that is cannot be identified as from a particular subject. The master list will be secured and kept in a locked cabinet with access limited to the PI and the faculty advisor. Full head photographs will be made of you at points during our work. We use these photographs to record positions of recording and stimulating electrode locations. At the end of your visit, each photograph will be edited to remove identifying information. This is typically done by blanking out eyes, noses, and lips. The original photographs will then be destroyed. You may participate in this process if you wish.

What will happen if you are injured by this research?

All research involves a chance that something bad might happen to you. This may include the risk of personal injury. In spite of all safety measures, you might develop a reaction or

injury from being in this study. If such problems occur, the researchers will help you get medical care, but any costs for the medical care will be billed to you and/or your insurance company. The University of North Carolina at Chapel Hill has not set aside funds to pay you for any such reactions or injuries, or for the related medical care. However, by signing this form, you do not give up any of your legal rights.

What if you want to stop before your part in the study is complete?

You can withdraw from this study at any time, without penalty. The investigators also have the right to stop your participation at any time. This could be because you have had an unexpected reaction, or have failed to follow instructions, or because the entire study has been stopped.

Will you receive anything for being in this study?

You will receive $20 for taking part in this study.

Will it cost you anything to be in this study?

It will not cost you anything to be in this research study.

What if you are a UNC student?

You may choose not to be in the study or to stop being in the study before it is over at any time. This will not affect your class standing or grades at UNC-Chapel Hill. You will not be offered or receive any special consideration if you take part in this research.

What if you are a UNC employee?

Taking part in this research is not a part of your University duties, and refusing will not affect your job. You will not be offered or receive any special job-related consideration if you take part in this research.

Who is sponsoring this study?

This research study is funded by internal laboratory funds.

What if you have questions about this study?

You have the right to ask, and have answered, any questions you may have about this research. If you have questions, or if a research-related injury occurs, you should contact the researchers listed on the first page of this form.

What if you have questions about your rights as a research subject?
All research on human volunteers is reviewed by a committee that works to protect your rights and welfare. If you have questions or concerns about your rights as a research subject you may contact, anonymously if you wish, the Institutional Review Board at 919-966-3113 or by email to IRB_subjects@unc.edu.

- -

Subject's Agreement:

I have read the information provided above. I have asked all the questions I have at this time. I voluntarily agree to participate in this research study.

_____ _____
Signature of Research Subject Date

_____
Printed Name of Research Subject

_____ _____
Signature of Person Obtaining Consent Date

_____
Printed Name of Person Obtaining Consent

BIBLIOGRAPHY

Advanced Bionics. (2003). *Electrical field imaging and modeling tool (EFIM) v 1.3 user guide*

ANSI/AAMI ES1. (1993). Safe current limits for electromedical apparatus, 3ed

Ary, J. P., Klein, S. A., & Fender, D. H. (1981). Location of sources of evoked scalp potentials: Corrections for skull and scalp thicknesses. *IEEE transactions on bio-medical engineering, 28*(6), 447-452.

Battmer, R. D., Gnadeberg, D., Lehnhardt, E., & Lenarz, T. (1994). An integrity test battery for the nucleus mini 22 cochlear implant system. *European archives of oto-rhino-laryngology : official journal of the European Federation of Oto-Rhino-Laryngological Societies (EUFOS) : affiliated with the German Society for Oto-Rhino-Laryngology - Head and Neck Surgery, 251*(4), 205-209.

Baumann, S. B., Wozny, D. R., Kelly, S. K., & Meno, F. M. (1997). The electrical conductivity of human cerebrospinal fluid at body temperature. *IEEE transactions on bio-medical engineering, 44*(3), 220-223.

Berg, P., & Scherg, M. (1994). A fast method for forward computation of multiple-shell spherical head models. *Electroencephalography and clinical neurophysiology, 90*(1), 58-64.

Briaire, J. J., & Frijns, J. H. (2000). Field patterns in a 3D tapered spiral model of the electrically stimulated cochlea. *Hearing research, 148*(1-2), 18-30.

Brody, D. A., Terry, F. H., & Ideker, R. E. (1973). Eccentric dipole in a spherical medium: Generalized expression for surface potentials. *IEEE transactions on bio-medical engineering, 20*(2), 141-143.

Burger, H., & van Milaan, J. (1943). Measurements of the specific resistance of the human body to direct current. *Acta Med.Scand, 114*, 584–607.

Carter, P. M. (2001). The use of surface potential testing for diagnosing cochlear implant electrode faults and cochlear pathologies. *the 2nd International Symposium and Workshop on Objective Measures in Cochlear Implantation,* Lyon, France.

Chatrian, G., Lettich, E., & Nelson, P. (1985). Ten percent electrode system for topographic studies of spontaneous and evoked EEG activities. *American Journal of EEG Technology, 25*, 83–92.

Christopher, P. (2003). A generic approach to monitoring cochlear implant function. *Master's Thesis in Biomedical Engineering,*

Clopton, B. M., & Spelman, F. A. (1982). Neural mechanisms relevant to the design of an auditory prosthesis. location and electrical characteristics. *The Annals of otology, rhinology & laryngology.Supplement, 98*, 9-14.

Coleman, T.F. and Y. Li, "An Interior, Trust Region Approach for Nonlinear Minimization Subject to Bounds," *SIAM Journal on Optimization*, Vol. 6, pp. 418-445, 1996.

Coleman, T.F. and Y. Li, "On the Convergence of Reflective Newton Methods for Large-Scale Nonlinear Minimization Subject to Bounds," *Mathematical Programming*, Vol. 67, Number 2, pp. 189-224, 1994.

Cuffin BN, Schomer DL, Ives JR, Blume H (2001). Experimental tests of EEG source localization accuracy in realistically shaped head models. *Clin Neurophysiol.* 112(12):2288-92.

Cuffin BN, Schomer DL, Ives JR, Blume H (2001). Experimental tests of EEG source localization accuracy in spherical head models. *Clin Neurophysiol.* 112(1):46-51.

Cullington, H. E., & Clarke, G. P. (1997). Integrity testing of cochlear implants in the awake child. *British journal of audiology, 31*(4), 247-256.

Cumming, G., Fidler, F., & Vaux, D. L. (2007). Error Bars in experimental Biology. *J Cell Biol. 177*(1), 7-11.

de Munck, J. C., & Peters, M. J. (1993). A fast method to compute the potential in the multisphere model. *IEEE transactions on bio-medical engineering, 40*(11), 1166-1174.

Duda, R. O., Hart, P. E., & Stork, D. G. (2000). *Pattern classification* Wiley-Interscience.

Ferree, T. C., Eriksen, K. J., & Tucker, D. M. (2000). Regional head tissue conductivity estimation for improved EEG analysis. *IEEE transactions on bio-medical engineering, 47*(12), 1584-1592.

Finley, C. C., Christopher, P., Eddington, D. K., & Herrmann, B. (2003). Seventh quarterly progress report. *Speech Processors for Auditory Prostheses, NIH Progress Report,*

Finley, C. C., Herrmann, B., & Eddington, D. K. (2004). Eleventh quarterly progress report. *Speech Processors for Auditory Prostheses, NIH Progress Report,*

Finley, C. C., Wilson, B. S., & White, M. W. (1990). Models of neural responsiveness to electrical stimulation. *Cochlear Implants: Models of the Electrically Stimulated Ear,* , 55-96.

Frijns, J. H., de Snoo, S. L., & Schoonhoven, R. (1995). Potential distributions and neural excitation patterns in a rotationally symmetric model of the electrically stimulated cochlea. *Hearing research, 87*(1-2), 170-186.

Garnham, J., Cope, Y., & Mason, S. M. (2000). Audit of 5-year post-implantation routine integrity tests performed on paediatric cochlear implantees. *British journal of audiology, 34*(5), 285-292.

Geddes, L. A. (1997). Historical evolution of circuit models for the electrode-electrolyte interface. *Annals of Biomedical Engineering, 25*(1), 1-14.

Geddes, L. A., & Baker, L. E. (1967). The specific resistance of biological material--a compendium of data for the biomedical engineer and physiologist. *Medical & biological engineering, 5*(3), 271-293.

Girzon, G. (1987). Investigation of current flow in the inner ear during electrical stimulation of intracochlear electrodes.

Hanekom, T. (2001). Three-dimensional spiraling finite element model of the electrically stimulated cochlea. *Ear and hearing, 22*(4), 300-315.

Hanekom, T. (2005). Modelling encapsulation tissue around cochlear implant electrodes. *Medical & biological engineering & computing, 43*(1), 47-55.

Heller, J. W., Sinopoli, T., Fowler-Brehm, N., & Shallop, J. K. (1991). The characterization of averaged electrode voltages from the nucleus cochlear implant. *IEEE Trans, Nov,*

Jasper, H. H. (1958). The ten-twenty electrode system of the international federation. *Electroencephalography and clinical neurophysiology, 10*(1), 371–375.

Kasper, A., Pelizzone, M., & Montandon, P. (1991). Intracochlear potential distribution with intracochlear and extracochlear electrical stimulation in humans. *The Annals of Otology, Rhinology, and Laryngology, 100*(10), 812-816.

Kileny, P. R., Meiteles, L. Z., Zwolan, T. A., & Telian, S. A. (1995). Cochlear implant device failure: Diagnosis and management. *The American Journal of Otology, 16*(2), 164-171.

Lagerlund, T. (1999). EEG source localization (model-dependent and model-independent methods). *Electroencephalography: Basic Principles, Clinical Applications, and Related Fields.Lippincott, Williams and Wilkins, Baltimore, MD,* , 809–822.

Law, S. K. (1993). Thickness and resistivity variations over the upper surface of the human skull. *Brain topography, 6*(2), 99-109.

Loeb, G. E. (1985). The functional replacement of the ear. *Scientific American, 252(2),* 104-111.

Malmivuo, J., & Plonsey, R. (1995). *Principles and Applications of Bioelectric and Biomagnetic Fields,*

Mens, L. H., Huiskamp, G., Oostendorp, T., & van den Broek, P. (1999). Modelling surface potentials from intracochlear electrical stimulation. *Scandinavian audiology, 28*(4), 249-255.

Mens, L. H., & Mulder, J. J. (2002). Averaged electrode voltages in users of the clarion cochlear implant device. *The Annals of Otology, Rhinology, and Laryngology, 111*(4), 370-375.

Mens, L. H., Oostendorp, T., & van den Broek, P. (1994a). Cochlear implant generated surface potentials: Current spread and side effects. *Ear and hearing, 15*(4), 339-345.

Mens, L. H., Oostendorp, T., & van den Broek, P. (1994b). Identifying electrode failures with cochlear implant generated surface potentials. *Ear and hearing, 15*(4), 330-338.

Micco, A. G., & Richter, C. P. (2006). Electrical resistivity measurements in the mammalian cochlea after neural degeneration. *Laryngoscope. 116(8),*1334-1341.

Mosher, J. C., Leahy, R. M., & Lewis, P. S. (1999). EEG and MEG: Forward solutions for inverse methods. *IEEE transactions on bio-medical engineering, 46*(3), 245-259.

Musha, T., & Okamoto, Y. (1999). Forward and inverse problems of EEG dipole localization. *Critical Reviews in Biomedical Engineering, 27*(3-5), 189-239.

National Institute on Deafness and other Communication Disorders. (2006). http://www.nidcd.nih.gov/

Oostenveld, R., & Praamstra, P. (2001). The® ve percent electrode system for high-resolution EEG and ERP measurements. *Clinical Neurophysiology, 112*, 713-719.

Rattay, F., Leao, R. N., & Felix, H. (2001). A model of the electrically excited human cochlear neuron. II. influence of the three-dimensional cochlear structure on neural excitability. *Hearing research, 153*(1-2), 64-79.

Rattay, F., Lutter, P., & Felix, H. (2001). A model of the electrically excited human cochlear neuron. I. contribution of neural substructures to the generation and propagation of spikes. *Hearing research, 153*(1-2), 43-63.

Reilly, JP (1998). Applied Bioelectricity: From Electrical Stimulation to Electropathology. Springer New York.

Roth, W., Ford, J., Pfefferbaum, A., & Elbert, T. (1995). Methodological issues in event-related brain potential and magnetic field studies. *Psycho-pharmacology, the Fourth Generation of Progress.Raven Press, New York,* , 895–910.

Rush, S., & Driscoll, D. A. (1969). EEG electrode sensitivity--an application of reciprocity. *IEEE transactions on bio-medical engineering, 16*(1), 15-22.

Salu, Y., Cohen, L. G., Rose, D., Sato, S., Kufta, C., & Hallett, M. (1990). An improved method for localizing electric brain dipoles. *IEEE transactions on bio-medical engineering, 37*(7), 699-705.

Salu, Y., & Mehrotra, P. (1984). A computerized system for localizing sources of cardiac activation. *Computers and biomedical research, an international journal, 17*(3), 222-228.

Scherg, M. (1990). Fundamentals of dipole source potential analysis. *Advances in audiology, 6*, 40-69.

Shallop, J. K. (1993). Objective electrophysiological measures from cochlear implant patients. *Ear and hearing, 14*(1), 58-63.

Skrandies, W. (1990). Global field power and topographic similarity. *Brain topography, 3*(1), 137-141.

Spelman, F. A., Clopton, B. M., & Pfingst, B. E. (1982). Tissue impedance and current flow in the implanted ear. implications for the cochlear prosthesis. *The Annals of otology, rhinology & laryngology.Supplement, 98*, 3-8.

Spelman, F. A., Clopton, B. M., Pfingst, B. E., & Miller, J. M. (1980). Design of the cochlear prosthesis: Effects of the flow of current in the implanted ear. *The Annals of otology, rhinology & laryngology.Supplement, 89*(2 Pt 2), 8-10.

Spelman, F. A., Pfingst, B. E., Miller, J. M., Hassul, M., Powers, W. E., & Clopton, B. M. (1980). Biophysical measurements in the implanted cochlea. *Otolaryngology and head and neck surgery, 88*(2), 183-187.

Vanpoucke, F., Zarowski, A., Casselman, J., Frijns, J., & Peeters, S. (2004). The facial nerve canal: An important cochlear conduction path revealed by clarion electrical field imaging. *Otology & neurotology : official publication of the American Otological Society, American Neurotology Society [and] European Academy of Otology and Neurotology, 25*(3), 282-289.

Vanpoucke, F. J., Zarowski, A. J., & Peeters, S. A. (2004). Identification of the impedance model of an implanted cochlear prosthesis from intracochlear potential measurements. *IEEE transactions on bio-medical engineering, 51*(12), 2174-2183.

von Békésy, G. (1951). The course pattern of the electrical resistance in the cochlea of the guinea pig(electro-anatomy of the cochlea). *The Journal of the Acoustical Society of America, 23*(1), 18-28.

von Békésy, G. (1960). *Experiments in hearing*McGraw-Hill New York.

Whiten, D. M. (2007). Electro-anatomical models of the cochlear implant.

WILSON, F. N., & BAYLEY, R. H. (1950). The electric field of an eccentric dipole in a homogeneous spherical conducting medium. *Circulation, 1*(1), 84-92.

Wilson, B. S., Finley, C. C., Lawson, D. T., Wolford, R. D., Eddington, D. K., & Rabinowitz, W. M. (1991). Better speech recognition with cochlear implants. *Nature, 352*(6332), 236-238.

World Health Organization. (2005). http://www.who.int/mediacentre/factsheets/fs300/en/

Xu, J., Xu, S. A., Cohen, L. T., & Clark, G. M. (2000). Cochlear view: Postoperative radiography for cochlear implantation. *The American Journal of Otology, 21*(1), 49-56.

Youngworth, R., Bates, R., Romero, R., & Aronstein, D. (2005). TRADING spaces. *SPIE,* , 29-33.

Zhang, Z. (1995). A fast method to compute surface potentials generated by dipoles within multilayer anisotropic spheres. *Physics in Medicine and Biology, 40*(3), 335-349.

Zhang, Z., & Jewett, D. L. (1993). Insidious errors in dipole localization parameters at a single time-point due to model misspecification of number of shells. *Electroencephalography and clinical neurophysiology, 88*(1), 1-11.